USGS
science for a changing world

Prepared in cooperation with the State of New York, Department of Education, New York Geological Survey

Bedrock Geologic Map of the Eagle Lake Quadrangle, Essex County, New York

By Gregory J. Walsh, Sean P. Regan, Phillip S. Geer, Arthur J. Merschat, Kaitlyn A. Suarez, Ryan J. McAleer, Matt S. Walton Jr., and E. Allen Crider, Jr.

Pamphlet to accompany

Scientific Investigations Map 3542

U.S. Department of the Interior
U.S. Geological Survey

U.S. Geological Survey, Reston, Virginia: 2026

Suggested citation:
Walsh, G.J., Regan, S.P., Geer, P.S., Merschat, A.J., Suarez, K.A., McAleer, R.J., Walton, M.S., Jr., and Crider, E.A., Jr., 2026, Bedrock geologic map of the Eagle Lake quadrangle, Essex County, New York: U.S. Geological Survey Scientific Investigations Map 3542, 1 sheet, scale 1:24,000, 57-p. pamphlet, https://doi.org/10.3133/sim3542.

Associated data for this publication:
Walsh, G.J., Regan, S.P., Geer, P.S., Merschat, A.J., Suarez, K.A., McAleer, R.J., Walton, M.S., Jr., and Crider, E.A., Jr., 2026, Database for the bedrock geologic map of the Eagle Lake quadrangle, Essex County, New York: U.S. Geological Survey data release, https://doi.org/10.5066/P9D6XYEL.

ISSN 2329-132X (online)

Cover: Springtime view looking south across Eagle Lake in May 2022. Photograph by Gregory J. Walsh, U.S. Geological Survey.

Acknowledgments

We would like to thank Peter Valley, John Aleinikoff, Randall Orndorff, Chris Kopf, Tim Grover, Graham Baird, William Peck, Mike Williams, Marian Lupulescu, Anji Shah, Cliff Taylor, and Ryan Taylor for comments and discussions during field work. John Aleinikoff, Ryan Taylor, Peter Valley, and Nancy Stamm are kindly acknowledged for thorough and helpful reviews. Sean Regan would like to extend thanks to Jeff Chiarenzelli, Neil Seifert, and Paxton Rountree-Jablin for valuable field assistance. Paul and Mary-Lloyd Borroughs are acknowledged for logistical support, hospitality, and kindness; without Paul and Mary-Lloyd, the quality of mapping would be diminished. Local residents have been extremely cooperative and are acknowledged for their support. Lyme Adirondack Timberlands allowed entry to their private forest lands via annual written permits, which provided essential access to Hammondville especially. Kathleen Bonk of the New York State Museum, New York State Geological Survey, kindly answered multiple requests for access to archival manuscript maps. The U.S. Geological Survey (USGS) Pathways program provided partial funding assistance to Sean Regan and Phillip Geer. The National Science Foundation (NSF) provided partial funding assistance to Kaitlyn Suarez through the USGS/NSF Intern Opportunity. Sean Regan, Phillip Geer, and Kaitlyn Suarez conducted research as part of their graduate degrees at the University of Massachusetts at Amherst, with Mike Williams their primary advisor.

Contents

Figures

Table

Conversion Factors

International System of Units to U.S. customary units

Multiply	By	To obtain
	Length	
centimeter (cm)	0.3937	inch (in.)
meter (m)	3.281	foot (ft)
kilometer (km)	0.6214	mile (mi)
meter (m)	1.094	yard (yd)

U.S. customary units to International System of Units

Multiply	By	To obtain
	Length	
mile (mi)	1.609	kilometer (km)

Datums

Horizontal coordinate information in the text is referenced to the World Geodetic System of 1984. Horizontal coordinates in the accompanying database are referenced to the North American Datum of 1983.

Vertical coordinate information is referenced to the National Geodetic Vertical Datum of 1929.

Elevation, as used in this report, refers to distance above the vertical datum.

Abbreviations

AMCG	anorthosite-mangerite-charnockite-granite suite
$^{40}Ar/^{39}Ar$	argon-40/argon-39
BSE	back scattered electron microscopy
°C	degrees Celsius
CL	cathodoluminescence
EDS	energy dispersive spectroscopy
Fe	iron
Ga	giga-annum (billion years before present)
GIS	geographic information system
GPa	gigapascals
GPS	global positioning system
HREE	heavy rare earth element
ICP-MS	inductively coupled plasma mass spectrometry
IOA	iron oxide-apatite
IOCG	iron-oxide-copper-gold
K-Ar	potassium-argon
km	kilometer
lidar	light detection and ranging
LREE	light rare earth element
Lu-Hf	lutetium-hafnium
m	meter
Ma	mega-annum (million years before present)
mi	mile
MRDS	Mineral Resources Data System
MSWD	mean square of the weighted deviates
NE	northeast
NW	northwest
NYF	niobium-yttrium-fluorine
ppm	part per million
P-T	pressure-temperature
P-T-X	pressure-temperature-composition
Q-P-A	quartz-plagioclase-alkali feldspar
REE	rare earth element
RG	reverse geometry

SEM	scanning electron microscopy
SHRIMP	sensitive high-resolution ion microprobe
Ti	titanium
µm	micron
U-Pb	uranium-lead
µR/h	microrems per hour
USGS	U.S. Geological Survey
U-Th/He	uranium-thorium/helium
U-Th-Pb	uranium-thorium-lead
V	vanadium
WGS 84	World Geodetic System of 1984
XRF	X-ray fluorescence

Bedrock Geologic Map of the Eagle Lake Quadrangle, Essex County, New York

By Gregory J. Walsh,[1] Sean P. Regan,[1,2] Phillip S. Geer,[1,3] Arthur J. Merschat,[1] Kaitlyn A. Suarez,[3] Ryan J. McAleer,[1] Matt S. Walton Jr.,[4] and E. Allen Crider, Jr.[1]

Abstract

The bedrock geology of the 7.5-minute Eagle Lake quadrangle, Essex County, New York, consists of deformed and metamorphosed Mesoproterozoic gneisses of the Adirondack Highlands unconformably overlain by weakly deformed lower Paleozoic sedimentary rocks of the Champlain Valley. The Mesoproterozoic rocks occur on the eastern edge of the Adirondack Highlands and represent an extension of the Grenville Province of Laurentia. Granulite facies Mesoproterozoic paragneiss, marble, and amphibolite hosted the emplacement of an anorthosite-mangerite-charnockite-granite (AMCG) suite, now exposed mostly as orthogneiss, at approximately 1.18–1.15 giga-annum (Ga, billion years before present). The earliest of four phases of deformation (D1) predated AMCG magmatism and is characterized by gneissosity, rarely preserved F1 isoclinal folds, and migmatite in the paragneiss host rocks. A sample of hornblende quartz syenite from the AMCG suite, collected from an abandoned railroad cut on Old Furnace Road, yielded a U-Pb zircon age of 1,149±10 million years before present. D2 deformation produced a composite penetrative gneissosity, migmatite, and isoclinal F2 folds. Towards the end of D2, felsic magmatism (including the regionally extensive Lyon Mountain Granite Gneiss) spread by penetrative migration as semiconcordant alkali feldspar granite sheets subparallel to S2 into the previously deformed lithologies. The Lyon Mountain Granite Gneiss crystallized at approximately 1.15 to 1.14 Ga and displays synkinematic F2 folds thus constraining the time of D2 deformation. Exhumation of the Marcy anorthosite began during D3 along a mylonitic extensional detachment as a type of core complex. Protracted D3 produced F3 folds (exhibited in regional domes and basins, such as the Hammondville antiform), reactivation of the S2 foliation, partial melting, metamorphism, metasomatism, iron ore remobilization, and intrusion of magnetite-bearing pegmatite both as layer-parallel sills and crosscutting dikes. D4 created NE- and NW-trending boudinage, local high-grade ductile shear zones, and crosscutting granitic pegmatite dikes. Kilometer (km)-scale lineaments readily observed in lidar data are Ediacaran mafic dikes and Phanerozoic brittle faults. Lower Paleozoic rocks are part of the Early Cambrian to Late Ordovician great American carbonate bank on the ancient margin of Laurentia. The Potsdam Sandstone preserves the Cambrian stratigraphy in outliers above the Great Unconformity. The Paleozoic rocks are weakly folded and block faulted. Parts of the quadrangle are covered by undifferentiated glacial deposits, but much of the quadrangle contains only a variably thick, veneer of unmapped glacial till over significant areas of exposed bedrock. The map also shows waste rock piles and locations of historical mining operations.

This study was undertaken to improve our understanding of the bedrock geology in the Adirondack Highlands, establish a modern framework for 1:24,000-scale bedrock geologic mapping in the Adirondack Mountains, and provide a modern context for historical mines. This Scientific Investigations Map of the Eagle Lake 7.5-minute quadrangle consists of a map sheet, an explanatory pamphlet, and a geographic information system database that includes bedrock geologic units, faults, outcrops, and structural geologic information. The map sheet includes a bedrock geologic map, a correlation of map units, a description of map units, an explanation of map symbols, and two cross sections. The explanatory pamphlet includes a discussion of the geology.

Plain Language Summary

The U.S. Geological Survey mapped the bedrock geology of the 7.5-minute Eagle Lake quadrangle, Essex County, New York, to establish a framework for 1:24,000-scale detailed bedrock geologic mapping in the Adirondack Mountains, and provide a modern context for historical iron, graphite, and feldspar mines that operated in the 1800s. The report includes the most detailed 1:24,000-scale bedrock geologic map ever published in the Adirondack Mountains. The region is underlain by highly complex Precambrian igneous and metamorphic rocks that range in age

[1]U.S. Geological Survey.

[2]University of Alaska, Fairbanks, Alaska.

[3]University of Massachusetts, Amherst, Mass.

[4]Yale University, New Haven, Conn. (deceased).

from about 1.2 to 1.0 billion years old. The high quality of the naturally occurring mineral magnetite extracted from local iron mines led to the first use of an electric motor in Ironville, proclaimed to be the birthplace of the electric age. Abandoned iron and pegmatite mines locally contain elevated abundances of rare earth elements; some of the deposits have elevated natural radioactivity above background concentrations.

Introduction

The bedrock geology of the 7.5-minute Eagle Lake quadrangle, Essex County, New York, consists of deformed and metamorphosed Mesoproterozoic gneisses of the Adirondack Highlands unconformably overlain by weakly deformed Cambrian sedimentary rocks of the Potsdam Sandstone (refer to the bedrock geologic map and fig. 1 on map sheet). Undifferentiated, unconsolidated Quaternary glacial sediments overlie the bedrock and conceal some of the bedrock geology in the valley bottoms and on some hill slopes, but the uplands generally contain abundant exposed bedrock and a veneer of glacial till. The surficial geology was previously mapped in a preliminary way (Ogilvie, 1905), and the new map only shows undifferentiated glacial deposits in three areas. The Mesoproterozoic rocks in the map area occur in the eastern edge of the Adirondack Highlands (fig. 1). The Adirondack Highlands and Lowlands represent an extension of the Grenville Province of Laurentia (fig. 1) (McLelland and others, 2013). The Paleozoic rocks are part of the Early Cambrian to Late Ordovician great American carbonate bank on the ancient margin of Laurentia (Landing, 2012), and their deposition on the Mesoproterozoic rocks created the Great Unconformity. Areas of Holocene waste rock piles and tailings from mining are also shown on the map.

Prior to this study, the only published geologic maps for the Eagle Lake quadrangle were the 1:62,500-scale map by Ogilvie (1905) of the Paradox Lake 15-minute quadrangle and the 1:250,000-scale State geologic map of New York (Isachsen and Fisher, 1970; Rickard and others, 1970). Unpublished manuscript text and maps at 1:24,000-scale by Walton (1954, 1960, 1966) were supplied by the New York State Geological Survey and provided a foundation for our new mapping. Walton and de Waard (1963) summarized their mapping in a small-scale synthesis of the eastern Adirondack Highlands, and it was largely Walton's work in the area that provided the source for the geology depicted in this area of the Adirondack sheet of the State geologic map of New York (Isachsen and Fisher, 1970). The only published synthesis of quadrangle-scale mapping in the immediate area before this study is the work of Walton and de Waard (1963) and de Waard and Walton (1967). Their primary conclusion was a hypothesis that the paragneisses in the Adirondack Highlands represented a supracrustal sequence of rocks that postdated the orthogneisses found in the area. This hypothesis disagreed with earlier work by Newland and Kemp (1908) and the seminal Adirondack work by Balk (1931) and Buddington (1939) who all recognized that the igneous rocks intruded into a series of marble, quartzite, amphibolite, and paragneiss. Subsequent advances in Adirondack geochronology showed that the supracrustal hypothesis was incorrect, and the State geologic map of New York (Isachsen and Fisher, 1970) reestablished the relative ages of map units in the Adirondack Mountains (or simply, Adirondacks). Walton and de Waard (1963) recognized the dome and basin architecture in the eastern Adirondacks, and their distribution of major structures and map units is generally valid and useful for guiding ongoing and future geologic mapping in the area.

This study was undertaken to (1) improve our understanding of the bedrock geology in the Adirondack Highlands, (2) establish a modern framework for 1:24,000-scale geologic mapping in the Adirondacks, and (3) provide a context for historically important iron, graphite, and pegmatite mines in the region (fig. 2 on map sheet).

The geologic mapping was initiated by Regan and Geer as students in 2014 under the guidance of Gregory J. Walsh on a 1:24,000-scale topographic base prior to the acquisition of light detection and ranging (lidar) topographic data. Geer mapped on an enlarged base at 1:10,000-scale and completed his work in his thesis (Geer, 2020). Regan's preliminary findings were reported in a guidebook article (Regan and others, 2015), and topical studies were reported in journal articles (Peck and others, 2018; Regan and others, 2019a). Modern base maps included lidar-derived percent-slope maps, high resolution leaf-off satellite imagery, and recently acquired geophysical data including airborne magnetic and radiometric surveys (Shah, 2016; Shah and others, 2019, 2021). Student data capture involved the use of hand-held Garmin eTrex global positioning system (GPS) receivers and data compilation in Microsoft Excel and ArcGIS. Digital data capture during mapping by Walsh, Merschat, and Suarez was conducted with an iPad mini 4 running the Fieldmove app (v. 1.3). Location information was obtained with a bluetooth-enabled GPS receiver, either Garmin GLO or Bad Elf GPS Pro+ paired to the iPad. Field data were exported to Esri ArcGIS and final cartography was completed in Adobe Illustrator. A geographic information system (GIS) database (Walsh and others, 2026) accompanies the bedrock geologic map. Representative photographs of map units from the Eagle Lake quadrangle were taken during fieldwork and are presented as figures in this report or in appendix 1.

Lithostratigraphy

Mesoproterozoic Metasedimentary and Metavolcanic Paragneiss

Paragneiss units of the Grenville Complex (Brown, 1979, 1988, 1989; Brown and Ayuso, 1985; Walsh and others, 2022) are the oldest rocks in the quadrangle and the host rock for several generations of igneous rock. The Grenville Complex has alternatively been called the "Grenville supergroup" (Wynne-Edwards, 1972; Davidson, 1998; Chiarenzelli and others, 2015). The Grenville Complex is likely correlative with parts of the Mount Holly Complex in Vermont (Ratcliffe and others, 2011). The age range is not well constrained, but the complex is likely correlative, in part, with rocks in the Adirondack Lowlands (to the northwest), which range in age from about 1,284 to 1,258 mega-annum (Ma, million years before present) (Chiarenzelli and others, 2015). Peck and others (2019) report detrital zircon ages from about 1.45–1.25 Ga (giga-annum, billion years before present) for quartzites sampled from Laurentian rocks in the Adirondack Highlands and correlative locations in the Morrin terrane of Québec and the New Jersey Highlands. The most abundant paragneiss units in the quadrangle are the migmatitic biotite gneiss member (Ybg) and amphibolite gneiss member (Ya) of the Grenville Complex. Less abundant metasedimentary units include the rusty garnet-sillimanite gneiss (Ysi) and marble and calc-silicate gneiss members (Ym). The two units Ya and Ym are intricately interlayered in places, and they are mapped based on the most abundant rock type observed. A minor unit that is a slight variation of the migmatitic biotite gneiss member (Ybg) includes the rusty weathering biotite-bearing paragneiss (Yrbg).

Mesoproterozoic Igneous Rocks

The Adirondack Highlands are predominately underlain by granulite facies igneous lithologies (McLelland and others, 2013). In this quadrangle, the paragneiss units predate the intrusion of the oldest plutonic rock in the area, the granitic augen gneiss (Yggn), which yielded an age of 1,185±11 Ma (Regan and others, 2019a). The dated granitic augen gneiss is contiguously mapped into the adjacent Crown Point quadrangle (Walsh and others, 2022) and provides an upper age limit for the oldest paragneiss units in the region. Regionally, the most voluminous plutonic rocks belong to the anorthosite-mangerite-charnockite-granite (AMCG) suite. The paragneiss units are the host for widespread igneous rocks of the AMCG suite, which underlie most of the Adirondack Highlands (Hamilton and others, 2004; McLelland and others, 2013). The AMCG suite has an age range of about 1,160 to 1,145 Ma (McLelland and others, 2013; Aleinikoff and others, 2021). The AMCG suite (Emslie, 1978; Martin, 2012) is widespread in the Eagle Lake quadrangle (Regan and others, 2015, 2019a; this study) (fig. 3 on map sheet). The AMCG suite was also briefly referred to as the anorthosite-mangerite-charnockite-granite-alaskite (AMCA) suite (McLelland and others, 1988b). The petrogenesis of AMCG suites has been debated for decades, but detailed uranium-lead (U-Pb) geochronologic work presented in Hamilton and others (2004) and McLelland and others (2004) shows that some granitoid lithologies (~1,158 Ma) are statistically older than anorthositic and other mafic members of the suite (~1,154 Ma) but overlap in age. These data were interpreted as showing that AMCG suites are "… coeval, but not necessarily comagmatic" (McLelland and others, 2004, p. 1300). Geochemical and isotopic analysis performed by Regan and others (2011) showed that coronitic metagabbros (unit Ygb) of the Adirondack Highlands are permissible as the parental magma for the anorthosite. Quartz-bearing endmembers were interpreted to have been derived from partial melting of lower continental crust, whereas anorthosite formed via fractional crystallization of an asthenospherically derived gabbroic magma (McLelland and others, 2004; Bickford and others, 2008; Regan and others, 2011). The largest body of anorthosite is the Marcy massif, which underlies the High Peaks region of the Adirondack Mountains (Balk, 1931; Buddington, 1939) and is exposed in the northwestern part of this quadrangle. The AMCG suite of rocks has been interpreted as the result of lithospheric-mantle delamination at the waning stages of Shawinigan orogenesis (McLelland and others, 2004). In this quadrangle, the MCG phases of the AMCG suite postdate the anorthositic phases. Relative ages based on crosscutting relationships show that the anorthositic rocks (Yan and Yanw) are the oldest, followed by the mangeritic and charnockitic rocks (Ych), and finally the granitic rocks of the Lyon Mountain Granite Gneiss (Ylg).

The Marcy massif is a classic "massif-type" Proterozoic anorthosite (Ashwal and Bybee, 2017). In the Eagle Lake quadrangle, the outer (southeastern) rim of the Marcy massif consists of a mapped zone (unit Yanw) of deformed heterogeneous anorthosite, leucogabbro, variably deformed coronitic metagabbro, and lesser ferrodiorite (McLelland and others, 1994). This marginal zone, informally referred to regionally as the "Whiteface facies" or "Whiteface type" anorthosite (Kemp, 1898; Miller, 1919a), ranges in width from <50 meters (m) to >1 kilometer (km). Miller (1918, 1919a) stated that the "Marcy type" of anorthosite (Yan) is coarse-grained, massive, and rarely foliated, whereas the Whiteface type is similar in composition, generally gneissic, and contains more mafic minerals making it locally a gabbroic anorthosite. According to Miller (1918) the Whiteface type has greater percentages of mafic minerals, more garnet, and the plagioclase is whiter than the more common blue-gray color within the Marcy; the latter being the result of fewer inclusions of ilmenite. Cushing (1917) and Miller (1919a) recognized that the border of the anorthosite massif contained a gabbroic outer rim, which they interpreted as a chilled border. In a petrographic study, Crosby (1969) noted the regional use of the terms "Marcy" and "Whiteface" and applied the latter to the border facies. Locally, but not in all

places, the State map (Isachsen and Fisher, 1970) shows areas of border zones of anorthosite depicted with a cartographic overprint pattern, but the names Whiteface type and Marcy type were not applied.

Along the margin of the Marcy massif, one of the striking differences between the leucogabbro (Yanw) unit and anorthosite (Yan) is the presence of mylonitic to protomylonitic textures within the leucogabbro; this high strain zone continues into the overlying igneous rocks and the Grenville Complex. The border unit Yanw has a gneissosity that generally parallels the margin of the anorthosite massif and contains ferrodioritic or gabbroic (Ygb) screens. Several low-strain portions of the border unit (Yanw) contain evidence for magmatic mixing or mingling between the gabbro, leucogabbro, and anorthosite, but the majority of exposure of Yanw contains a granulite to amphibolite facies tectonic overprint (Regan and others, 2019a). Faults have long been recognized along the border of the Marcy massif (Cushing, 1917), but recent work has suggested that the border zone developed as an extensional detachment zone during gravitational collapse in the Ottawan phase of the Grenville orogeny (Regan and others, 2019a).

Metagabbro (Ygb) bodies are mapped in several parts of the quadrangle, especially along the border of the Marcy massif, both within the Yanw unit and within the charnockitic gneiss unit (Ych). The metagabbroic rocks occur throughout the Adirondack Mountains, most notably as satellite plutons exposed along the margin of the Marcy massif (Buddington, 1939). Regionally forming km-scale plugs, dikes, and lozenges, these bodies are locally cored by olivine metagabbro with little to no penetrative fabric, preserve ophitic to subophitic textures (Whitney and McLelland, 1983), and contain spinel clouded plagioclase laths. The metagabbro unit (Ygb) contains evidence for a high grade and static metamorphic overprint similar to the Marcy-type anorthosite (Peck and others, 2018). The metamorphic assemblage varies, but consistently contains early biotite-clinopyroxene-hornblende-garnet coronitic textures around primary olivine, spinel clouded plagioclase, and orthopyroxene (Whitney and McLelland, 1973). In the Eagle Lake quadrangle, the metagabbro intruded the Grenville Complex rocks but predated the charnockitic gneiss unit (Ych) and the leucogranite gneiss (Ylg). Vestiges of metagabbro also occur locally within the amphibolite gneiss member (Ya) of the Grenville Complex at several places where the amphibolite is a migmatitic border phase of the metagabbro, notably on the southwest flank of Mount Lewis. Ages, interpreted as igneous, from a metagabbro dike at Dresden Station, N.Y., in the eastern Adirondack Highlands include 1,144±7 Ma (McLelland and others, 1988a; McLelland and others, 2004) and 1,134±3 Ma (Walsh and others, 2016), but the metagabbro mapped in this quadrangle was not observed as dikes. Instead, the metagabbro bodies appear as intrusive plugs.

The petrologic, geochemical, and isotopic systematics of rocks belonging to the AMCG suite have been extensively studied (Hamilton and others, 2004; McLelland and others, 2004; Bickford and others, 2008). We refer to the "MC" rocks of this suite as locally orthopyroxene-bearing (Opx) hornblende granitoids (unit Ych). Frost and Frost (2008a, p. 41) define charnockite as, "an Opx-(or Fay[alite]-) bearing granitic rock that is clearly of igneous origin or that is present as an orthogneiss within a granulite terrane," and the Ych unit is generally a charnockite orthogneiss. However, although the "MC" rocks have historically been referred to as mangerites and charnockites, most occurrences do not contain orthopyroxene. It is possible that the occurrence of orthopyroxene was much more widespread but that it has been replaced by retrograde reactions that include hornblende as a product phase. Relict orthopyroxene confirming such a reaction is rare. In the Eagle Lake quadrangle, the Ych unit represents the "MC" part of the suite and ranges in composition from granite to granodiorite, monzonite, quartz monzonite, and syenite, thus it is loosely a charnockite, but not everywhere. The different granitoid rock types are, however, complexly interlayered and look similar in outcrop, and for these reasons they are shown as an undifferentiated map unit at the scale of this map. In the map area, the Ych unit postdated the Yan and Yanw units based on locally observed crosscutting relationships. In general, the Ych unit is strongly deformed throughout most of the quadrangle where it occurs in a high-strain zone structurally above the Marcy massif. Hornblende and garnet are typically metamorphic phases associated with granulite or upper amphibolite facies conditions. Given the structural and petrologic similarity, and geochronologic data confirming an approximately equivalent age, Hamilton and others (2004) and McLelland and others (2004) considered these granitoid gneisses as part of the same suite together with other charnockitic lithologies regionally. Aleinikoff and others (2021) noted that Opx granitoids are also regionally part of the Hawkeye Granite Gneiss, which yielded U-Pb zircon ages from four samples at about 1,160–1,155 Ma and overlap with the ages of other dated MCG rocks (Hamilton and others, 2004; McLelland and others, 2004). A sample of unit Ych, a hornblende quartz syenite, from an abandoned railroad cut on Old Furnace Road yielded a U-Pb zircon age of 1,149±10 Ma (2σ) interpreted to reflect the time of magma crystallization (table 1 on map sheet) (refer to U-Th-Pb Geochronology section).

The most widespread orthogneiss in the quadrangle is the Lyon Mountain Granite Gneiss (map unit Ylg), which occupies about half of the Mesoproterozoic exposure on the map (fig. 3). Although the rock was originally named the Lyon Mountain Granite by Miller (1919b, 1926) for exposures in the hamlet of Lyon Mountain, located in the town of Dannemora in Clinton County, New York, the name "Lyon Mountain Granite Gneiss" was formally adopted by Postel (1951, 1952). The rock was called the "ore formation" granite by Kemp and Alling (1925, p. 51), and all workers recognized the occurrence of historically significant iron ore magnetite deposits within it or adjacent to it. Some confusion exists in the literature regarding proper nomenclature, and the rocks within the unit have also been called the Lyon Mountain

Granitic Gneiss (McLelland and others, 2002), Lyon Mountain gneiss (Whitney and Olmsted, 1988, 1993; Foose and McLelland, 1995), Lyon Mountain Granite suite (Lupulescu and others, 2012; Chiarenzelli and others, 2017), or simply the Lyon Mountain Granite (Valley and others, 2009, 2010, 2011; Miller, 1919b, 1926). Despite the nomenclature issue, we and most workers agree that it is the youngest widespread granite exposed within the Adirondack Highlands (Buddington, 1939; Postel, 1951, 1952; Buddington and Leonard, 1962; McLelland and others, 2001, 2002; Selleck and others, 2005; Valley and others, 2009, 2010, 2011; Lupulescu and others, 2012; Chiarenzelli and others, 2017; Aleinikoff and others, 2021).

The Lyon Mountain Granite Gneiss is a ferroan A-type leucogranite (Chiarenzelli and others, 2017; Aleinikoff and others, 2021) that is locally hydrothermally altered (Valley and others, 2011). Alkali feldspar bearing phases locally show alteration to quartz-albite rock, most likely the result of fluid alteration, especially near magnetite seams (Foose and McLelland, 1995; McLelland and others, 2002; Valley and others, 2011). Previous geochronology studies concluded that the Lyon Mountain Granite Gneiss intruded at about 1,050 Ma, concluding that zircon rims represented the time of igneous crystallization and zircon cores were inherited (McLelland and others, 2001; Selleck and others, 2005; Valley and others, 2009, 2010, 2011; Chiarenzelli and others, 2017). New interpretations of the U-Pb geochronology (Aleinikoff and Walsh, 2015; Walsh and others, 2016; Aleinikoff and others, 2021) report evidence that shows the Lyon Mountain Granite Gneiss represents the "granite" part of the AMCG suite, with ages from nine samples that range from about 1,163–1,141 Ma. Aleinikoff and others (2021) show that the zircon cores are igneous and mostly not inherited, and that the rims are metamorphic with ages ranging from about 1,080–990 Ma. The Lyon Mountain Granite Gneiss may be similar to ferroan granites found in other granulite terranes, which evolved from charnockitic melts (Frost and Frost, 2008a). It is permissible that the Lyon Mountain Granite Gneiss is an end member of melts evolved from tholeiitic magmas, to anorthosite, to ferroan granites (Frost and Frost, 2008b), and thus the end of the AMCG suite (Aleinikoff and others, 2021).

Several undifferentiated rock types occur in the mapped Ylg unit including microperthite granite, microcline granite, quartz syenite, alkali feldspar granite (alaskite), syenogranite, monzogranite, and quartz-albite rock, all of which contain magnetite. Low percentage of mafic minerals, generally <5 percent, characterizes this map unit. Despite our higher resolution mapping (1:24,000 vs. 1:62,500), we agree with Postel (1951, 1952) that the different rock types cannot be mapped separately in the field, and subdivision therefore is "a microscopic rather than a megascopic task" (Postel, 1951). Since no one has of yet successfully mapped the different rock types (lithodemes) within the Lyon Mountain Granite Gneiss, there is no justification for using the suggested term "Lyon Mountain Granite suite" (Chiarenzelli and others, 2017) according to the North American Stratigraphic Code (North American Commission on Stratigraphic Nomenclature, 2021). The Lyon Mountain Granite Gneiss occurs as large sills, intrusive sheets, or slab-shaped plutons originally described as phacoliths by Buddington (1939). Layering is interpreted as mostly primary igneous layering formed as flow-banding during syn- to post-tectonic emplacement. Much of the fine layering does not appear to be due to subsolidus deformation processes as equigranular quartz and feldspar only rarely show grain size reduction and preferred grain shapes, and the rock has a general paucity of fabric-forming minerals (such as biotite and hornblende), which are only locally aligned. The granoblastic texture could also, in part, be due to recrystallization and grain boundary migration during slow cooling and uplift and is common in high grade gneiss (Passchier and others, 1990). Some aspects of the layering may be due to metamorphic differentiation that took place after emplacement, and the Lyon Mountain Granite Gneiss is clearly deformed and contains complex internal structure that is well-illustrated by foliation formline trends (fig. 3*B*). Xenoliths (fig. 4), screens, and schlieren are widespread in the Lyon Mountain Granite Gneiss. Mapped screens are especially apparent in the eastern lobe of the Hammondville pluton on Beach Hill and Knob Mountain where belts of the biotite paragneiss (Ybg) and amphibolite (Ya) members of the Grenville Complex can be traced for kilometers. The rocks near the contacts with Ylg are generally migmatites (figs. 5, 6) in zones that may be many tens or hundreds of meters wide and are locally mappable as unit Ylgt especially where in contact with the biotite paragneiss (Ybg). Local tight to isoclinal folding (F2) of the banding suggests that the rock was emplaced at a late stage of the main foliation-forming event (D2), but we cannot rule out that some of the deformation may be younger and Ottawan age (about 1.09–1.03 Ga, McLelland and others, 2013). Map patterns show that the Lyon Mountain Granite Gneiss both truncates F2 folds in some rocks, yet it is also deformed by F2 folds. This is most apparent east of Dudley Pond to an unnamed ridge east of Railroad Hill where units Ych and Ybg are tightly folded in a north-south trending F2 fold and enveloped within the Hammondville pluton (bedrock geologic map, fig. 3*A*, *B*). In the Hogan Hill pluton, layered amphibolite gneiss (Ya) in an F2 fold is truncated and enveloped by the Lyon Mountain Granite Gneiss northwest of Hogan Hill and there the Lyon Mountain Granite Gneiss flow-banding is also deformed by the D2 folding. Dome-stage F3 folds postdate emplacement of the Lyon Mountain Granite Gneiss (bedrock geologic map, fig. 5).

The youngest Mesoproterozoic igneous rocks include granite pegmatite (Yp) that occurs as small bodies of highly irregular dikes, or tabular semiconcordant to discordant sills and dikes. Small, outcrop-scale, locally mapped dikes or sills are shown on the map by strike and dip symbols. The semiconcordant bodies are foliation-parallel sills, and the crosscutting dikes occur as either irregular dikes, tabular straight-walled dikes, pegmatite-filled ductile shear bands, axial planar segregations in F3 or F4 folds, and boudin necks

Figure 4. Photograph of partly assimilated xenoliths of amphibolite, quartzite, and calc-silicate rock in white-weathered leucogranite gneiss (Ylg, Lyon Mountain Granite Gneiss) in the Hammondville pluton. The xenoliths preserve the older S2 foliation subparallel to the flow-banding and exhibit limited rotation. Faint layering in the leucogranite is interpreted as magmatic flow-banding, and in this example, is locally self-truncating along an annealed dextral shear zone. Hammer is shown for scale. Photograph by Gregory J. Walsh, U.S. Geological Survey. Location of photograph: 43.900753°, –73.586587° (WGS 84).

Figure 5. Photograph of complex migmatite zone along the contact between the Lyon Mountain Granite Gneiss (Ylg) and amphibolite gneiss member of the Grenville Complex (Ya) on the southern edge of the Hammondville pluton near Little Knob Mountain. Light-colored rock is leucogranite gneiss (Ylg) and dark-colored rock is amphibolite (Ya). The migmatitic rocks and S2 foliation are deformed by late upright F3 folds and are crosscut by late irregular pegmatite segregations. Hammer is shown for scale. Photograph by Gregory J. Walsh, U.S. Geological Survey. Location of photograph: 43.89670167°, –73.59489833° (WGS 84).

related to D3 to D4 extensional fabrics. Statistically, the measured tabular dikes show a prominent northeast-striking near vertical principal trending plane at 38°, 88° (fig. 7).

Pegmatite occurs in all the Mesoproterozoic rocks but is not mapped everywhere at the scale of the map, and masses of irregularly shaped unmapped pegmatite occur throughout the area. Most of the mapped pegmatite is relatively young and crosscuts the dominant foliation in the rock, but relatively older pegmatite is also present in the migmatitic paragneiss units as evidenced by locally preserved isoclinally folded and highly foliated pegmatite segregations. Pegmatites in the Adirondack Highlands range in age from about 1,222 to 949 Ma, but crosscutting pegmatites range from about 1,090 to 949 Ma (Lupulescu and others, 2011). Two pegmatites were dated in the Eagle Lake quadrangle. A dated pegmatite (Yp) at Spar Bed Hill (also known as Roe's Spar Bed; Lupulescu and others, 2011) yielded a U-Th-Pb zircon age of 1,030.7±9.9 Ma determined by laser ablation-multicollector-inductively coupled plasma-mass spectrometry (LA-MC-ICP-MS) (Lupulescu and others, 2011; table 1). On Spar Bed Hill, the pegmatite (Yp) cuts the Ych and Ygb units and is itself cut by a Neoproterozoic mafic dike (Rowley, 1962a, b; Tan, 1966; this study). Valley and others (2011) report ages of about 1,030 to 1,016 Ma from crosscutting granite pegmatites in the Lyon Mountain Granite Gneiss (Ylg), including a location from a roadcut on the south side of Route 74, north of Eagle Lake, near the southern border of the quadrangle. The granite pegmatite at the Route 74 location is an undeformed irregular dike that intruded a microcline phase of the Lyon Mountain Granite Gneiss and yielded a SHRIMP U-Pb zircon age 1,030.4±11 Ma (Valley and others, 2011; table 1).

Figure 6. Photographs showing rocks along an internal contact of the leucogranite gneiss (Ylg, Lyon Mountain Granite Gneiss) with an unmapped screen of migmatitic amphibolite in the Hammondville pluton near the Dog Alley mine. Outcrop photographs showing *A*, migmatitic amphibolite with large clinopyroxene-hornblende (Cpx-Hb) rafts; and *B*, banded leucogranite. Photograph *B* is located about 3 meters structurally beneath and to the west (to the left) of photograph *A*. Both photographs are looking east and the dominant foliation (in *A*) and layering (in *B*) is parallel to the hammer handle and strikes northeast at about 020° (to the left) and dips moderately at about 30°, into the picture, to the southeast. Hammer is shown for scale. Photographs by Gregory J. Walsh, U.S. Geological Survey. Location of photographs: 43.918385°, –73.601550° (WGS 84).

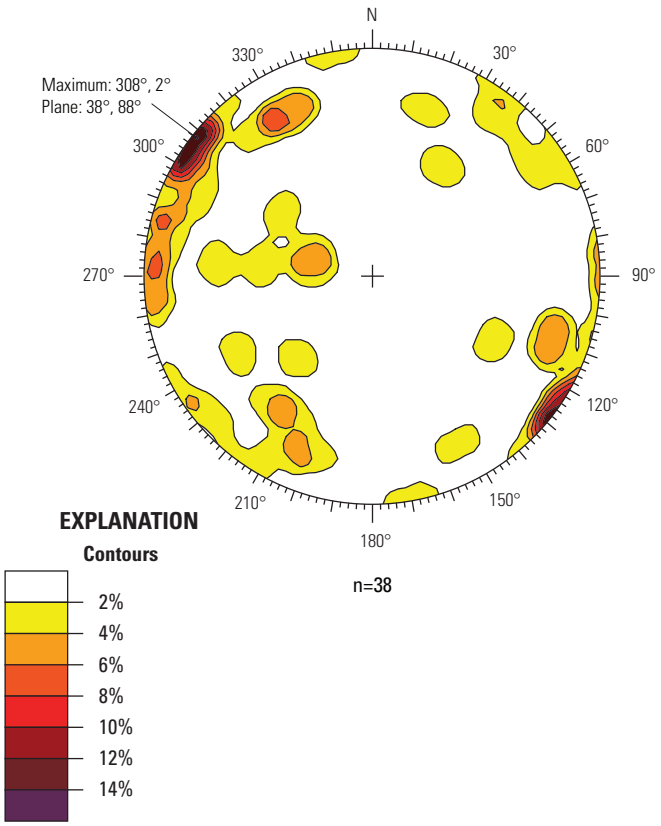

Figure 7. Stereonet showing the orientation of measured outcrop-scale pegmatite dikes (Yp) in the Eagle Lake quadrangle. The stereonet shows a lower-hemisphere equal-area projection of contoured poles to dikes. The orientation of the statistical maximum pole is indicated, with the corresponding strike and dip of the plane. The number of structural measurements in the dataset is indicated by "n." The diagram was plotted using the Structural Data Integrated System Analyser (DAISY 3, version 5.14a) software by Salvini and others (1999) and Salvini (2016).

Neoproterozoic Igneous Rocks

Northeast striking fractures and lineaments are locally prominent in areas of abundant exposed bedrock. Steeply dipping unmetamorphosed mafic diabase dikes cut the Mesoproterozoic rocks and are locally exposed within prominent fractures that principally trend northeast. Statistically, the measured dikes show a prominent northeast-striking near vertical principal trend with a statistical maximum strike and dip of 34°, 86° (fig. 8). This is the regional dike trend seen on the edge of Laurentia due to the breakup of Rodinia (Burton and Southworth, 2010). Regionally, the dikes predate deposition of the Cambrian Potsdam Sandstone and the Great Unconformity (Kemp and Marsters, 1893; Cushing, 1898; Isachsen and others, 1988), but the dikes observed in this quadrangle were not seen near or in the limited exposures of Potsdam Sandstone. The dikes are interpreted as Iapetan rift-related igneous rocks (Coish and Sinton, 1992; Burton and Southworth, 2010). Regionally, the dikes display a range of compositions and yield ages analyzed by various methods including a dike swarm in the Ottawa graben (U-Pb baddeleyite age of 590+2/–1 Ma, Kamo and others, 1995); the Callander alkaline complex intrusive body in the Ottawa graben (U-Pb zircon age of 577±1 Ma, Kamo and others, 1995); diabase dikes at Rand Hill in New York (whole-rock K-Ar ages from 588 to 542 Ma, Isachsen and others, 1988); a trachytic dike at Dannemora, N.Y. (provisional U-Pb zircon age of 643±4 Ma, Chiarenzelli and Regan, 2015), and trachytic dikes from Rand Hill and Dannemora (provisional U-Pb zircon and $^{40}Ar/^{39}Ar$ biotite ages of about 640 Ma, Valley and others, 2023).

Paleozoic Sedimentary Rocks

The Great Unconformity is a worldwide gap in the geological record between 500 million and 1 billion years long (DeLucia and others, 2017) that in most regions separates continental crystalline basement rock from much younger Cambrian shallow marine deposits (Yochelson, 2006; Peters and Gaines, 2012; Walsh and others, 2022). In the Eagle Lake quadrangle, the Great Unconformity is marked by the Potsdam Sandstone overlying Mesoproterozoic igneous and metamorphic rocks and is a gap of about 525 million years (Yp pegmatites, ~1,025 Ma, overlain by Potsdam Sandstone, ~500 Ma). The Potsdam Sandstone is not widespread in the Eagle Lake quadrangle and occurs in three small outliers in the eastern part of the map; along McMurtry Road, near Breed Hill and Sherm Ross Roads, and along Buck Mountain Road. Walton (1954, 1960) showed a very small area of Potsdam Sandstone near Chilson, but this exposure could not be confirmed during our mapping. However, an outlier of Potsdam Sandstone does occur south of the unconfirmed exposure, south of Chilson in the Graphite quadrangle (Ogilvie, 1905), and this may represent a buried extent of the Potsdam Sandstone in the valley of the Penfield Pond graben, which is largely occupied by swamp in the Eagle Lake quadrangle. Bedding in the Potsdam Sandstone is very gently dipping to subhorizontal and locally deformed in the vicinity of brittle faults.

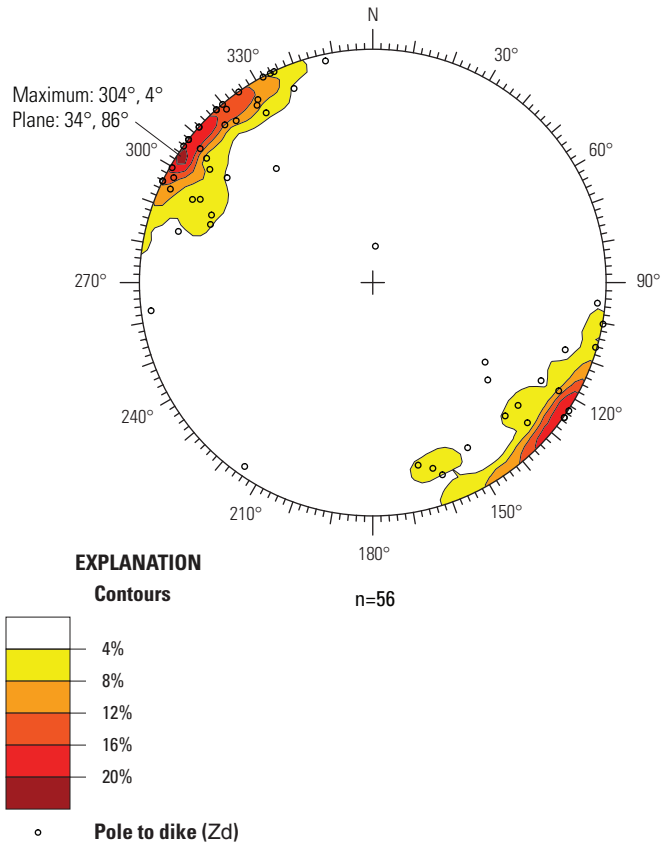

Figure 8. Stereonet showing the orientation of measured outcrop-scale diabase dikes (Zd) in the Eagle Lake quadrangle. The stereonet shows a lower-hemisphere equal-area projection of contoured poles to dikes. The orientation of the statistical maximum pole is indicated, with the corresponding strike and dip of the plane. The number of structural measurements in the dataset is indicated by "n." The diagram was plotted using the Structural Data Integrated System Analyser (DAISY 3, version 5.14a) software by Salvini and others (1999) and Salvini (2016).

Gamma Radiation Measurements

While mapping the Proterozoic rocks, a portable radiation detector documented background gamma radiation and locally elevated gamma radiation. Locally, elevated readings can be a proxy for identifying rocks with higher thorium (Th) that is associated with elevated rare earth element (REE) concentrations in mineral deposits (Meleik and others, 1978; Force and others, 1982; McCafferty and others, 2014; Shah and others, 2017, 2021; Wang and others, 2023; this study). The device (Polimaster PM1703MO-1) has two built-in detectors, a CsI (Tl) (cesium iodide thallium activated) scintillation detector and a Geiger-Muller detector. Background readings averaged about 10 microrems per hour (μR/h), with marble units showing the lowest background of about 5–10 μR/h and the Lyon Mountain Granite Gneiss showing the highest background counts of about 10–15 μR/h. Quantitative gamma-ray spectrometer data on selected units in the area confirms the semiquantitative gamma radiation readings (Shah and others, 2019, 2021). Continuous data were not collected, and the device was not used at all observed outcrops in the quadrangle because it was not available the entire time of the survey. Readings were recorded in the GIS database (Walsh and others, 2026) when the device detected more than approximately two times background, and those locations are shown on the bedrock geologic map. Most places with elevated readings occur in pegmatite or are within the Lyon Mountain Granite Gneiss (unit Ylg). A total of 21 measurements exceeded 20 μR/h, with high values in the pegmatite ranging from 25 to 101 μR/h and highs in the Lyon Mountain Granite Gneiss ranging from 22 to 36 μR/h. A single high value in the biotite paragneiss unit (Ybg, migmatitic biotite gneiss member of the Grenville Complex) measured 36 μR/h. A maximum reading of 298 μR/h was observed in the fluorapatite-magnetite ore seam at the Dog Alley mine, which has some of the highest concentrations of rare earth elements in the region (Singer and Lupulescu, 2016; Taylor and Adams, 2019; Taylor and others, 2019, and Geochemistry section). The Lyon Mountain Granite Gneiss (Ylg) in the Crown Point quadrangle contains clusters of allanite (Walsh and others, 2022). Allanite locally occurs in Adirondack pegmatites and is reported from the Spar Bed Hill pegmatite along with REE-bearing and other radiogenic mineral phases (Rowley, 1962a, b; Tan, 1966; Lupulescu and others, 2011). Monazite is common in some apatite-bearing magnetite ore seams (Regan and others, 2019b). Taylor and Adams (2019) report allanite, monazite, and thorite from metasomatically altered apatite from the Dog Alley mine and Hammond pit.

Suarez and others (2023, 2025a, b) report results on the integration of multiple techniques to characterize the alteration near REE-bearing and REE-poor deposits in Hammondville and on Skiff Mountain, using handheld gamma-ray spectroscopy, portable X-ray fluorescence (pXRF), airborne geophysics, and petrography. The gamma-ray spectrometer and pXRF proved to be successful at distinguishing the relative intensity of alteration in the granites based on potassium (K) abundance. The K-poor values occur as haloes immediately adjacent to the iron deposits, in agreement with McLelland and others (2002). Away from iron ore seams, K content increases such that the magnitude and width of the gradient is similar along strike of the deposits. Elevated U and Th values are also present in host rocks adjacent to REE-bearing deposits. The pXRF and gamma-ray spectrometer K values are remarkably consistent with laboratory-based whole-rock XRF geochemical data and, therefore, useful for semiquantitative analysis. Potassium radiation data from airborne geophysics (Shah, 2016; Shah and others, 2021) could not be correlated with ground-based K data, as the scale of heterogeneity is finer than can be resolved by the 250-m-wide flight line spacing. Mineral modes and textures associated with K and sodium (Na) metasomatism were evaluated from compositional maps of thin sections. The lowest K values detected by the handheld devices correspond

to rocks with pure albite and no K-feldspar. High-K outcrops are dominated by K-feldspar that may reflect K-metasomatism or unaltered granite. Medium K-values may suggest partial alteration.

Structural Geology

Ductile Structures

McLelland and others (2013) summarized the structural geology of the Adirondack Highlands as follows, from oldest to youngest features: rare intrafolial and isoclinal F1 folds, widespread map-scale recumbent isoclinal F2 folds related to the dominant gneissic fabric, upright east-west-trending F3 folds, and upright north-northeast trending F4 folds, the latter two produced dome and basin structures. In this model, AMCG rocks were strongly deformed and folded during the D2/F2 event. The presence of penetrative solid-state fabrics indicated that the hornblende-bearing charnockitic gneisses (regionally including the Hawkeye Granite Gneiss) were older than the Lyon Mountain Granite Gneiss, with which we agree. The Lyon Mountain Granite Gneiss was thus viewed as post-tectonic with respect to D2; all D1 and D2 fabrics are cut by pegmatite dikes dated at about 1.04–1.03 Ga.

Aleinikoff and others (2021) present an updated four-stage model for the structural evolution of the Adirondack Highlands during the Shawinigan, Ottawan, and Rigolet orogenic events. For Stage 1, at about 1,160 Ma, charnockitic gneiss of the AMCG suite was emplaced during D2 deformation. Most examples of the charnockitic gneisses show penetrative deformation, thus supporting the interpretation that they are pre- to syn-D2. Stage 1 occurred after the development of an older S1 gneissic fabric that has been attributed to an early phase of the Shawinigan orogeny at about 1,170 Ma (Wasteneys and others, 1999; Heumann and others, 2006). During Stage 1, S2 developed as a composite fabric with a preexisting gneissosity (S1) in Grenville Complex lithologies. The S2 fabric formed the axial surfaces of large isoclinal folds and affected rocks of the ~1,155 Ma AMCG plutonic suite and older rocks, producing a widespread penetrative gneissosity. During Stage 2, at about 1,160–1,140 Ma, the Lyon Mountain Granite Gneiss intruded subparallel to S2. In Stage 2, leucogranitic magmatism spread via penetrative migration, forming semiconcordant layers in previously deformed lithologies; emplacement was locally associated with migmatization of the host rocks, perhaps during biotite dehydration melting (Williams and others, 2019). The Lyon Mountain Granite Gneiss was emplaced late to post-D2, and locally displays synkinematic F2 folds. Flow banding, "ghost foliation," and schlieren formed at this time, and schollen and xenoliths of country rock (particularly restitic amphibolite) are common (figs. 4, 5). In places, the Lyon Mountain Granite Gneiss exhibits subsolidus deformational features, which are attributed to subsequent, local reactivation of S2. The older paragneisses and AMCG orthogneisses have a very strong penetrative D2 fabric that largely, but not entirely, predates Lyon Mountain Granite Gneiss emplacement. During Stage 3, at about 1,050 Ma, the AMCG suite and older rocks were deformed by D3 events under upper amphibolite to lower granulite facies conditions. A consequence of Stage 3 east-west folding (F3 of McLelland and others, 2013) was deformation of the Lyon Mountain Granite Gneiss into sheet-like bodies now exposed in domes and basins; these are the phacoliths of Buddington (1939). The S2 foliation was locally reactivated and pegmatite intruded both along the axial surfaces of F3 folds and subparallel to S2 due to partial melting. Limited biotite dehydration melting (Williams and others, 2019) and onset of extensional collapse (Selleck and others, 2005; McLelland and others, 2011; Regan and others, 2019a) occurred at this time. During Stage 4, at about 1,050–980 Ma, metasomatism, metamorphism, ore mobilization, limited migmatization, and intrusion of layer-parallel and crosscutting pegmatite accompanied D4 extension and boudinage. Local shear bands and mylonite zones developed with associated crosscutting granite pegmatite dikes in dilational zones during regional extension. Muscovite is rare or absent in these pegmatites, which were emplaced at P-T-X conditions above muscovite + quartz stability. Limited partial melting and metamorphic differentiation during D3 and D4 occurred due to decompression as the Adirondack Highlands began to unroof. During Stages 3 and 4, the gneissic rocks were annealed. Hydrothermal iron-oxide ore petrogenesis in the Lyon Mountain Granite Gneiss occurred at this time (Valley and others, 2009, 2010, 2011). In places, quartz ribbons, deformed feldspar, and mylonites occur within shear zones that are related to extension and exhumation of the Adirondack Highlands (Regan and others, 2019a); this occurred during D3-D4 and involved reactivation of D2 fabrics. The late D3 and D4 extensional structures are largely syn- to post-pegmatite emplacement; locally, mylonites postdate the pegmatites (Selleck and others, 2005; Wong and others, 2012). Stage 4 coincides with the F4 terminal extensional collapse of McLelland and others (2013).

In the Eagle Lake quadrangle, the oldest foliation is a relict gneissosity in the Mesoproterozoic Grenville Complex. The relict gneissosity (S1) is preserved only in the hinge regions of rootless folds of metasedimentary rocks (fig. 9). S1 contains layer-parallel leucosome and pegmatite segregations that are foliated and isoclinally folded implying that it developed during a relict high-temperature tectonothermal event, which may correspond to an early part of the Shawinigan orogeny (about 1.2–1.14 Ga; McLelland and others, 2013).

The S1 gneissosity is parallel to a widespread penetrative foliation that is the second-generation (S2) foliation in the Mesoproterozoic rocks (fig. 9). This S2 gneissosity is axial planar to abundant isoclinal and reclined folds in the Grenville Complex rocks (fig. 9). The S2 gneissosity is also the most conspicuous deformational fabric in the orthogneiss

units. Major map-scale F1 and F2 folds define interference patterns that reflect two periods of isoclinal folding. The Ironville basin in the center of the map forms a classic Type 2 mushroom-shaped interference pattern due to the intersection of two sets of isoclinal folds (F1 and F2) (Ramsay, 1962, 1967). The Lyon Mountain Granite Gneiss crosscuts this interference pattern yet exhibits local F2 folding (bedrock geologic map, fig. 10), supporting the interpretation that emplacement occurred late in D2. Subsequent younger upright D3 folding created additional dome and basin interference patterns. Thousands of measurements of the dominant foliation show a generally northeast-striking and moderately to gently dipping trend (fig. 11). The S2 measurements (fig. 11*A*) include the S2 foliation in all rocks older than the Lyon Mountain Granite Gneiss, plus the compositional banding in the Lyon Mountain Granite Gneiss, which is in many places, but not all, is subparallel to S2. A girdle of S2 poles defines a great circle with a β-axis trend and plunge of 116°, 31°; this is close to the mean trend and plunge (136°, 26°) of measured L2 mineral lineations and F2 fold axes (fig. 11*B*) in these high-strain, isoclinally folded gneisses. F2 folds associated with S2 are isoclinal with down-plunge fold axes that generally trend subparallel to the L2 mineral lineation (fig. 11*B*). The lineation is present in all Mesoproterozoic rocks except the late pegmatites and is only locally observed in the Lyon Mountain Granite Gneiss, partly due to the limited presence of dark mafic minerals. This trend is considered an average because the D2 fabrics were subsequently deformed. The wide scatter in poles to the S2 foliation and L2 lineation reflects the later deformation (fig. 11*A*, *B*). Williams and others (2018) report a U-Pb zircon age of 1,177±10 Ma from unit Ymig in the adjacent Ticonderoga quadrangle and Regan and others (2019a) report an U-Pb zircon age of 1,185±11 Ma from a sample of unit Yggn collected in this quadrangle; in both cases the rocks are strongly foliated by S2 implying that the D2 deformation is younger than about 1,177 Ma making it Shawinigan or younger. Largely undeformed fayalite granite of the Lyon Mountain Granite Gneiss in the northern Adirondack Highlands, yield U-Pb zircon ages of 1,143±6 Ma and 1,141±8 Ma interpreted to provide a minimum age constraint on D2 (Aleinikoff and others, 2021). Monazite geochronology supports the interpretation that D2 was reactivated in the Ottawan orogenic event between about 1,070 to 1,060 Ma at granulite facies conditions (Regan and others, 2019a).

Both S1 and S2 are deformed by a minimum of two younger ductile fabrics (S3 and S4). The third generation of planar fabrics include upright, open to tight folds (F3) that are very rarely expressed by an axial planar cleavage in the gneissic rocks (fig. 5). The F3 axial surfaces have many different orientations, although they most commonly strike northeast and dip steeply (fig. 12*A*). The F3 map-scale folds are broad features related to dome and basin formation and are most conspicuous in the Hammondville anticlinorium, the Towner Hill Road antiform, the Penfield Pond synform, the Skiff Mountain antiform, and the Moose Mountain synform. Axial surfaces of F3 folds locally contain thin pegmatite segregations that crosscut S2. Regional pegmatite ages between about 1,090 to 949 Ma (Lupulescu and others, 2011) and local pegmatite ages in this quadrangle (about 1,030 Ma; table 1) indicate that D3 deformation is likely Ottawan in age.

The youngest ductile deformation (D4) in the area occurs as parallel sets of low-amplitude, long-wavelength open folds, boudinage, and related shear bands. The dilatant extensional D4 structures are filled with pegmatite (fig. 12*D*). The boudinage shows variable orientations but includes dominant, conjugate trends that strike north-northeast and west-northwest and dip subvertically (fig. 12*C*). The F3 and F4 folds have somewhat similar orientations and geometry, and it was not always possible to differentiate between F3 and F4 in the field in this quadrangle. Outcrop scale open F4 folds form conjugate northwest and more common north-northeast crossfolds, shear bands, and boudinage (fig. 12*B*, *C*, *D*). Both F3 and F4 folds have muscovite-free pegmatite in their axial surfaces, indicating that they formed at high-grade during similar conditions. Steeply dipping, northwest and northeast striking shear bands and shear zones (fig. 12*B*, *C*) locally exhibit quartz ribbons and recrystallized feldspar, similar to features observed along the Moose Mountain detachment.

The Moose Mountain Detachment

Recent work identified southeast-directed granulite to amphibolite facies extensional shear zones in the Adirondack Highlands (Regan and others, 2019a). One of these shear zones, the "Marcy massif detachment zone," was first recognized in the Eagle Lake quadrangle by new 1:24,000-scale mapping. Regional reconnaissance was used to support the interpretation that this shear zone may wrap around the entire Marcy massif (Regan and others, 2019a). Subsequent mapping in this quadrangle has demonstrated that the shear zone contains an anastomosing series of faults herein named the "Moose Mountain detachment" for exposures on the north and west side of the named mountain. The mapped detachment faults are generally planar and dip moderately at about 20–30° to the east-southeast and occur in a shear zone of varying width, up to about 1–2 km wide, and few hundred meters thick. The mean lineation trend along the detachment is 147°, 22° (fig. 11*D*), which differs from the overall mean lineation trend of L2 lineations and F2 fold axes 124°, 29° (fig. 11*C*). The Lyon Mountain Granite Gneiss (unit Ylg) occurs in the upper plate of the detachment and is not found within the shear zone in this quadrangle, as reported by Regan and others (2019a). Brittle faults truncate the detachment in multiple places. High strain in the shear zone is evident in both orthogneiss and paragneiss units. Coarse-grained leucogabbroic and anorthositic rocks show clear grain-size reduction and rotated porphyroclasts. Within the mapped detachment, mylonitic textures transpose older fabrics, and quartz-bearing rocks exhibit quartz ribbons (fig. 13). Rotated porphyroclasts and C′-type shear bands (fig. 13*C*) show top-down to the southeast kinematics, consistent with the

Figure 9. Photograph of the migmatitic biotite gneiss member (Ybg) of the Grenville Complex southwest of Cedar Bridge Pond and south of Old Furnace Road. Photograph shows rarely preserved isoclinally folded S1 foliation in rootless F2 folds of older leucosome. The dominant foliation S2 is parallel to the axial surfaces of the F2 folds. A late crosscutting pegmatite dike occurs in a D4 shear band showing dextral offset (center) as well is in an irregular dike without apparent offset (lower right). Photograph by Gregory J. Walsh, U.S. Geological Survey. Location of photograph: 43.92575167, –73.58275 (WGS 84).

interpretations presented by Regan and others (2019a). On Moose Mountain, the detachment occurs at the base of the charnockitic gneiss (unit Ych) where it is in contact with rocks of the Marcy massif. Splays of the detachment branch out around the west side of Moose Mountain and extend into the adjacent Paradox Lake quadrangle. The detachment also contains two splays in the northwestern part of the quadrangle, which wrap around leucogabbroic gneiss (unit Yanw) on Blue Hill. Highly strained and locally mylonitic rocks within the detachment also show "block structure"[5], illustrating a complex history involving both early igneous and subsequent tectonic processes (fig. 13). The relative ages observed in this quadrangle demonstrate the following sequence of events:

- Anorthosite crystallized.
- Blocks of anorthosite were incorporated into leucogabbro and subsequently deformed.
- Charnockitic rocks intruded the deformed anorthosite and leucogabbro.
- These rocks were all deformed by penetrative granulite to amphibolite facies deformation.
- Deformation associated with the Moose Mountain detachment formed subparallel to, and locally, truncated earlier fabrics. The detachment postdated

[5]"Block structure" was defined in the Marcy massif by Balk (1931) and recognized by Buddington (1939). Ashwal (1983) and Ashwal and Bybee (2017) report this structure from other anorthosite massifs world-wide. McLelland and others (2016) use the terms "intrusion breccia" for this feature.

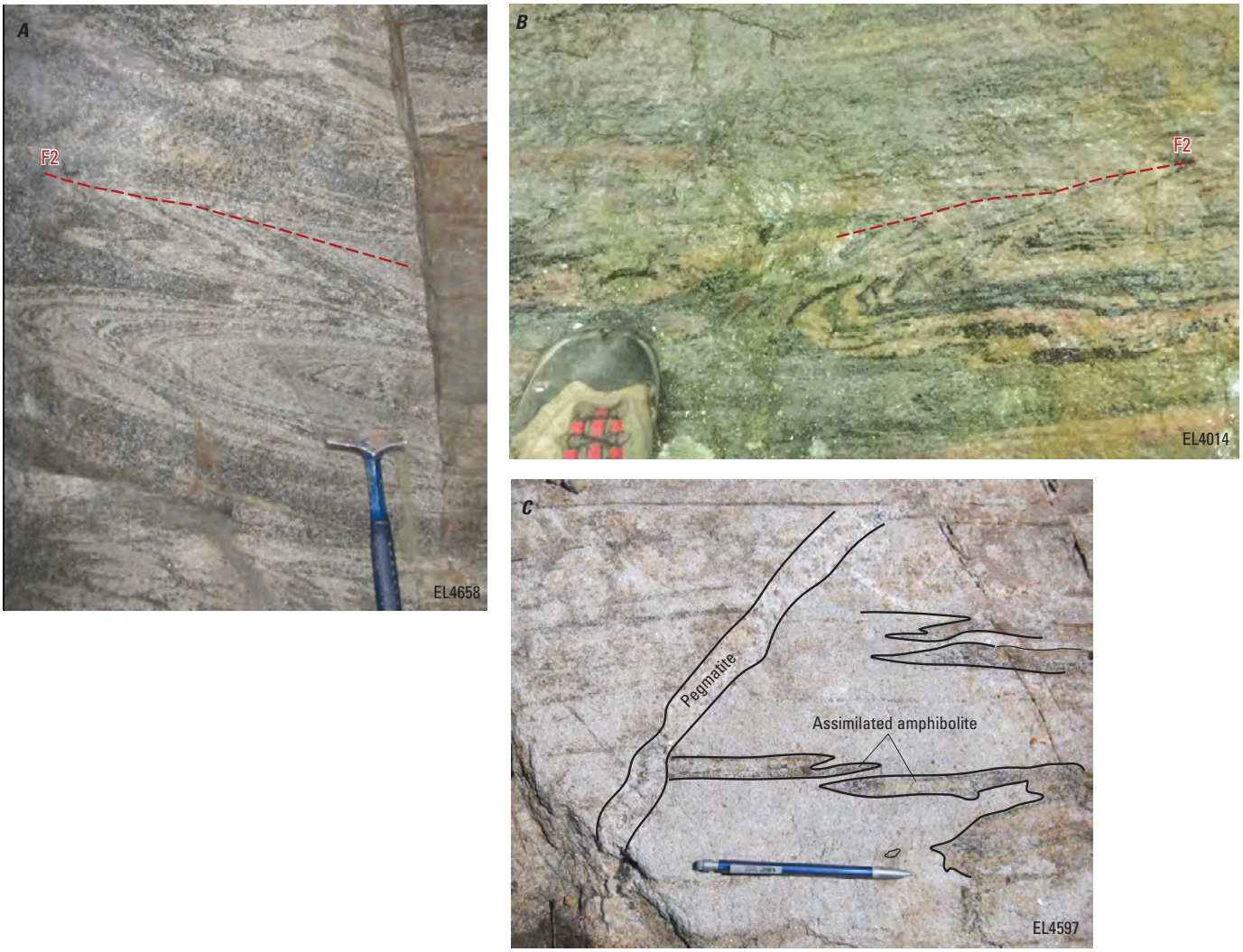

Figure 10. Photographs of the Lyon Mountain Granite Gneiss (Ylg) showing isoclinal F2 folds. Such folds are rarely observed in the Ylg unit, due to the timing of granite emplacement and the generally low percentage of dark minerals such as magnetite, clinopyroxene, and amphibole. Photographs *A* and *B* show examples where the rock is a well-layered migmatite that contains lean ore with dark bands of magnetite and mafic minerals. Photograph *C* shows an example where folded amphibolite screens are partly assimilated and crosscut by a pegmatite dike. Photograph *A* is from the North Pit in the Hammondville district; location: 43.91604, –73.616608 (WGS 84). Photograph *B* is from the No. 5 mine in the Hammondville district; location: 43.911042, –73.616608 (WGS 84). Photograph *C* is from the east slope of Little Knob Mountain; location: 43.900786, –73.584673 (WGS 84). Associated station numbers are shown in each photograph (for example, EL4658 in *A*). Hammer, boot, and pen are shown for scale. Photographs *A* and *C* by Phillip S. Geer, U.S. Geological Survey and University of Massachusetts. Photograph *B* by Gregory J. Walsh, U.S. Geological Survey.

the regionally extensive deformation, evidenced by tectonic clasts of anorthositic rocks with a relict foliation and a new lineation trend. Grain-size reduction and quartz ribbons formed in the detachment.

- The Moose Mountain detachment was gently warped by dome stage folds.
- Post-tectonic garnet porphyroblasts overprinted quartz ribbons in the detachment.

Regan and others (2019a) concluded that the deformation within these extensional shear zones occurred at about 1,070–1,060 Ma based on U-Pb-Th monazite geochronology from samples collected in the vicinity of the shear zone, but not within the detachment proper. This interpretation may be regionally valid, but future work remains to determine the precise age of the textures within structures like the Moose Mountain detachment. Regionally, post-tectonic garnet has yielded remarkably consistent ages of about 1,022 Ma from skarn near Willsboro (U-Pb age of 1,022 9±16 Ma, Seman and others, 2017) and from Adirondack Highlands anorthosite (lutetium-hafnium [Lu-Hf] ages of 1,022.3±2.9

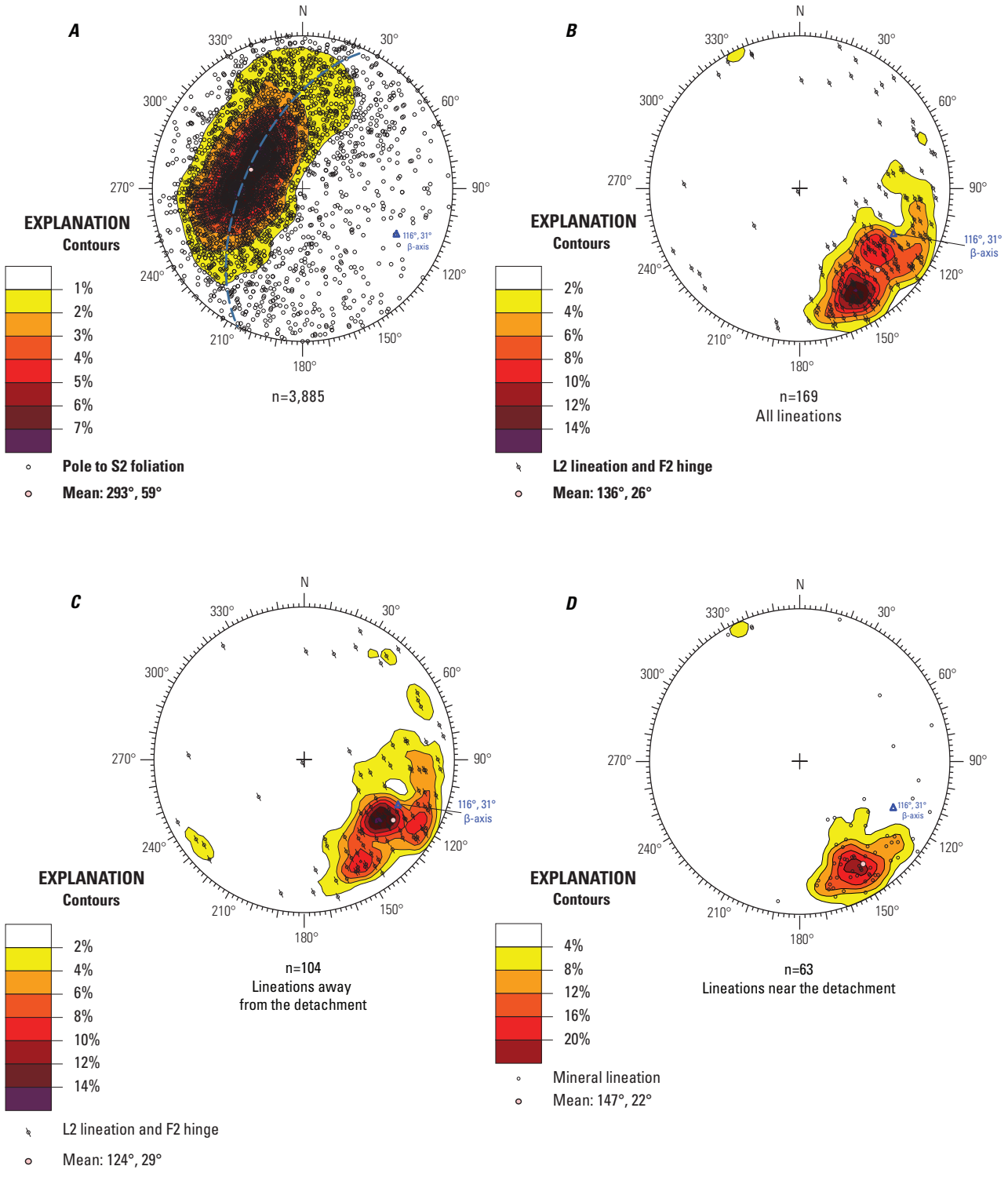

Figure 11. Stereonets showing synoptic diagrams with the orientation of the D2 structures in the Eagle Lake quadrangle. The stereonets show lower-hemisphere equal area projections of *A*, contoured poles to S2 foliation; and *B*, *C*, *D*, contoured L2 mineral lineations and F2 fold axes. Diagram *A* shows the best-fit great circle to the poles and the corresponding β-axis (116°, 31°). Diagram *B* shows all lineations and fold axes with a mean trend and plunge of 136°, 26° (see "Mean"). Diagram *C* shows a subset of the lineations measured away from the Moose Mountain detachment (>1.5 kilometers [km]), and diagram *D* shows a subset of the lineations measured near the detachment, within approximately 1.5 km. The number of structural measurements in the dataset is indicated by "n" at the bottom of each diagram. Stereonets were plotted using the Structural Data Integrated System Analyser (DAISY 3, version 5.14a) software by Salvini and others (1999) and Salvini (2016).

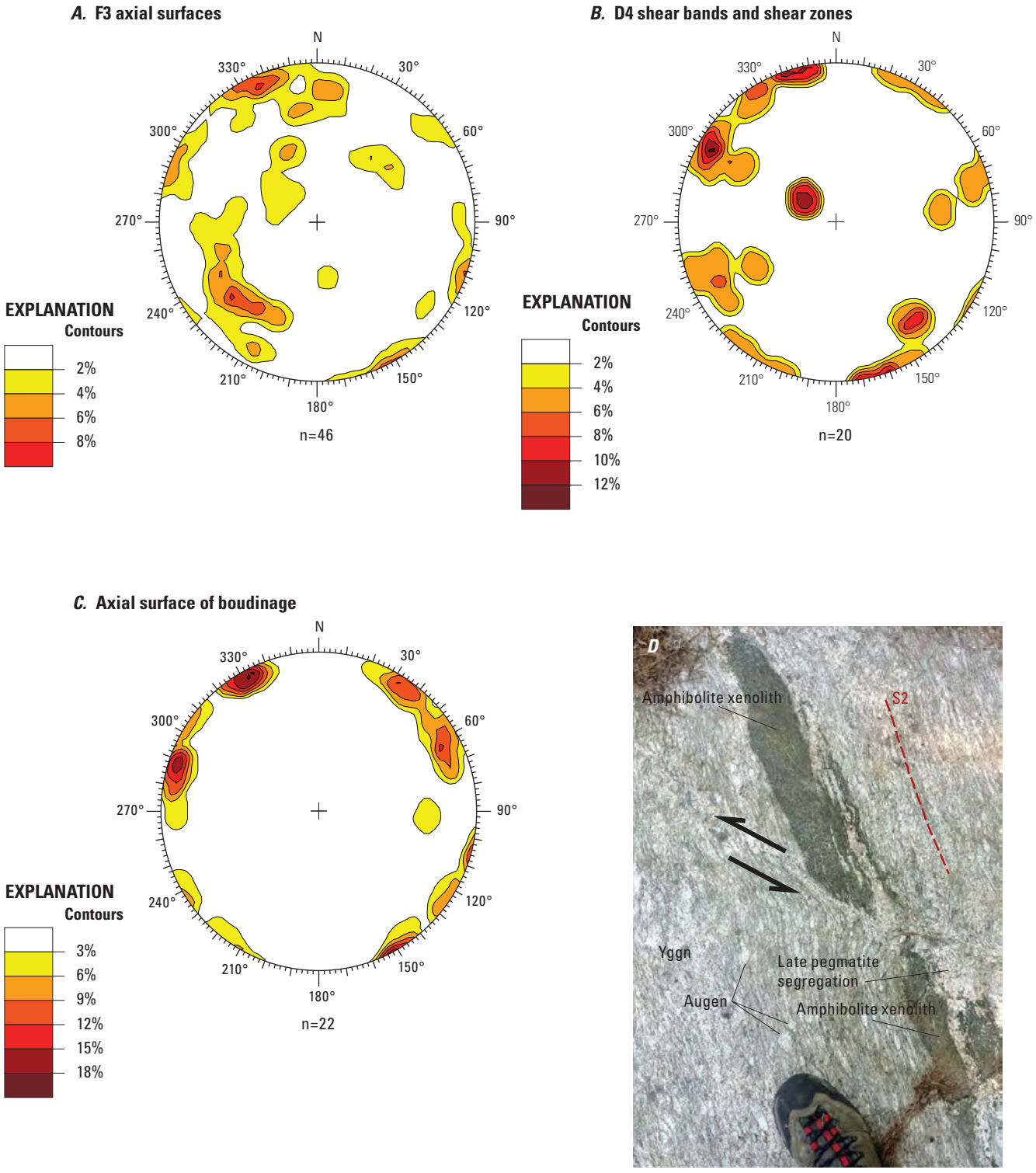

Figure 12. Stereonets and photograph of D3 and D4 structures in the Eagle Lake quadrangle. Synoptic diagrams show the orientation of measured outcrop-scale features. The stereonets show lower-hemisphere equal area projections of *A*, contoured poles to F3 axial surfaces; *B*, contoured poles to D4 shear bands and shear zones; and *C*, contoured poles to the axial surface of boudinage. The number of structural measurements in the dataset is indicated by "n" at the bottom of each diagram. Stereonets were plotted using the Structural Data Integrated System Analyser (DAISY 3, version 5.14a) software by Salvini and others (1999) and Salvini (2016). Photograph *D* shows a D4 sinistral shear zone that offsets the S2 foliation and an amphibolite xenolith in the granitic augen gneiss (Yggn); the dilatant shear zone is locally filled with pegmatite. Arrows show direction of shearing. Boot is shown for scale. Photograph by Gregory J. Walsh, U.S. Geological Survey. Location of photograph: 43.90587333, –73.531345 (WGS 84).

and 1,021.9±2.7 Ma) (Aleinikoff and others, 2018). Thus, it is interpreted that the Moose Mountain detachment is an Ottawan-age extensional structure that developed between about 1,070 and 1,020 Ma.

Brittle Structures

Joints

Summary diagrams show the structural orientations of over 1,000 measured outcrop-scale joints and joint sets across the map area (fig. 14). Most measured joints are steeply dipping and northeast-striking (fig. 14*A*, *B*). Fewer than 10 percent of measured joints have a dip less than 60°. The strike and dip of outcrop-scale joints are not plotted on the bedrock geologic map but are included in the GIS database (Walsh and others, 2026). The principal trend of steeply dipping joints is 55°±29° with subordinate trends to the northwest (fig. 14*B*). Many of the joints are subparallel to brittle faults or Neoproterozoic dikes.

Faults

Brittle faults are characterized by breccia, hematite-calcite-quartz veins, and locally observed pseudotachylyte (fig. 15). Maroon-colored hematite-bearing breccia zones, usually in the vicinity of steep-sided canyons or cliff faces, are the most commonly observed indicators of brittle faults. Slickensides on surfaces are only locally preserved. Some Neoproterozoic dikes show evidence for brittle faulting, which occurred either during emplacement or during subsequent reactivation. Many of the brittle faults show normal relative offset with east-side-down displacement. The principal trends of measured brittle faults are steeply dipping northeast and north-south striking (fig. 15). The same trends are seen in the mapped brittle faults. The strike and dip of outcrop-scale faults are not plotted on the bedrock geologic map but are included in the GIS database (Walsh and others, 2026). Faults were mapped by the surface expression of lineaments on the lidar percent-slope map (fig. 3*B*), observed brittle structures, and by observed minor offset of geologic units. It is likely that many more linear features seen in the modern lidar data, but not mapped in detail, may represent brittle faults with very minor offsets or zones of abundant joints with minimal to no offset. Apatite fission track and apatite U-Th/He data from the Adirondacks record Middle Jurassic through the Late Cretaceous ages (about 170 to 70 Ma; Roden-Tice and others, 2000; Roden-Tice and Tice, 2005) indicating about 3–5 km of exhumation since that time. Thermal modelling based on these data and U-Pb calcite ages indicate that the passive margin may have experienced renewed tectonic activity at about 105, 85 to 65, and 20 Ma and these times may correlate with episodes of renewed brittle fracturing and faulting (Roden-Tice and others, 2000; Roden-Tice and Tice, 2005; Amidon and others, 2016; Robbins and Amidon, 2018). For example, recent work shows that calcite veins in the Champlain Valley yield U-Pb ages that document fracturing from about 115 to 75 Ma followed by renewed fracturing in the Miocene to Plicoene with ages from about 50 to 3 Ma (Amidon and others, 2022), suggesting that brittle tectonics were active from the Late Jurassic to the Neogene. The entire Adirondack dome may be experiencing anomalously high uplift (Isachsen, 1981).

Veins

Tabular crosscutting veins were mapped in the Mesoproterozoic rocks and are shown on the bedrock geologic map with strike and dip symbols. Not all veins are shown on the geologic map for cartographic reasons, but all measurements (n=21) are included in the GIS database (Walsh and others, 2026) and shown in figure 16. The veins contain quartz, hematite, magnetite, ilmenite, amphibole, and locally small amounts of epidote, calcite, and garnet. Maroon-weathering veins consist of hematite and fractured country rock; they are relatively young and related to brittle deformation (fig. 16*B*). Locally, quartz veins occur in the Lyon Mountain Granite Gneiss as tabular sills, parallel to the layering, or as crosscutting veins, and these veins are locally deformed and likely old and related to pegmatite and iron-ore seam emplacement. Similarly, garnet-bearing magnetite-ilmenite veins are relatively old and may be related to the same high-temperature metamorphic or metasomatic event. Epidote veins locally show marginal bleached zones due to hydrothermal alteration during greenschist facies retrogression and are related to saussurite alteration of plagioclase seen in thin section. The veins show a variety of steeply dipping orientations from limited data (fig. 16*C*).

Figure 13. Photographs illustrating shear zone structures in and near the Moose Mountain detachment. Photograph *A* shows rarely preserved examples of block structure from a loose boulder at an outcrop consisting of anorthosite (Yan) in leuocogabbro gneiss (Yanw), cut by charnockitic gneiss (Ych). The large anorthosite block in the center has variable amounts of mafic minerals ranging from about 1 to 5 percent (Yan 1% and Yan 5%) and an internal contact that is tectonically truncated against Ych and Yanw. Smaller blocks of strained anorthosite occur near the bottom in Yanw. A finer-grained version of Yanw occurs near the top and contains plagioclase megacrysts. The charnockitic gneiss intruded the anorthositic rocks and contains a well-developed tectonic foliation (red line). Hammer for scale is 30 centimeters (cm) long. Photograph *B* shows highly strained Ych showing a younger tectonic foliation (red lines) that postdated and truncated an older tectonic fabric in xenoliths of leucogabbroic gneiss (Yanw). Pen for scale is 14 cm long. Photograph *C* of mylonitic texture in a thin section of magnetite-garnet-biotite-K-feldspar-quartz-plagioclase straight gneiss in the migmatitic biotite gneiss member of the Grenville Complex (unit Ybg). The rock shows well-developed mylonitic quartz ribbons and C′-type shear bands (thin black line) that indicate top to the left (down to the east-northeast) kinematics; the view is looking south-southeast. Post-tectonic garnet porphyroblasts postdate the mylonite and overgrew the quartz ribbons. The thin section contains trace amounts of zircon, apatite, and chlorite (not visible). Most of the left side of the thin section is stained for plagioclase (light pink) and K feldspar (deep yellow). Arrows in photograph *C* show direction of shearing. The slide measures 25 x 45 millimeters. Photographs by Gregory J. Walsh, U.S. Geological Survey. Locations of photographs: *A*, west of Trout Pond, 43.986108, –73.573311 (WGS 84); *B*, east side of Pigeon Hill, 43.956466, –73.583025 (WGS 84); *C*, north of Goosepuddle Pond, 44.00141, –73.546974 (WGS 84). Grt, garnet; Kfs, K-feldspar; Pl, plagioclase; Qz, quartz; %, percent.

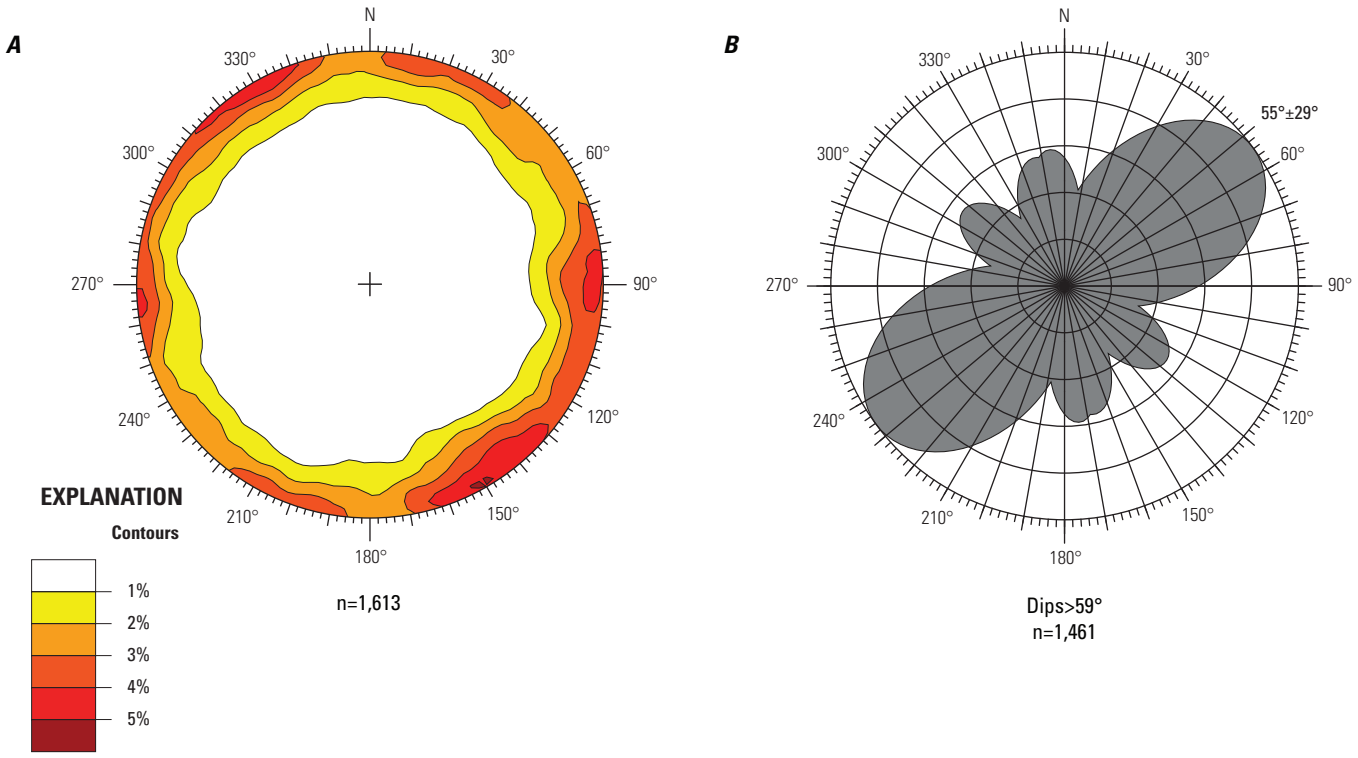

Figure 14. Stereonet and rose diagram showing the orientations of measured joints. *A*, Stereonet showing a lower-hemisphere equal area projection of poles and contoured poles to joints. *B*, Rose diagram showing a normalized subset of the data for dips >59°, and the statistical peak trend is shown with 1 standard deviation error (for example, 55°±29°). The number of structural measurements in each dataset is indicated by "n" at the bottom of each diagram. Stereonet and rose diagram were plotted using the Structural Data Integrated System Analyser (DAISY 3, version 5.14a) software by Salvini and others (1999) and Salvini (2016).

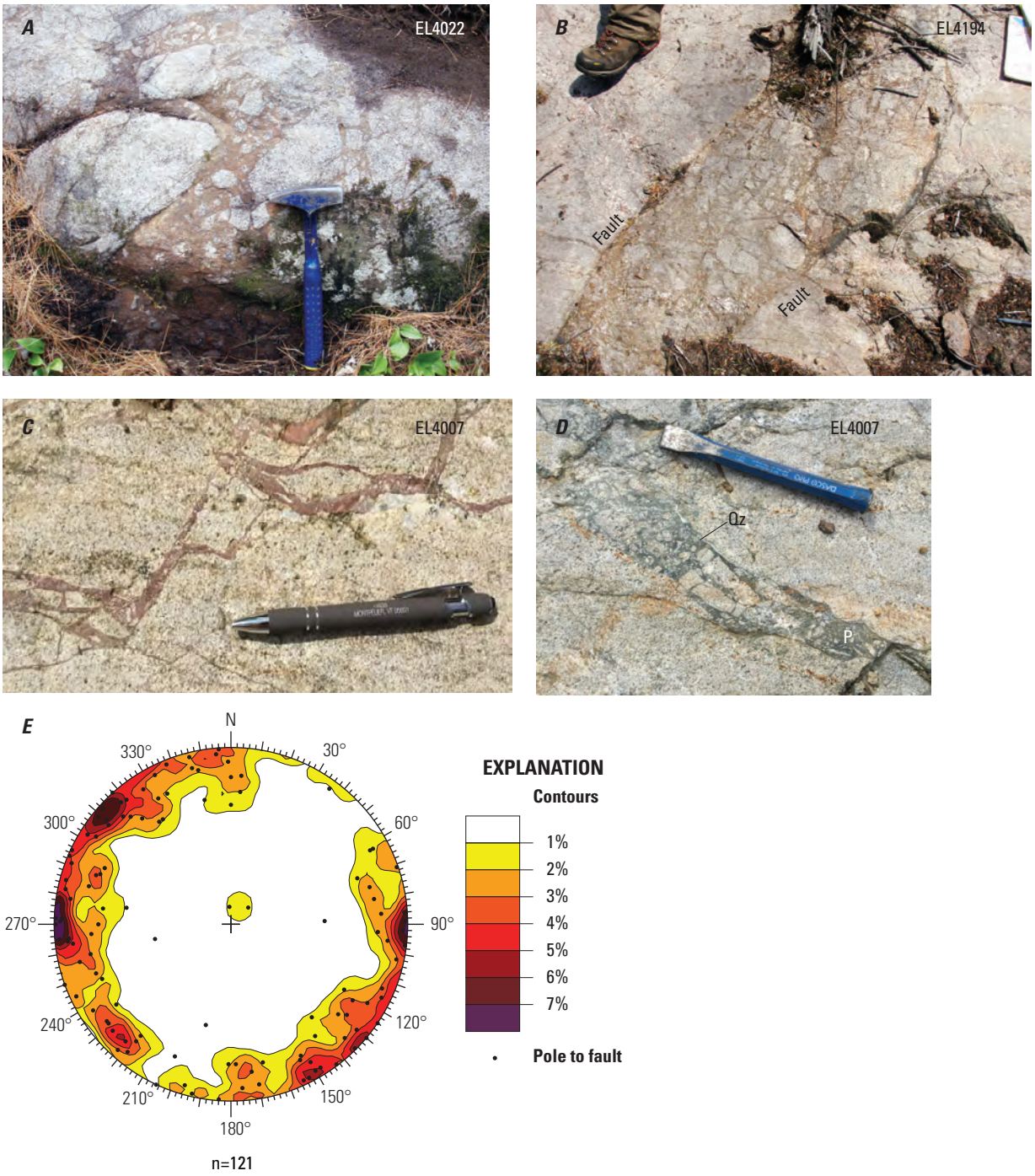

Figure 15. Photographs and stereonet of brittle faults in the Eagle Lake quadrangle. Photographs *A*–*D* show outcrop-scale fault breccia in the Lyon Mountain Granite Gneiss. Photographs *A*, *B*, and *C* show maroon-colored hematite veins and breccia; hammer, boot, and pen are shown for scale, respectively. Photograph *D* shows dark-gray pseudotachylyte (P), quartz veins (Qz), and breccia; chisel is shown for scale. Associated station numbers are shown in each photograph (for example, EL4022 in *A*). Photograph *A* by Phillip S. Geer, U.S. Geological Survey and University of Massachusetts; location: 43.916991, –73.608751 (WGS 84). Photograph *B* by Phillip S. Geer, U.S. Geological Survey and University of Massachusetts; location: 43.909977, –73.57078 (WGS 84). Photographs *C* and *D* by Gregory J. Walsh, U.S. Geological Survey; location: 43.921128, –73.602158 (WGS 84). Diagram *E* is a stereonet showing the orientations of measured brittle faults. The stereonet shows a lower-hemisphere equal area projection of contoured poles to faults. The number of structural measurements in the dataset is indicated by "n" at the bottom of the diagram. Stereonet was plotted using the Structural Data Integrated System Analyser (DAISY 3, version 5.14a) software by Salvini and others (1999) and Salvini (2016).

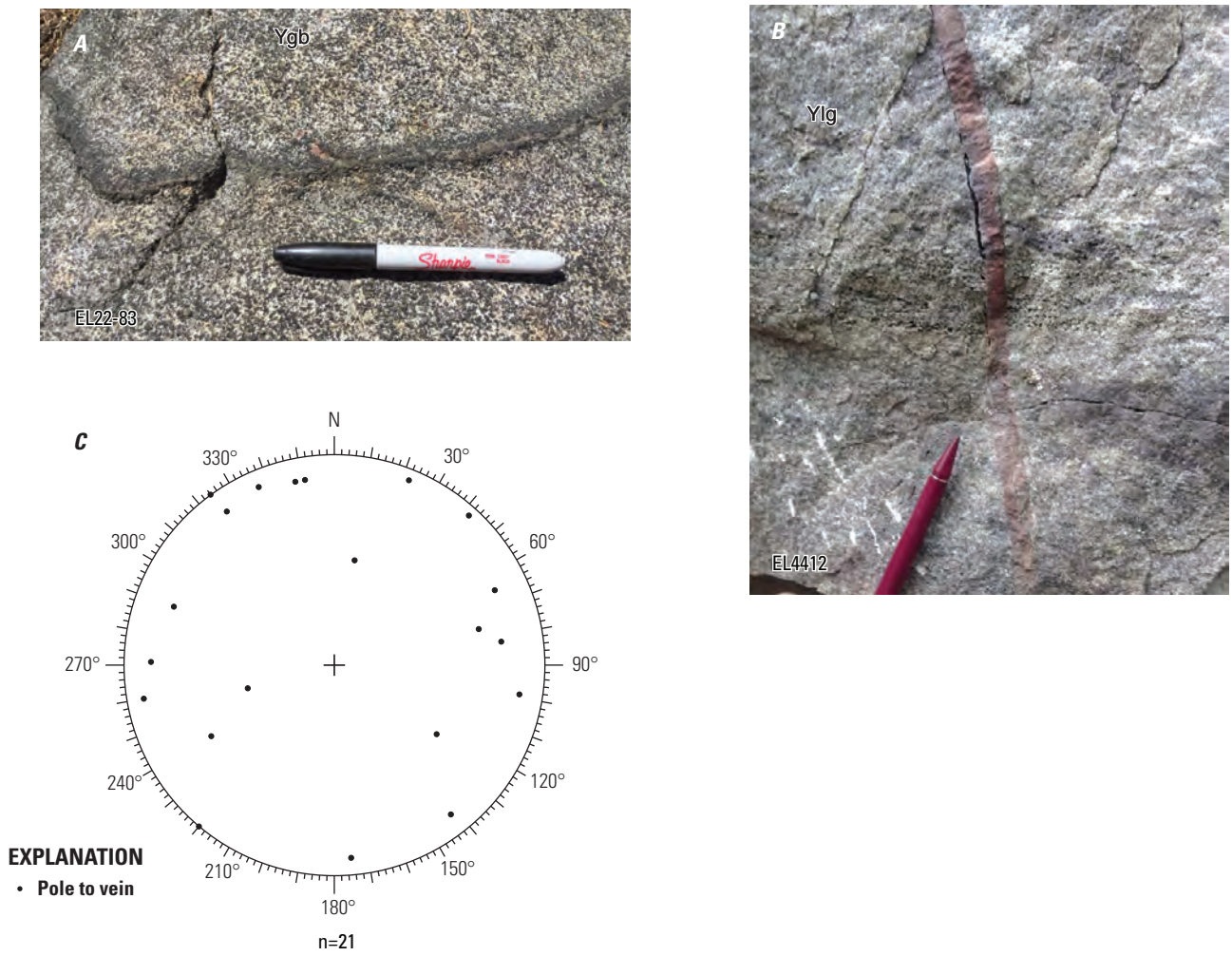

Figure 16. Photographs and stereonet of veins in the Eagle Lake quadrangle. Photograph *A* shows a garnet-magnetite-ilmenite vein in a metagabbro (Ygb) on Skiff Mountain; location: 43.884792, –73.602858 (WGS 84). Marker is shown for scale. Photograph *B* shows a hematite vein in the Lyon Mountain Granite Gneiss; location: 43.908783, –73.613488 (WGS 84). Pencil is shown for scale. Associated station numbers are shown in *A* and *B* (EL22-83 and EL4412, respectively). Photographs by Gregory J. Walsh, U.S. Geological Survey. Diagram *C* is a stereonet showing a lower-hemisphere equal area projection of poles to veins. The number of structural measurements in the dataset is indicated by "n" at the bottom of the diagram. Stereonet was plotted using the Structural Data Integrated System Analyser (DAISY 3, version 5.14a) software by Salvini and others (1999) and Salvini (2016).

Tectonics and Metamorphism

Tectonic and metamorphic events in the Adirondack Highlands of the Grenville Province are associated with three major events called the Elzevirian (about 1.25–1.22 Ga), Shawinigan (about 1.2–1.14 Ga), and Ottawan (about 1.09–1.03 Ga) orogenies (McLelland and others, 2013). The last, or fourth, event has been called the Rigolet phase (about 1.01–0.98 Ga) of the Grenville orogeny (Rivers, 2012; McLelland and others, 2013). Plutonic calc-alkaline arc-related rocks related to the Elzevirian orogeny occur in the southern Adirondack Highlands and the Mount Holly Complex in the Green Mountains (Ratcliffe and others, 1991, 2011; Aleinikoff and others, 2011; McLelland and others, 2013) but they do not occur in the Eagle Lake quadrangle.

The multiple high-grade metamorphic events and polyphase ductile deformation have challenged researchers working on the Grenville Province for well over a century (Rivers, 2015). In the Adirondack Highlands, Walton and de Waard (1963, p. 98) noted that "metamorphism in the hornblende or pyroxene granulite facies strongly modified all preexisting rock relationships and totally recrystallized most of the rocks." They suggested that much of the geologic history of the Adirondack Mountains was, "hidden behind a screen of diastrophism." Research in the last 60 years, however, has helped to more fully understand the geologic history of the Adirondacks.

The Adirondack Highlands experienced peak metamorphism at granulite facies followed by upper amphibolite facies conditions. Bohlen and others (1985)

documented approximately 0.6–0.8 gigapascals (GPa) at about 750–850 °C in the Adirondack Highlands. Spear and Markussen (1997) presented pressure-temperature (P-T) data from anorthosite from the northern part of the Marcy massif. A P-T path for these rocks was calculated as having initiated at ~0.8 GPa and 800 °C and cooling to ~700 °C and 0.65 GPa. Petrologic analysis by Storm and Spear (2005) showed that peak metamorphic conditions attained within the southern Adirondack Highlands were 0.8–0.9 GPa and 790 °C, followed by a two-phase cooling history defined by slow then rapid cooling. The number of high-grade metamorphic events has been a challenge to unravel. Peak granulite facies conditions have been interpreted as the result of the Ottawan orogeny from about 1,090 to 1,030 Ma with earlier high-grade metamorphism the result of the Shawinigan orogeny (McLelland and others, 2013). To better constrain the timing of metamorphism, Peck and others (2018) analyzed zircon in situ by laser ablation-inductively coupled plasma-mass spectrometry from a metagabbroic rock (unit Ygb) on the north side of Moose Mountain to determine the age of garnet corona growth formed during cooling from peak metamorphic conditions around the southern edge of the Marcy massif. Metamorphic zircon ages range from 1,060 to 1,035 Ma, suggesting that peak metamorphic conditions recorded in the margin of the Marcy massif occurred during the Ottawan phase of the Grenville orogeny. In contrast, zircon rims from quartzite in the southern Adirondack Highlands, in the same region where thermobarometry data were acquired by Storm and Spear (2005), yielded Shawinigan ages ranging from 1,170 to 1,130 Ma (Peck and others, 2010). Williams and others (2019) show that the rocks in the eastern part of the Adirondacks Highlands experienced at least two periods of melting, related to biotite dehydration, with the first major event at about 1,160 to 1,150 Ma (Shawinigan orogeny) and a second high-temperature event with less melting at about 1,050 Ma (Ottawan orogeny). These results indicate that although peak metamorphic conditions adjacent to the Marcy massif and the southern Adirondack Highlands are similar, two separate periods of high-grade metamorphism may be recorded in different parts of the Highlands. This polyphase metamorphism is also documented in Adirondack Highlands anorthosite and rocks along the margin of the Marcy massif from samples collected in or adjacent to this quadrangle (refer to table 1 on map sheet; Peck and others, 2018; Regan and others, 2019a). Dated pegmatites in the area postdate the peak of metamorphism and the dominant foliation and yield ages at about 1,030 Ma (table 1) and are interpreted as representing granitic melts produced at the end of the Ottawan orogeny (Lupulescu and others, 2011; Valley and others, 2011). Metamorphism and fluid alteration took place from the Ottawan orogeny to the Rigolet phase of the Grenville orogeny, and the ages of mineral growth are documented by zircon, garnet, monazite, titanite, and apatite dated from about 1,050 to 980 Ma (McLelland and others, 2001, 2002; Valley and others, 2009, 2010, 2011; Aleinikoff and Walsh, 2015, 2016, 2019; Aleinikoff and others, 2018, 2021; Peck and others, 2018; Regan and others, 2019a, b; Krestianinov and others, 2021).

Mineral assemblages in the paragneiss units are consistent with lower granulite facies to upper amphibolite facies conditions, sometimes called the clinopyroxene-almandite subfacies of the granulite facies (de Waard, 1965). Representative assemblages include the following:

- Pelitic and psammitic rocks: garnet-sillimanite-biotite-plagioclase-K-feldspar-quartz-graphite.
- Marble: diopside-forsterite-scapolite-calcite-dolomite-wollastonite-graphite.
- Mafic rocks: garnet-hornblende-clinopyroxene-plagioclase±orthopyroxene.
- Granitoid gneisses: garnet-hornblende-biotite-clinopyroxene-plagioclase-K-feldspar-quartz±orthopyroxene.

Sillimanite occurs aligned with both L2 mineral lineations and F3 fold axes indicating second sillimanite conditions during both these events in this quadrangle and in the adjacent Crown Point quadrangle (Walsh and others, 2022). The late pegmatites do not contain muscovite; they crystallized mainly above muscovite stability and can be classified as abyssal pegmatites related to adiabatic melting during uplift and unroofing (Cerny and Ercit, 2005). The granitic gneisses commonly show blebs or planar to lenticular microperthite lamellae textures, which are common in granulite facies rocks where temperatures peak above the alkali feldspar solvus and two feldspars exsolve during slow cooling (Hyndman, 1972). Locally “two stage” microperthite texture with blebs and lamellae occur, and these are characteristic of granulite facies rocks (Parsons and others, 2005). Common trace minerals include apatite, titanite, monazite, magnetite, pyrite, graphite, and zircon. Greenschist facies minerals mark retrograde assemblages. Muscovite is absent except in rocks that show retrograde assemblages, which are most common as muscovite replacing sillimanite or alkali feldspar, or fine-grained sericite in saussurite. This indicates that all the Mesoproterozoic rocks were metamorphosed above the muscovite stability curve or the activity of water was low in these dry rocks (Storm and Spear, 2005; Williams and others, 2019). Chlorite is a common retrograde mineral after biotite, garnet, and amphibole, but retrograde assemblages are not widespread. Epidote is a common retrograde mineral and is locally found in veins; plagioclase is commonly saussuritized to varying degrees where observed in thin section. Actinolite is locally observed, and serpentine minerals are retrograde products of olivine in marbles (Walsh and others, 2022). Tremolite locally, replaced diopside in calc-silicate granofels. Calcite and dolomite coexist in Adirondack marbles (Valley and O’Neil, 1981) but were not independently verified in this study.

U-Th-Pb Geochronology

A sample (EL-4067A, fig. 17) was collected from the hornblende granitoid gneiss (unit Ych) along the abandoned railroad cut, on the north side of the "tracks" just north of Old Furnace Road, west of Cedar Bridge Pond and the junction with Hogback Road in the town of Crown Point (43.929512, -73.585793, WGS 84 datum), to determine the primary intrusive age and high-grade metamorphic history of this rock in the quadrangle. U-Th-Pb data are available in Walsh and others (2023). The rock is a medium-grained, granoblastic, microperthite hornblende quartz syenite. Hand samples and the outcrop exhibit a moderate to weak foliation, which is not readily apparent in the thin section (fig. 17*B*). Approximate mineral modes estimated from 394 point-counts, are as follows: quartz (10 percent), plagioclase (18 percent), microperthite (49 percent), amphibole (8 percent), brown to olive-green hornblende (7 percent), clinopyroxene (4 percent), magnetite/ilmenite (3 percent), apatite (trace), zircon (trace), pyrite (trace), and chlorite (trace). The rock has a quartz-plagioclase-alkali feldspar (Q-P-A) ratio of 14–23–63. Plagioclase and albite may be undercounted because it was counted with microperthite. Microperthite locally exhibits thin rims of albite. The rock contains minor amounts of magnetite, ilmenite, and dark-green clinopyroxene with relict lamellae of orthopyroxene. The clinopyroxene is altered to a fine-grained and commonly Fe-rich amphibole (fig. 17E). The rock contains crosscutting secondary veins of fine-grained, fibrous, matted, yellowish-brown Fe-rich amphibole (fig. 17E). The same yellowish-brown alteration also occurs as irregularly shaped secondary felty clusters and blobs, and aggregates arranged parallel to compositional lamellae in microperthite, clinopyroxene, and inside hornblende, due to retrograde replacement. Exploratory energy dispersive spectroscopy (EDS) demonstrates that the yellow-brown alteration and vein filling amphibole is similar in composition regardless of textural variations, indicating all occurrences are cogenetic. The sample contains trace amounts of pyrite, apatite, chlorite, and relatively large zircon grains (0.2–0.54 millimeters; fig. 17*D*). Allanite-Ce overgrowths on apatite (fig. 17*H*) are evidence for late remobilization of REEs, possibly associated with the aforementioned amphibole veins and partial replacement of K-feldspars. Electron microscopy shows that micron (µm)-scale fluorite is associated with the partial replacement of K-feldspar domains in microperthite (fig. 17*J*).

The sample was processed through a jaw crusher and a disk mill, then sieved at 250 micron (60 mesh). Zircons were separated using a Wilfley table, Franz magnetic separator, and heavy liquids. The sample yielded a large quantity of anhedral zircon grain fragments and rare soccer-ball-shaped whole grains. Scanning electron microscopy (SEM)-EDS analysis confirmed that the grains are zircon. Because most of the grains were fragments, additional processing of >250-µm fraction from the disk mill was conducted to locate whole grains from the coarser grained population. Although most coarser grains were fragmented, some large grains (>250 µm) occur in two color populations: (1) >80 percent are peach colored, transparent, and blocky to anhedral. Rare grains that appear to be whole or at least have clear crystal faces indicate the original morphology of the zircon was equant; and (2) <20 percent are dark-brown zircon with similar morphology as the peach-colored zircons. On average, the darker grains more commonly show crystal faces and are closer to whole grains. The observed whole grains are prismatic. Smaller grains (<250 µm) also comprise two color populations, with the darker grains more commonly occurring as doubly terminated whole grains. Also present are clear reddish soccer-ball-shaped grains that are hard to distinguish on a binocular microscope from fragments of nominal soccer ball shape.

Zircon was hand-picked, mounted in epoxy, ground to half-thickness (to expose interior zones), and polished sequentially with 6 µm and 1 µm diamond suspension. The grains were then imaged using a Hitachi SU-5000 field emission electron microscope at the U.S. Geological Survey (USGS) in Reston. Zircon imaging by back scattered electron microscopy (BSE) and cathodoluminescence (CL) (figs. 18, 19) suggests that there were large (>500 µm) oscillatory- and fir-tree-zoned zircon grains that were broken apart into large fragments because the external grain morphology does not match the internal zoning shape. The broken grains were then overgrown and (or) replaced by a dark CL/bright BSE zircon that is unzoned in CL and rarely sinuously zoned in BSE. Associated with this zircon growth was fluorapatite growth that occurs in a subset of dark CL zones in the zircon (figs. 18, 19). In detail, some zircon grains show multiple episodes of rim growth identifiable by crosscutting relations in high contrast BSE images. However, typically individual rim zones were narrow (<25 µm) or the rims were mottled in BSE rather than showing a clear replacement stratigraphy. For these two reasons, the analytical spot locations were broken into only two categories: (1) oscillatory zircon cores, and (2) zircon rims that are uniformly dark in CL but may exhibit some zoning in BSE images.

Following spot selection in Reston, Virginia, the polished grains were analyzed for U, Th, and Pb isotopes using the USGS/Stanford sensitive high-resolution ion microprobe reverse geometry (SHRIMP-RG) at Stanford University.

The analytical spot (~25 µm diameter x 1 µm depth) was excavated using a primary oxygen beam of ~4–5 nanoamps. The magnet was cycled through 9 mass positions in 5 cycles, and signals were collected on an electron multiplier. Raw data were reduced using Squid v. 2.51 (Ludwig, 2009) and plotted using IsoplotR (Vermeesch, 2018). The measured ages were referenced to zircon standard R-33, which was analyzed after every four unknowns (419±1 Ma; Black and others, 2004). Five interspersed analyses of secondary standard Z1242 (2,679.8±0.2 Ma; Davis and others, 2019) yielded an $^{207}Pb/^{206}Pb$ age of 2,682±6 Ma. U and Th concentrations were

measured relative to trace element standard MAD-559 located on the same mount (3,940±210 parts per million [ppm] U, 483±30 ppm U; Coble and others, 2018).

SHRIMP spot locations, guided by CL imaging (figs. 18, 19), typically allowed analysis of single textural zones, designated by us as "cores" and "rims." Following removal of discordant results from data for cores (defined here as any data point where error ellipse does not overlap concordia, n=3 of 35), all data were plotted as "cores" regardless of age. The uncertainty of the ages (either Concordia Age or weighted average age) is +/- 2-sigma. One analysis with a high uncertainty was kept in the calculated age because it is concordant (fig. 18*C*). We note also that the reported summary ages are weighted by the uncertainties of individual analyses and the inclusion of this one analysis does not change the reported summary final age within the quoted limits of uncertainty. The cores (fig. 18) have typically low U (median of 69 ppm) and Th (median of 28 ppm), and a median Th/U value of ~0.39, typical of igneous zircon Th/U values of ≥0.5 (Hoskin and Schaltegger, 2003). Thirty-two concordant analyses of zircon cores yield a Concordia Age of 1,145.0±7.7 Ma (2 sigma) with a mean square of the weighted deviates (MSWD) of concordance of 0.33, in agreement with the ^{207}Pb-corrected $^{206}Pb/^{238}U$ weighted average age of 1,149.3±9.6 Ma (fig. 18*C*, MSWD = 0.76, rounded to 1,149±10 Ma). For the cores, the weighted average age is considered the time of crystallization of the rock. In contrast, data for zircon rims (fig. 19) are considered to reflect the time of subsequent metamorphism. Following removal of discordant data (defined here as any data point where the error ellipse does not overlap concordia, n=2 of 31) all data were plotted as "rims" regardless of age. Relative to core analyses, the rim analyses have high U (median of 950 ppm) and high Th (median of 120 ppm) concentrations. Rim analyses also have a lower median Th/U value (0.11) commonly interpreted to reflect a metamorphic origin (Hoskin and Schaltegger, 2003). Because the rims were high in U and Th concentration the $^{207}Pb/^{206}Pb$ ages were used to determine a weighted average age. In general, zircon rim analyses yield younger $^{207}Pb/^{206}Pb$ ages than the zircon cores, however, significant age scatter is present, and a few rim analyses are similar to the Concordia Age for cores (5 of 29). The remaining 24 ages yield a weighted average ^{204}Pb-corrected $^{207}Pb/^{206}Pb$ age of 1,038.6±8.2 (fig. 19*C*, MSWD = 2.4, rounded to 1,039±8 Ma), interpreted to be the approximate time of metamorphism. Based on BSE zoning, this age may reflect the average of several distinct episodes of metamorphism (fig. 19), but these episodes were not resolvable analytically.

The five older rim ages could indicate (1) misidentification of core material for those analytical spots, (2) an older episode of metamorphism, or (3) a mixed isotopic signature of igneous and metamorphic domains. We suggest option 1 is unlikely given that the analytical spots are in zones that embay oscillatory zones in cores, have high U and Th concentrations, and relatively low Th/U ratios. We cannot rule out options 2 or 3. More data would be required to distinguish between these two hypotheses. In conclusion, the data suggest that the protolith of sample EL-4067A crystallized at 1,149±10 Ma and was subject to at least one episode of metamorphism at about 1,040 Ma.

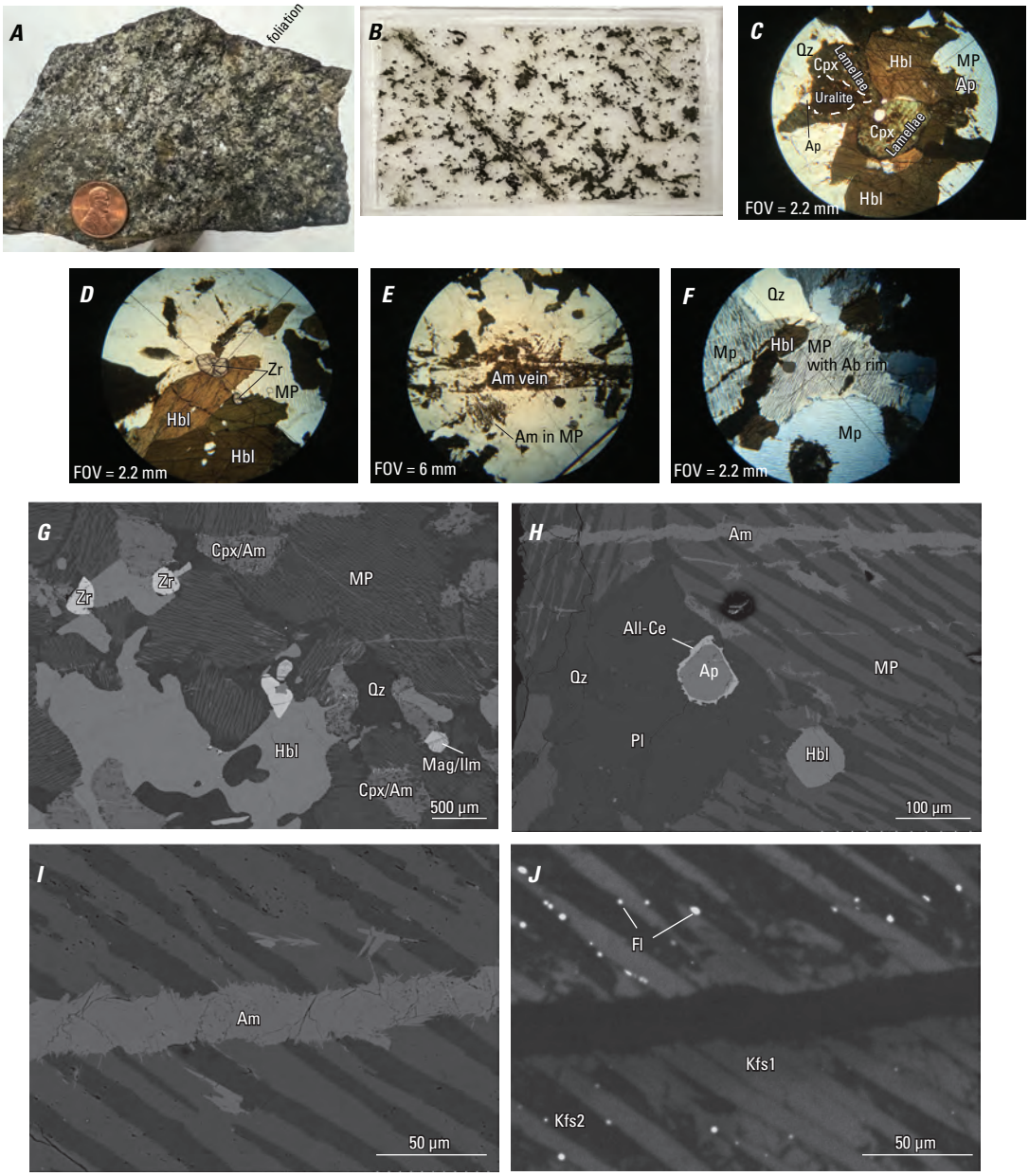

Figure 17. Photographs of the dated microperthite hornblende quartz syenite (sample EL-4067A) from the hornblende granitoid gneiss (unit Ych). *A*, Photograph of the sampled rock showing a weak foliation from lower left to upper right. Penny is shown for scale. *B*, Photograph of an entire thin section showing black magnetite and dark-green amphibole (about 15 percent amphibole and 3 percent magnetite). The sample contains crosscutting amphibole veins from upper left to lower right. The slide measures 25 x 45 millimeters (mm). Photographs *C*–*F* show photomicrographs in polarized light. *G*, BSE image showing typical microtexture in sample EL-4067A. Note the abundant microperthite (MP), altered clinopyroxene (Cpx), and coarse zircon (Zr or Zrn). *H*, BSE image showing apatite (Ap) with overgrowth of allanite-Ce (All-Ce) in a matrix of plagioclase (Pl) and microperthite (MP), and crosscutting veins of amphibole (Am). *I*, BSE image of vein composed of fine-grained amphibole (Am) crosscutting microperthite. *J*, Cathodoluminescence image of area shown in *I*. Two distinct types of K-feldspar (Kfs) lamellae are present, CL-bright (Kfs1) and CL-dark (Kfs2). Kfs2 replaces Kfs1 and micron-sized fluorite (Fl) is disseminated in Ksp2. Scalebars in *G*–*J* are in microns (µm). Ab, albite; BSE, backscattered electron; Chl, chlorite; Fl, fluorite; FOV, field of view; Hbl, hornblende; Mag/Ilm, magnetite/ilmenite; Qz, quartz. Photographs by Gregory J. Walsh and Ryan J. McAleer, U.S. Geological Survey. Sample location: 43.929496, –73.585815 (WGS 84) on the east end of the abandoned railroad cut on the north side of "tracks," just north of Old Furnace Road.

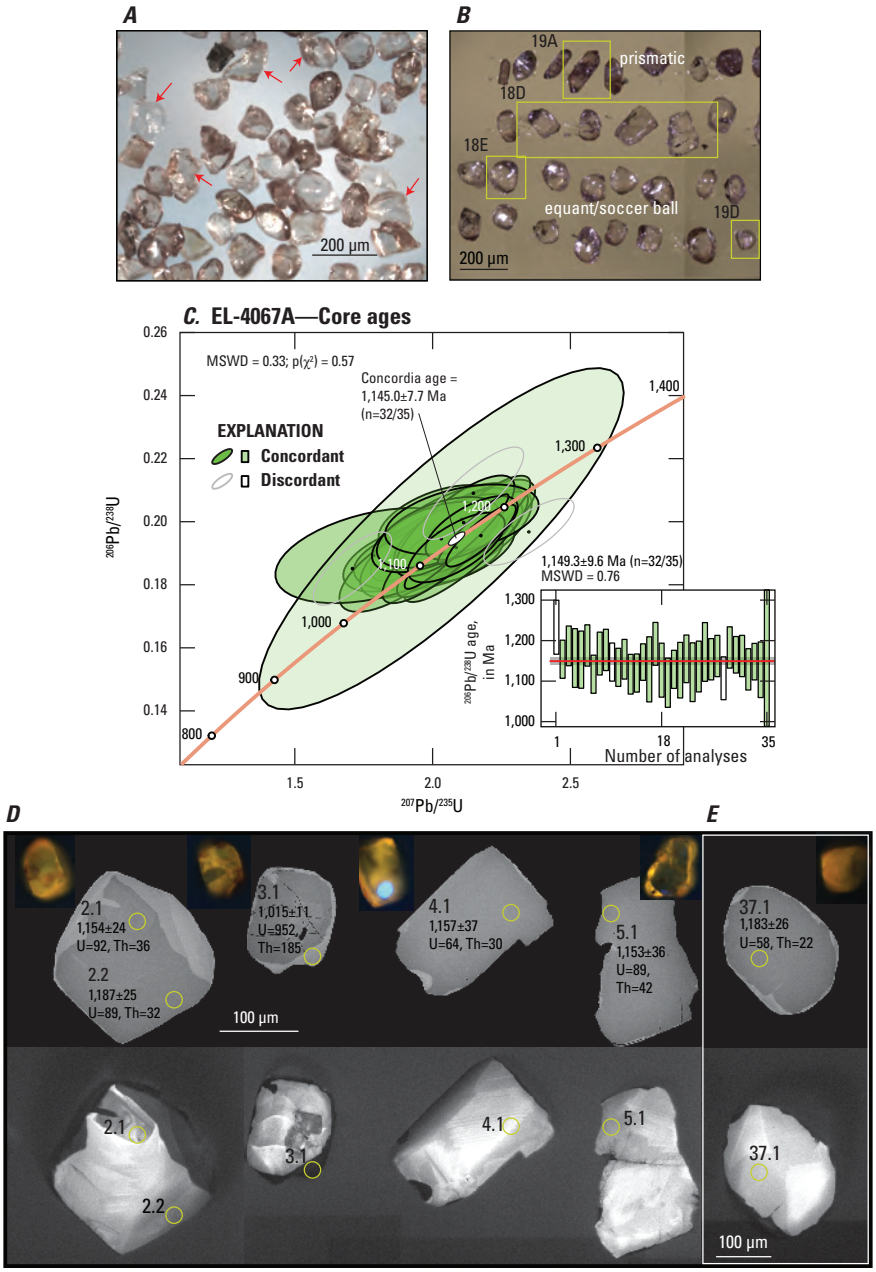

Figure 18. Photographs of zircon grains and U-Th-Pb geochronology data showing zircon-core age results. *A*, Incident light image of zircon separate from sample EL-4067A. The zircon grains are dominantly transparent, peach in color, and fragmental (subset of fragments indicated with red arrows). *B*, Subset of selected zircon grains for geochronology on Kapton tape prior to polishing. Grains with crystal faces were preferentially selected to maximize the likelihood of capturing the latest growth history. *C*, Wetherhill concordia plot of SHRIMP data from 35 analytical spots on cores of zircon grains. Thirty-two concordant analyses yield a Concordia Age of 1,145.0±7.7 Ma (2σ). The MSWD and chi-squared p-value for concordance are shown at top. The inset in *C* shows a weighted average plot of ^{207}Pb-corrected ^{206}Pb/^{238}U ages of cores (n=32). Three analyses are excluded due to discordance. *D*, BSE and CL images of cross-section of grains indicated in *B*. Spot number, age (^{207}Pb-corrected ^{206}Pb/^{238}U for cores, ^{204}Pb-corrected ^{207}Pb/^{206}Pb for rims) and 1σ uncertainty, and U and Th concentrations in parts per million are indicated. *E*, BSE and CL image of "soccer ball-shaped" grain. Yellowish-orange insets in the top of images *D* and *E* are photoluminescence images of the zircons taken prior to polishing excited under ~365 nanometers light using a petrographic microscope and a tin-halide bulb (McAleer and others, 2020); the zircon grains typically photoluminesce yellowish orange with a reddish rim. Yellow circles in *D* and *E* show spots of age analyses. The light-blue spot in *D* is reflected light. BSE, backscattered electron; CL, cathodoluminescence; Ma, mega-annum (million years before present); MSWD, mean squared weighted deviation; n, number of analyses; Pb, lead; SHRIMP, sensitive high-resolution ion microprobe; Th, thorium; U, uranium; µm, micron.

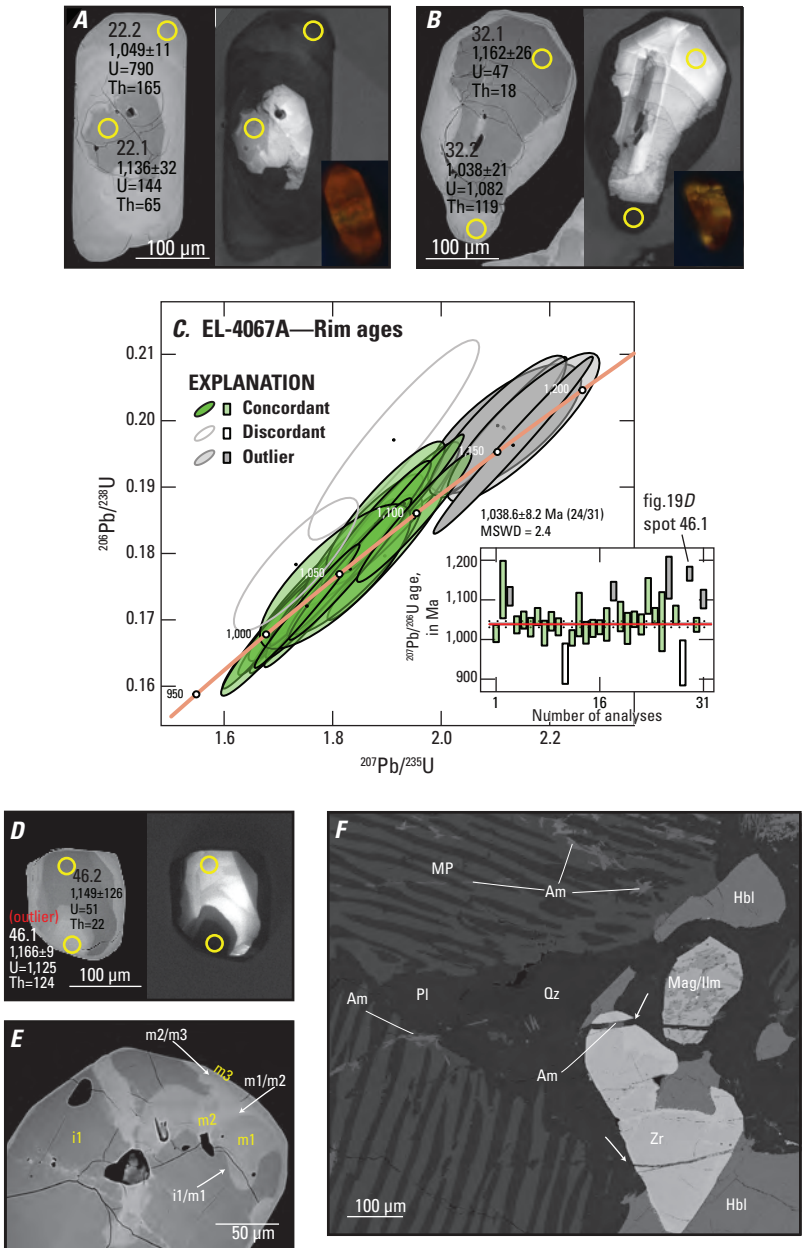

Figure 19. Photographs of zircon grains and U-Th-Pb geochronology data showing zircon-rim age results. *A* and *B*, representative BSE and CL images of dated zircon grains. Spot ages (^{207}Pb-corrected ^{206}Pb/^{238}U for cores, ^{204}Pb-corrected ^{207}Pb/^{206}Pb for rims) along with 1σ uncertainty, and U and Th concentrations in parts per million are indicated. Bright-BSE/dark-CL rims embay and replace dark-BSE/bright-CL cores. Orangish-yellow inset images in the lower right of *A* and *B* are photoluminescence images of zircon excited under ~365 nanometers light using a petrographic microscope and a tin-halide bulb (McAleer and others, 2020); compare with inset images in figure 18*D*. Yellow circles show spots of age analyses. *C*, Wetherhill concordia plot of SHRIMP data from 31 analytical spots on rims of zircon grains. The inset in *C* shows a weighted average plot of ^{204}Pb-corrected ^{207}Pb/^{206}Pb ages of rims (n=24). Two analyses are excluded due to discordance along with 5 outliers yielding a preferred age of 1,038.6±8.2 Ma (2σ). *D*, BSE and CL images of a grain with an outlier age for the rim analysis. Yellow circles show spots of age analyses. *E*, BSE zoning and truncations (indicated by white arrows) indicate multiple episodes of rim growth (m1 to m3) following igneous crystallization (i1). This metamorphic "stratigraphy" is not evident in most grains, instead most rims have mottled zoning not easily linked to an m1 to m3 history. *F*, SEM image showing that amphibole-filled fractures crosscut all metamorphic zircon domains (white arrows), indicating that this set of fractures and mineralization is younger than about 1,040 Ma. Am, retrograde amphibole; BSE, backscattered electron; CL, cathodoluminescence; Hbl, hornblende; Ma, mega-annum (million years before present); Mag/Ilm, magnetite-ilmenite intergrowth; MP, microperthite; MSWD, mean squared weighted deviation; n, number of analyses; Pb, lead; Pl, plagioclase; Qz, quartz; SEM, scanning electron microscope; SHRIMP, sensitive high-resolution ion microprobe; Th, thorium; U, uranium; µm, micron.

Geochemistry

Forty-six samples of magnetite ore (n=29) and adjacent host rock (n=17) in the Lyon Mountain Granite Gneiss (Ylg) were analyzed at Bureau Veritas Commodities Canada Ltd., of Vancouver, British Columbia, Canada, for whole-rock major, trace, and REE geochemistry (Geer, 2020), and those data are summarized here (figs. 20, 21). The data are available in Walsh and others (2023) and are also included in the accompanying GIS database (Walsh and others, 2026). Major element analyses were conducted by X-ray fluorescence (XRF) and trace elements and REEs by inductively coupled plasma-mass spectrometry (ICP-MS). Samples largely focused on the Hammondville pluton to characterize the ore and host rock from this historically important mining district, but a few samples come from the Long Pond and Skiff mines in the Skiff Mountain pluton.

Previous regional studies demonstrated that the Lyon Mountain Granite Gneiss is a ferroan A-type leucogranite (Chiarenzelli and others, 2017; Aleinikoff and others, 2021) that is locally hydrothermally altered (Valley and others, 2011). Whole rock geochemistry confirms these findings (fig. 20). The data show that the granitic samples plot as altered ferroan, alkalic to calc-alkalic, metaluminous to peraluminous, alkali feldspar granite to quartz alkali feldspar syenite (fig. 20*A–D*). On the iron oxide (FeO) versus silica (SiO_2) diagram (fig. 20*A*), the sampled granitoids plot in approximately the same field as other MCG phases of the AMCG suite of rocks in the Adirondacks, but only three samples plot in the unaltered field of the Lyon Mountain Granite Gneiss of Chiarenzelli and others (2017). On a major element classification diagram (fig. 20*E*), the granitoids plot largely as rhyolites with some overlap into the trachydacite and dacite fields with SiO_2 varying from about 67 to 76 percent. The granitic samples plot in the sodic (Na) alteration field (fig. 20*F*) for the Lyon Mountain Granite Gneiss as defined by Valley and others (2011), which is consistent with observations that the collected samples are altered quartz-albite rocks adjacent to Fe-ore seams. Geer (2020) reports that the plagioclase is greater than Ab_{90}, consistent with findings reported by McLelland and others (2002) and Valley and others (2011). Due to the sodic alteration, the quartz-albite rocks plot as trondhjemite on a normative An-Ab-Or (anorthite-albite-orthoclase) classification diagram (fig. 20*G*). Despite the observation that immobile elements are enriched in the sodic-altered rocks (Valley and others, 2011), the granitic samples plot consistently on trace element discrimination diagrams (fig. 20*H–J*). On a trace element tectonic diagram, the samples plot in the overlapping area between "within plate granite" and "ocean ridge granites" (fig. 20*H*). Samples with Nb (niobium) + Y (yttrium) >60 ppm and Yb (ytterbium) + Ta (tantalum) >6 ppm are considered A-type granites (Whalen and Hildebrand, 2019) and only one sample (EL4409B) does not fit these criteria; the rest of the samples plot in the "A2" field (fig. 20*I, J*). A2-type samples, in general, have compositions similar to rocks generated from melts in the lower crust at the end of continental collisions (anorogenic) perhaps during terminal extensional collapse (Eby, 1992; Murphy and others, 2018; Whalen and Hildebrand, 2019).

Twenty-nine iron ore samples show a linear distribution of SiO_2 vs Fe_2O_3, with iron (measured as Fe_2O_3) ranging from about 34 to 96 percent; the highest iron concentrations occur in samples with the lowest silica (fig. 21*A*). Quartz is a common mineral phase in the ore seams, which also contain albite, hornblende, clinopyroxene, apatite, allanite, and monazite (Taylor and others, 2019; Geer, 2020). For comparison, Fe_2O_3 in the sampled host rocks (Lyon Mountain Granite Gneiss) ranges from about 2 to 9 percent (fig. 21*A*). Total REEs versus Th show a relatively linear distribution; samples with the highest Th also have the highest REEs (fig. 21*B*). Adjacent host rocks, in most cases, show elevated Th when compared with the ore seams (fig. 21*B*). The ratio of heavy to light REEs (HREE vs LREE) is linear, with LREEs>HREEs, in agreement with findings reported by Taylor and others (2019) for sampled ore, host rock, waste rock, and tailings from abandoned mines in the eastern Adirondack Highlands. The highest concentrations of REEs occur in samples collected from a belt of rocks that extends from the Dog Alley mine to the No. 1E mine in Hammondville (fig. 21*C*). Other relatively high concentrations of REEs occur at the No. 8 mine in Hammondville, and the Long Pond and Skiff mines on Skiff Mountain (fig. 21*C*). A relatively linear correlation between REEs and phosphate occurs for apatite-bearing granitoids and ores, and samples without reported phosphate (P_2O_5) (Walsh and others, 2023, not plotted) have the lowest REEs (fig. 21*D*). REE diagrams show slight enrichment in LREEs, negative Eu anomalies, and comparable REE values between most host rock (Lyon Mountain Granite Gneiss) and ore samples (fig. 21*E–G*). Ore samples with the highest values again occur in the belt of rocks from the Dog Alley mine to the No. 1E mine in Hammondville (fig. 21*F, G*). These data are consistent with the interpretation that sodic alteration led to mobilization of iron (Fe) and REEs from the host rocks to the ore seams (Taylor and others, 2019).

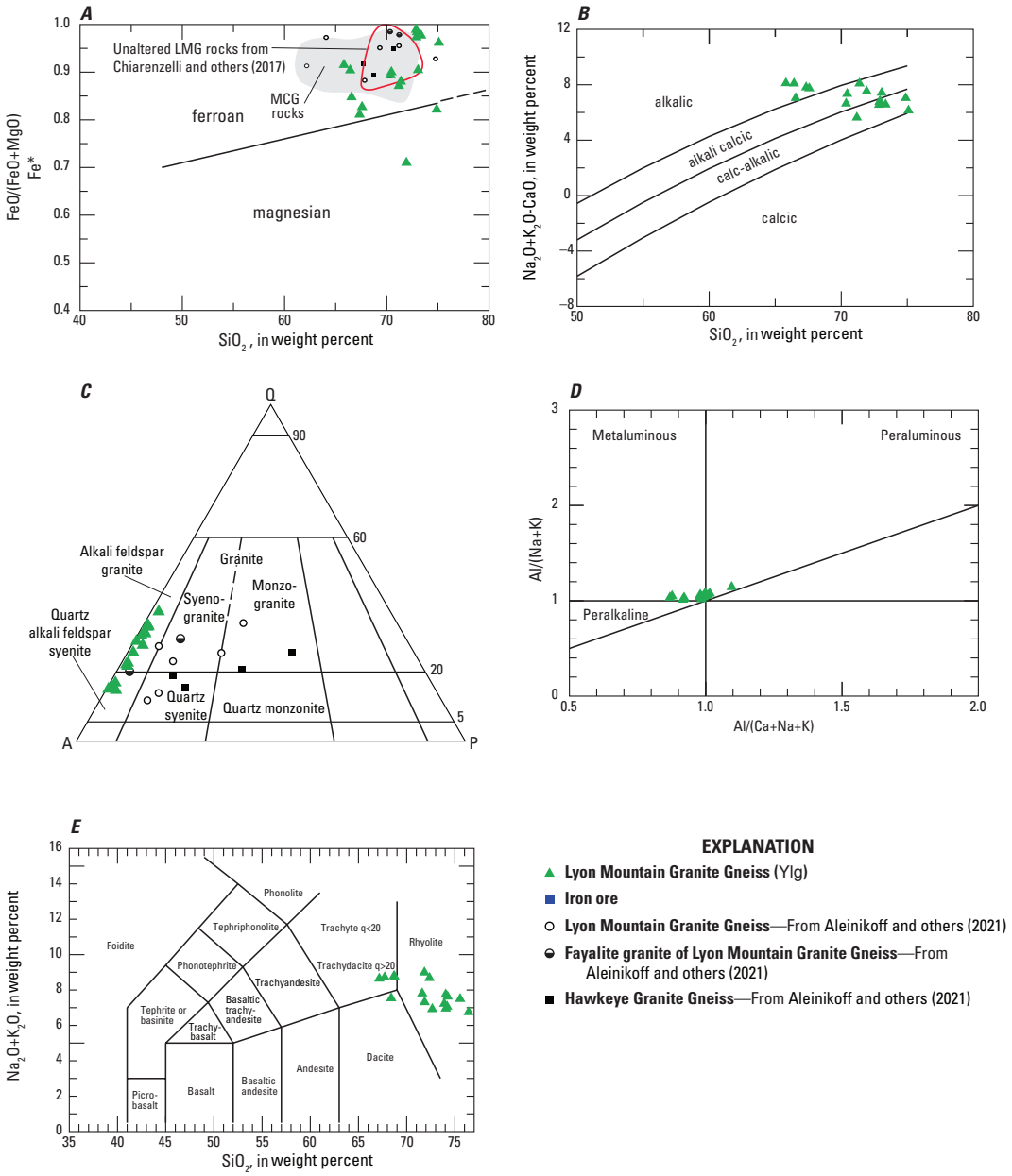

Figure 20. Plots of major and trace element geochemistry from samples of Lyon Mountain Granite Gneiss (unit Ylg) collected in the Eagle Lake quadrangle; comparisons with iron ore samples and previous work also shown in some diagrams. *A*, Fe-index (Fe*) = FeO/(FeO + MgO) versus SiO_2 plot after Frost and others (2001). *B*, Modified alkali-lime index plot after Frost and others (2001). *C*, IUGS classification diagram of igneous rocks after Le Bas and Streckeisen (1991) showing quartz (Q), alkali feldspar (A) and plagioclase (P) plots of normalized CIPW (Cross, Iddings, Pirsson, and Washington) geochemical modes; point-counted mineral modes from Aleinikoff and others (2021) are shown for comparison. *D*, Alumina saturation diagram after Shand (1951) and Maniar and Piccoli (1989). *E*, Alkalis-silica plot after Le Bas and others (1986) showing comparable volcanic rock names; q<20 means quartz is less than 20 percent in a QAPF classification, and q>20 means quartz is greater than 20 percent in a QAPF classification. *F*, Plot of Na_2O-K_2O normalized to Al_2O_3 showing Na and K alteration field from Valley and others (2011); low K and variably elevated Na suggests that the Fe ores are related to Na metasomatism and not K alteration. *G*, Normative An-Ab-Or (anorthite-albite-orthoclase) classification diagram of O'Connor (1965) and Barker (1979). *H*, Trace element tectonic discrimination diagram after Pearce and others (1984) showing that granitoids of the AMCG suite plot in the area of overlap between plate granites (WPG) and ocean ridge granites (ORG). *I*, Trace element diagram showing arc, slab failure, and A-type discrimination after Whalen and Hildebrand (2019). *J*, Trace element diagram showing A-type (A1, A2) discrimination after Eby (1992). Geochemistry diagrams are plotted with IgPet2022 software by RockWare. AMCG, anorthosite-mangerite-charnockite-granite suite; Ce, cerium; IUGS, International Union of Geological Sciences; LMG, Lyon Mountain Granite Gneiss; MCG, mangerite-charnockite-granite suite; Nb, niobium; VAG, volcanic arc granitoids; syn-col., syncollisional; Y, yttrium.

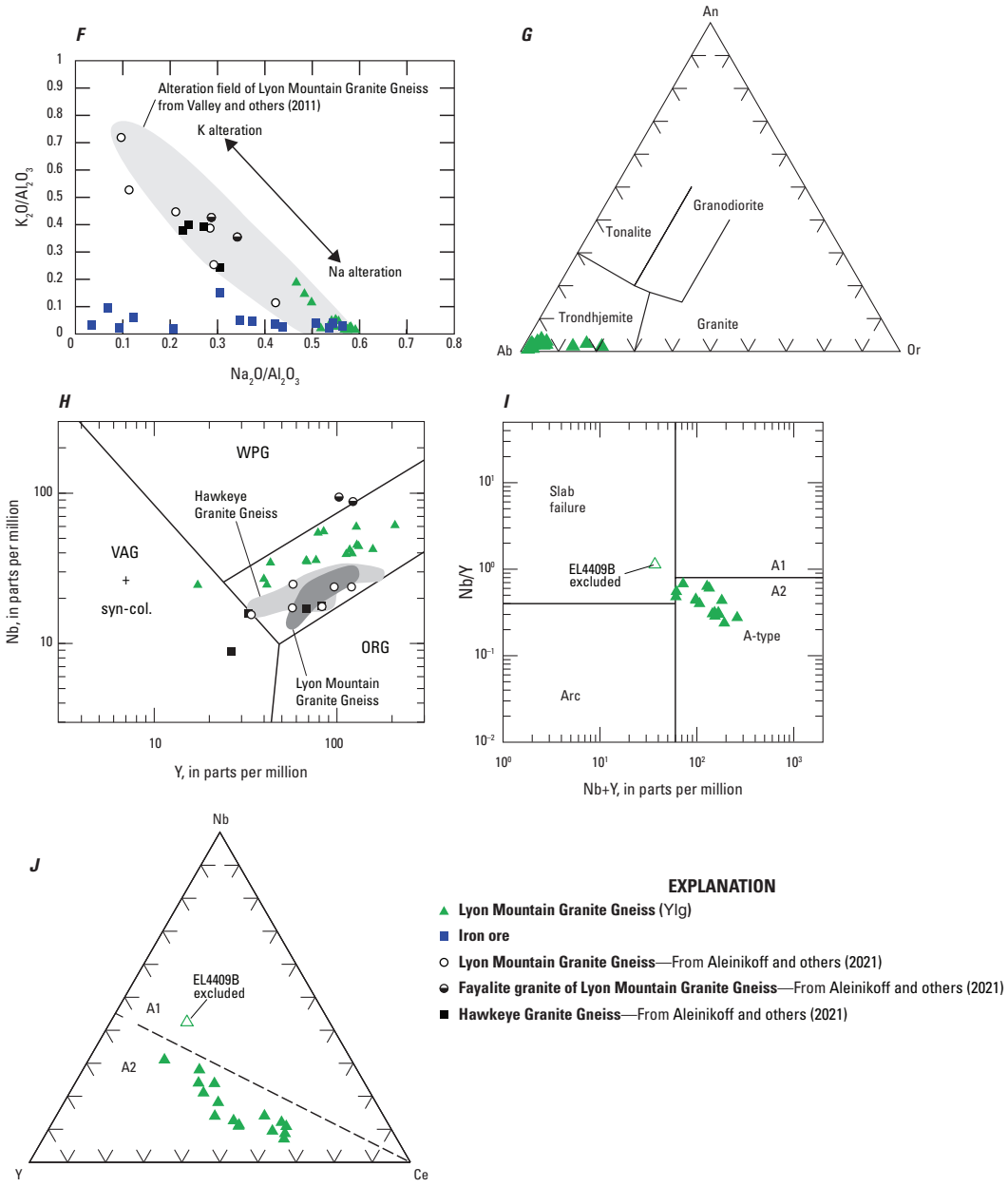

Figure 20. Plots of major and trace element geochemistry from samples of Lyon Mountain Granite Gneiss (unit Ylg) collected in the Eagle Lake quadrangle; comparisons with iron ore samples and previous work also shown in some diagrams. *A*, Fe-index (Fe*) = FeO/(FeO + MgO) versus SiO_2 plot after Frost and others (2001). *B*, Modified alkali-lime index plot after Frost and others (2001). *C*, IUGS classification diagram of igneous rocks after Le Bas and Streckeisen (1991) showing quartz (Q), alkali feldspar (A) and plagioclase (P) plots of normalized CIPW (Cross, Iddings, Pirsson, and Washington) geochemical modes; point-counted mineral modes from Aleinikoff and others (2021) are shown for comparison. *D*, Alumina saturation diagram after Shand (1951) and Maniar and Piccoli (1989). *E*, Alkalis-silica plot after Le Bas and others (1986) showing comparable volcanic rock names; q<20 means quartz is less than 20 percent in a QAPF classification, and q>20 means quartz is greater than 20 percent in a QAPF classification. *F*, Plot of Na_2O-K_2O normalized to Al_2O_3 showing Na and K alteration field from Valley and others (2011); low K and variably elevated Na suggests that the Fe ores are related to Na metasomatism and not K alteration. *G*, Normative An-Ab-Or (anorthite-albite-orthoclase) classification diagram of O'Connor (1965) and Barker (1979). *H*, Trace element tectonic discrimination diagram after Pearce and others (1984) showing that granitoids of the AMCG suite plot in the area of overlap between plate granites (WPG) and ocean ridge granites (ORG). *I*, Trace element diagram showing arc, slab failure, and A-type discrimination after Whalen and Hildebrand (2019). *J*, Trace element diagram showing A-type (A1, A2) discrimination after Eby (1992). Geochemistry diagrams are plotted with IgPet2022 software by RockWare. AMCG, anorthosite-mangerite-charnockite-granite suite; Ce, cerium; IUGS, International Union of Geological Sciences; LMG, Lyon Mountain Granite Gneiss; MCG, mangerite-charnockite-granite suite; Nb, niobium; VAG, volcanic arc granitoids; syn-col., syncollisional; Y, yttrium.

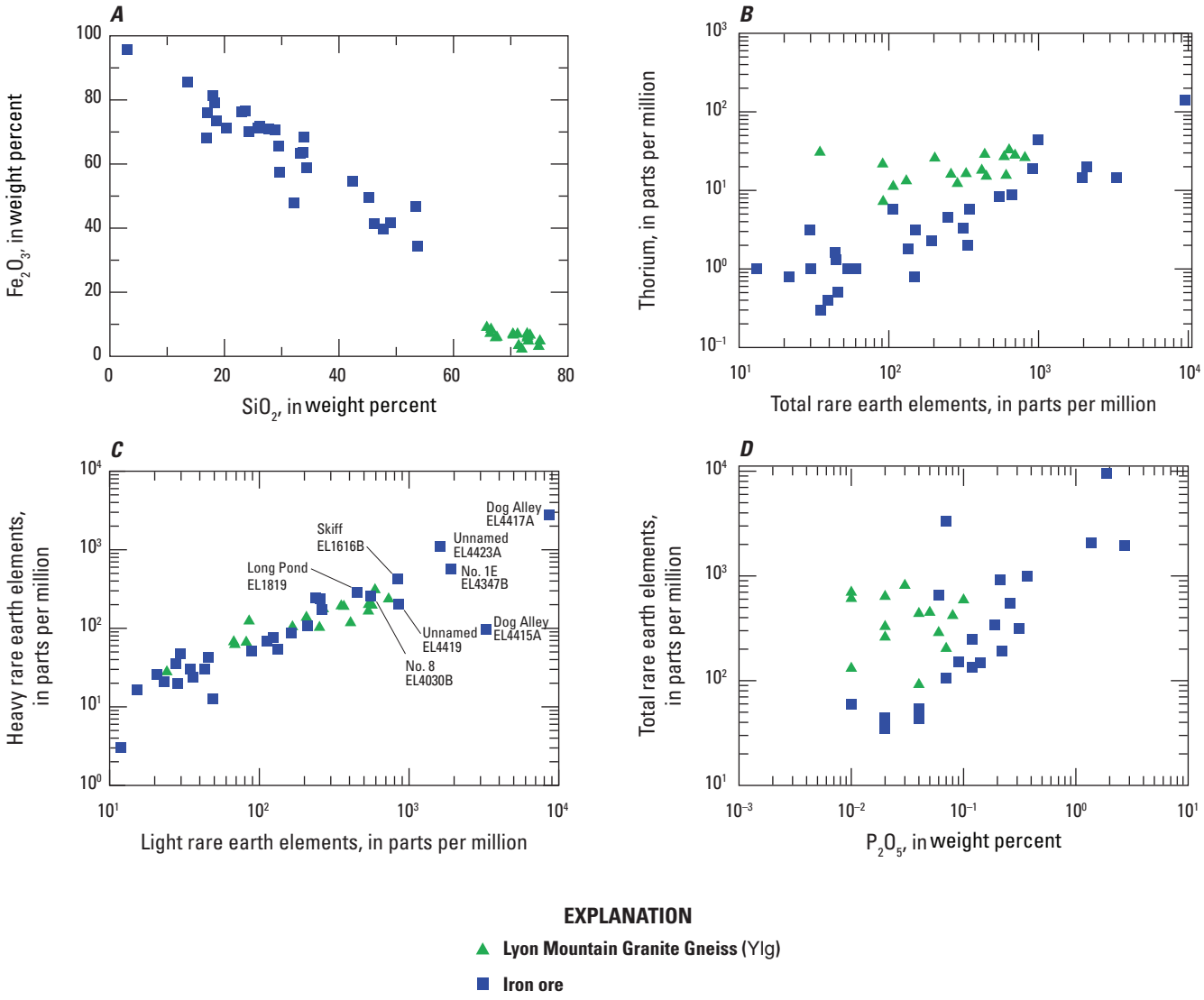

Figure 21. Plots of major, trace, and rare earth element geochemistry from iron ore and Lyon Mountain Granite Gneiss (unit Ylg) samples collected in the Eagle Lake quadrangle. *A*, Plot of iron oxide (Fe_2O_3) versus silica (SiO_2). *B*, Plot of thorium (Th) versus total rare earth elements (REEs). *C*, Plot of heavy versus light REEs; labelled points with the highest values in iron ores show mines and sample numbers. *D*, Plot of total REEs versus phosphate (P_2O_5). *E*, Plot of REEs for host rocks (Ylg). *F*, Plot of REEs for iron ores. *G*, Plot of cerium (Ce) versus lanthanum (La) for host rocks (Ylg) and iron ores.

Economic Geology

Abandoned hard rock mines and prospects occur throughout the quadrangle (fig. 2) and were developed in the 1800s for the extraction of iron, graphite, marble, and feldspar. Many small prospects also occur and are included in the GIS database (Walsh and others, 2026) along with the mines. Only one small active hard rock quarry currently exists, and the material is currently used for road metal on private logging roads (fig. 2). In this study, we accurately located and field checked most of the hard rock mines and prospects (fig. 2). In a few places, especially in the Hammondville district, we mapped small prospect pits based on the interpretation of the new lidar topography; some of these locations have not been field checked. The current USGS Mineral Resources Data System (MRDS) database either does not include many mine locations or it lists many of the locations incorrectly (Mineral Resources Data System, 2005). The USGS MRDS also lists multiple sand and gravel pits in the area. A few sand

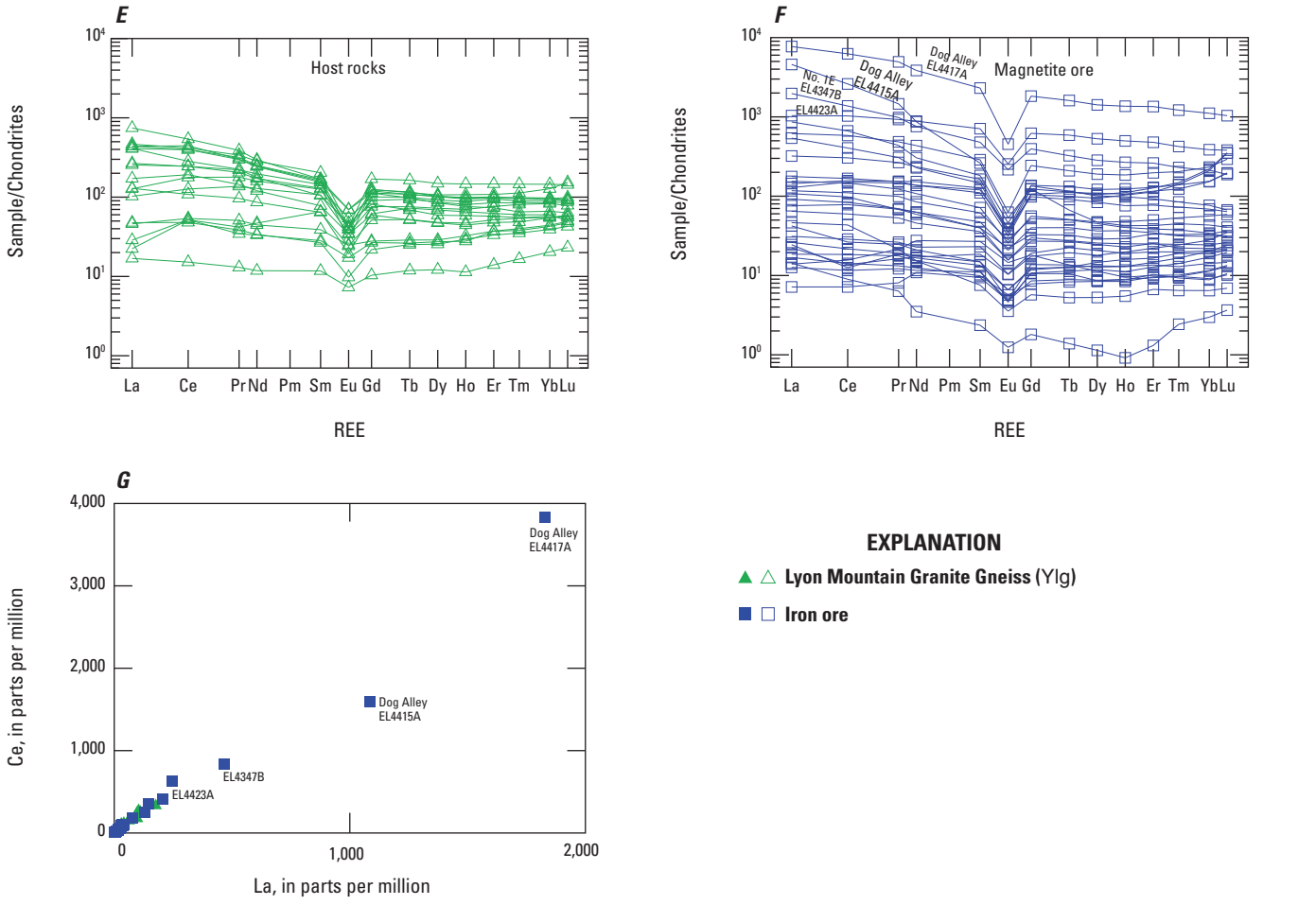

Figure 21. Plots of major, trace, and rare earth element geochemistry from iron ore and Lyon Mountain Granite Gneiss (unit Ylg) samples collected in the Eagle Lake quadrangle. *A*, Plot of iron oxide (Fe_2O_3) versus silica (SiO_2). *B*, Plot of thorium (Th) versus total rare earth elements (REEs). *C*, Plot of heavy versus light REEs; labelled points with the highest values in iron ores show mines and sample numbers. *D*, Plot of total REEs versus phosphate (P_2O_5). *E*, Plot of REEs for host rocks (Ylg). *F*, Plot of REEs for iron ores. *G*, Plot of cerium (Ce) versus lanthanum (La) for host rocks (Ylg) and iron ores.

and gravel pits were active at the time of mapping, but the Quaternary geology remains to be mapped and we did not field check or map these pits.

The largest mining operation in the area occurred in the Hammondville district. The abandoned village of Hammondville operated as a company mining town for the Crown Point Iron Company from 1873 to 1895. A brief history of Hammondville is described by Pope (1971). Sportman (2011) provides an in-depth history of Hammondville from an archeological perspective. More than 700 people lived and worked in the Hammondville district in the late 1800s (Northey, 1940; Sportman, 2011). Smaller magnetite mines and prospects in the quadrangle are subordinate to the deposits in Hammondville. Two sites called Skiff and Long Pond occur in magnetite deposits on Skiff Mountain (Newland and Kemp, 1908). Small magnetite deposits occur on Hogan Hill and Moose Mountain.

Iron

Historic iron mines occur in magnetite deposits categorized as iron oxide-apatite (IOA) end-member deposits of the low-titanium (Ti) iron-oxide-copper-gold (IOCG) system (Foose and McLelland, 1995; McLelland and others, 2002; Valley and others, 2009; Lupulescu, 2018; Taylor and others, 2019). Most iron deposits occur in the Lyon Mountain Granite Gneiss (unit Ylg), but the Moose Mountain deposit occurs in metagabbro (unit Ygb). Iron deposits in metagabbro have higher concentrations of Ti (Newland and Kemp, 1908; Lupulescu, 2018) and locally higher concentrations of vanadium (Taylor and others, 2019), but the Moose Mountain deposit, now accurately located, has not yet been analyzed and was described as a small iron-rich metagabbro deposit containing about 40 percent iron with magnetite and pyrite (Newland and Kemp, 1908).

Iron mining in the Adirondack Mountains significantly impacted the history of the United States including the Revolutionary War, the birth of the U.S. Navy, the development of the railroads and canals, the Industrial Revolution, and the first and second World Wars (Barker, 1942; Farrell, 1996; Pickands, 2018). The magnetite deposits were mined for iron in the 1800s and supplied local furnaces early, and furnaces at Ironville and Crown Point on Lake Champlain later on (Newland and Kemp, 1908). In 1824, the Penfield mine was the first to open in the district, and in 1828 the first forge was operated in Ironville (Newland and Kemp, 1908). Ruins of the Hammond mine furnace, constructed in 1845 (Newland and Kemp, 1908), remain along Old Furnace Road near the junction of the old road to Hammondville; a waste pile of slag is located northeast of the old furnace. Iron mining in the region ceased in 1973 with the closing of the operations in Mineville (Farrell, 1996) in the adjacent Witherbee quadrangle, about 17 km north-northeast of Hammondville.

The main period of iron mining in the Adirondacks occurred from 1860 to 1880 (Newland and Kemp, 1908) and peaked in New York during the Civil War (Pickands, 2018). The history of the iron industry in the region is described by Witherbee (1906), Newland and Kemp (1908), Newland (1921), and Barker (1942). Pickands (2018) provides a modern summary of the history of the iron industry in New York State. Locally in 1872, according to Barker (1942), the Crown Point Iron Company built a narrow-gauge railroad that connected furnaces on the shore of Lake Champlain at Crown Point to the western upland operations at Ironville and the mines at Hammondville. Peak operation and profitability for the company took place between 1876 and 1882. In 1900, the railroad was removed, and in 1905 the Crown Point furnaces were dismantled in response to changing economic conditions and the citing of new iron deposits west of Lake Superior. The deposits and historic workings are now greatly modified by time, and in many places, overgrown by dense forest. Locating and mapping of the abandoned mines, waste rock piles, and the trace of the railroad bed were made possible by recently acquired lidar topographic data, in a similar process described by Walsh and Walsh (2023).

The iron deposits are hosted in the quartz-albite leucogranite of the Lyon Mountain Granite Gneiss (Ylg), pegmatite (Yp), and the metagabbro (Ygb). The deposits occur as rich ore veins (0.5 centimeters [cm] to several meters thick) that are in most places semiconcordant to the principal layering in the host rocks (fig. 22). Crosscutting magnetite veins and magnetite-rich pegmatite also occur. Locally, the deposits observed in the smaller workings and prospects consist of finely banded migmatitic lean ore (fig. 10*A*, *B*). The magnetite within the metagabbro at the Moose Mountain deposit locally contains pyrite, which made it less suitable for the iron furnace (Newland and Kemp, 1908). Several small mines or prospects occur in marble (Ym) or in thin marble horizons within amphibolite (Ya); these deposits served as flux for the iron furnaces.

Graphite

Graphite deposits were mined in the Adirondacks beginning in the mid-1800s (Alling, 1918). In the early 1900s, New York led national graphite production (Bastin, 1909). Several small graphite mines and prospects were in operation in the area, but all were abandoned by the summer of 1917 (Alling, 1918). The observed deposits are flake graphite associated with complex geology mostly involving members of the Grenville Complex including marble (Ym), but also amphibolite (Ya), sillimanite gneiss (Ysi), augen gneiss (Yggn), and pegmatite (Yp). Flake graphite was observed in marble, amphibolite, calc-silicate rock, pegmatite, and rusty garnet-sillimanite gneiss with interlayered quartzite and quartz-rich gneiss rocks of the Grenville Complex. Graphite flakes up to 2 cm across occur in the deposits, but most flakes are less than 1 cm (fig. 23). The deposits operated by the Crown Point Graphite Company south of Stoney Lonesome Road and by the Columbia Graphite Company west of Hebron Hill were the two largest workings in the quadrangle (Alling, 1918), and each site contains foundations and ruins from abandoned structures. The Crown Point Graphite Company deposit was in operation in 1908 (Bastin, 1909) and operated from 1907 to 1910 (Alling, 1918). The main ore occurs in a belt of strike-parallel marble (called “limestone” by Alling) about 1 to 2 m thick (3–7 feet [ft]) and about 300 m long

Figure 22. Photograph of dark, “rich ore” magnetite (Mt) seams interlayered with light-colored leucogranite at the Hammond Pit. Geologist’s arm and hand are shown for scale; location: 43.92231, –73.604875 (WGS 84). Photograph by Gregory. J. Walsh, U.S. Geological Survey.

(1000 ft) (Alling, 1918). The marble horizon is too thin to map at 1:24,000-scale and it is enclosed in a mappable body of amphibolite (Ya). The Columbia Graphite Company deposit was in operation from 1903 to 1904 and the main ore is in a belt of strike-parallel marble and pegmatite (Alling, 1918). Alling (1918) called the marble "verde antique limestone" and noted that it was serpentinized; fibrous asbestiform serpentine minerals are reported from the Buck Mountain Pond graphite deposit in calcite marble located in the adjacent Crown Point quadrangle (Walsh and others, 2022). The marble occurs within quartz-rich gneiss, quartzite, sillimanite gneiss and abundant pegmatite. The thin mapped marble (Ym) horizon occurs near the eastern contact of a belt of sillimanite gneiss where it was intruded by pegmatite (Yp) and augen gneiss (Yggn).

The deposits known as Towne, Penfield Pond, and Betsy Cooke now consist of small collapsed and overgrown prospect pits. The Towne prospect was opened in 1902 and the host rock contains biotite-hornblende schist, pyroxene, flake graphite, and pyrite (Alling, 1918). We noted and mapped marble (Ym), augen gneiss (Yggn), pegmatite (Yp) and biotite paragneiss (Ybg, migmatitic biotite gneiss member of the Grenville Complex) at the site. The Penfield Pond prospect contains flake graphite in marble (Ym). The marble is enclosed within a larger belt of amphibolite (Ya). Alling (1918) noted that the marble ("limestone") was white, pink, and red. Alling (1918) did not provide a date of prospection. The Betsy Cooke prospect is located in rusty weathering amphibolite, and Alling (1918) reports graphite, pyroxenes, scapolite, hornblende, plagioclase feldspar, pyrite, biotite, and titanite from the prospects. Alling (1918, p. 20) stated that the deposit was marked by a "long chain of shallow pits running northwesterly in a curved line" but we did not locate all of the pits. Alling (1918) did not provide a date of prospection.

Feldspar

Economic feldspar in the quadrangle came from a quarried pegmatite body on the south slopes of Spar Bed Hill near Sherman Lake. The quarry on Spar Bed Hill was also named Roe's Spar Bed (Ogilvie, 1905; Tan, 1966). Newland stated that the quarry extracted material for pottery 15 years before his report, so in 1905 (Newland, 1921). This was a year before a processing mill was built in 1906 in Crown Point on the west shore of Lake Champlain near Spar Mill Bay (Tan, 1966; Walsh and others, 2022). The pegmatite is syenitic and consists mostly of coarse microcline and plagioclase (oligoclase) with quartz, biotite, and black tourmaline (Rowley, 1962a; Tan, 1966). Both authors noted that the pegmatite is cut by diabase dikes (Zd) and veins of pyrrhotite. The pegmatite body strikes northeast. Tan (1966, p. 63) shows a detailed map of the Spar Bed Hill quarry and noted at least four zones; however, Rowley stated that the pegmatite was unzoned. Rowley (1962a, b) reported the occurrence of rare-earth element bearing minerals in the pegmatite including the following: uraninite, uranophane, sklodowskite, fergusonite, kasolite, lanthanite, cyrtolite, thorite (uranothorite), fourmarierite, monazite, allanite, and zircon. Rowley (1962a, p. 341) noted that the quarry contained "the first known occurrences of fergusonite, kasolite, thorite (uranothorite), fourmarierite, sklodowskite, uranophane, montmorillonite, and spodumene in New York State, and the first recorded occurrence of uraninite" in the eastern Adirondacks. Lupulescu and others (2011) classify the rock as a NYF (niobium-yttrium-fluorine)-type pegmatite.

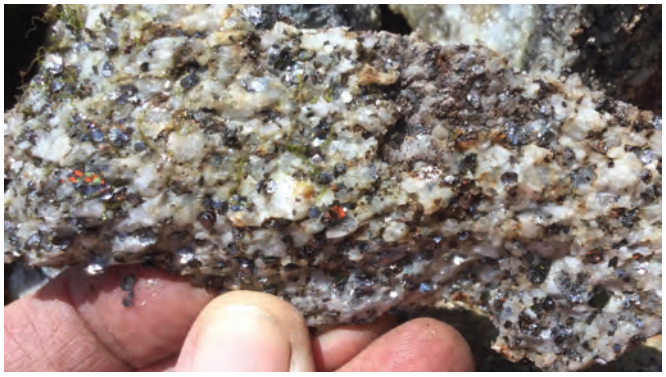

Figure 23. Photograph of flake graphite in marble at the Crown Point Graphite Company deposit; location: 43.894544, –73.572131 (WGS 84). Photograph by Gregory J. Walsh, U.S. Geological Survey.

References Cited

Aleinikoff, J.N., Ratcliffe, N.M., and Walsh, G.J., 2011, Provisional zircon and monazite uranium-lead geochronology for selected rocks from Vermont: U.S. Geological Survey Open-File Report 2011–1309, 46 p. [Also available at https://doi.org/10.3133/ofr20111309.]

Aleinikoff, J.N., and Walsh, G.J., 2015, A new interpretation for the ages of Adirondack plutonism—Implications for the nature and timing of Mesoproterozoic deformation and metamorphism [abs.]: Geological Society of America Abstracts with Programs, v. 47, no. 7, p. 722. [Also available at https://gsa.confex.com/gsa/2015AM/webprogram/Paper264276.html.]

Aleinikoff, J.N., and Walsh, G.J., 2016, Ages and origins of low-Ti magnetite deposits of the eastern Adirondacks—SHRIMP U-Pb and REE evidence from complexly zoned zircon [abs.]: Geological Society of America Abstracts with Programs, v. 48, no. 2. [Also available at https://doi.org/10.1130/abs/2016NE- 272005.]

Aleinikoff, J.N., and Walsh, G.J., 2019, New SHRIMP U-Pb evidence for multiple ages of anorthosite emplacement, Marcy massif, Adirondacks, NY [abs.]: Geological Society of America Abstracts with Programs, v. 51, no. 1. [Also available at https://doi.org/10.1130/abs/2019NE-328144.]

Aleinikoff, J.N., Walsh, G.J., and McAleer, R.J., 2021, New interpretations of the ages and origins of the Hawkeye Granite Gneiss and Lyon Mountain Granite Gneiss, Adirondack Mountains, NY—Implications for the nature and timing of Mesoproterozoic plutonism, metamorphism, and deformation: Precambrian Research, v. 358, no. 106112, 37 p. [Also available at https://doi.org/10.1016/j.precamres.2021.106112.]

Aleinikoff, J.N., Walsh, G.J., and Vervoort, J.D., 2018, SHRIMP U-Pb ages of zircon and monazite, and garnet Lu-Hf ages in anorthosite of the Marcy massif, Adirondack Highlands, NY—Recognizing inherited, igneous, and metamorphic components [abs.]: Geological Society of America Abstracts with Programs, v. 50, no. 2. [Also available at https://doi.org/10.1130/abs/2018NE-310391.]

Alling, H.L., 1918, The Adirondack graphite deposits: New York State Museum Bulletin 199, 150 p.

Amidon, W.H., Kylander-Clark, A.R.C., Barr, M.N., Graf, S.F.I., and West, D.P., Jr., 2022, Pace of passive margin tectonism revealed by U-Pb dating of fracture-filling calcite: Nature Communications, v. 13, no. 1953, 9 p. [Also available at https://doi.org/10.1038/s41467-022-29680-z.]

Amidon, W.H., Roden-Tice, M., Anderson, A.J., McKeon, R.E., and Shuster, D.L., 2016, Late Cretaceous unroofing of the White Mountains, New Hampshire, USA—An episode of passive margin rejuvenation?: Geology, v. 44, no. 6, p. 415–418. [Also available at https://doi.org/10.1130/G37429.1.]

Ashwal, L.D., 1983, Anorthosites: Springer-Verlag, Berlin, Germany, 422 p.

Ashwal, L.D., and Bybee, G.M., 2017, Crustal evolution and the temporality of anorthosites: Earth-Science Reviews, v. 173, p. 307–330. [Also available at https://doi.org/10.1016/j.earscirev.2017.09.002.]

Balk, R., 1931, Structural geology of the Adirondack anorthosite—A structural study of the problem of magmatic differentiation: Journal of Crystallography, Mineralogy and Petrography, v. 41, p. 308–434 [Also available at https://doi.org/10.1007/BF02938750.]

Barker, E.E., 1942, The story of Crown Point iron: New York History, v. 23, no. 4, p. 419–436. [Also available at https://www.jstor.org/stable/23134763.]

Barker, F., 1979, Trondhjemite—Definition, environment and hypotheses of origin, chap. 1 *of* Barker, F., ed., Trondhjemites, dacites, and related rocks: Elsevier, Amsterdam, Netherlands, v. 6, p. 1–12.

Bastin, E.S., 1909, Graphite, *in* Mineral resources of the United States, calendar year 1908, Part II—Nonmetallic products: U.S. Geological Survey, Mineral Resources of the United States, p. 717–738.

Bickford, M.E., McLelland, J.M., Selleck, B.W., Hill, B.M., and Heumann, H.J., 2008, Timing of anatexis in the eastern Adirondack Highlands—Implications for tectonic evolution during ca. 1050 Ma Ottawan orogenesis: Geological Society of America Bulletin, v. 120, nos. 7–8, p. 950–961 [Also available at https://doi.org/10.1130/B26309.1.]

Black, L.P., Kamo, S.L., Allen, C.M., Davis, D.W., Aleinikoff, J.N., Valley, J.W., Mundil, R., Campbell, I.H., Korsuch, R.J., Williams, I.S., and Foudoulis, C., 2004, Improved $^{206}Pb/^{238}U$ microprobe geochronology by the monitoring of a trace-element-related matrix effect; SHRIMP, ID-TIMS, ELA-ICP-MS and oxygen isotope documentation for a series of zircon standards: Chemical Geology, v. 205, nos. 1–2, p. 115–140, accessed January 24, 2025, at https://doi.org/10.1016/j.chemgeo.2004.01.003.

Bohlen, S.R., Valley, J.W., and Essene, E.J., 1985, Metamorphism in the Adirondacks—I. Petrology, pressure and temperature: Journal of Petrology, v. 26, no. 4, p. 971–992, accessed January 24, 2025, at https://doi.org/10.1093/petrology/26.4.971.

Brown, C.E., 1979, Differential deformation of the Grenville Complex and its basement in St. Lawrence County, New York, *in* Geological Survey research 1979: U.S. Geological Survey Professional Paper 1150, p. 59. [Also available at https://doi.org/10.3133/pp1150.]

Brown, C.E., 1988, Geology of the Birch Creek area, St. Lawrence County, New York: U.S. Geological Survey Miscellaneous Investigations Series Map I–1645, 1 sheet, scale 1:12,000. [Also available at https://doi.org/10.3133/i1645.]

Brown, C.E., 1989, Geologic map of the Beaver Creek area in the Grenville lowlands, St. Lawrence County, New York: U.S. Geological Survey Miscellaneous Investigations Series Map I–1725, 1 sheet, scale 1:18,000, 7-p. pamphlet. [Also available at https://doi.org/10.3133/i1725.]

Brown, C.E., and Ayuso, R.A., 1985, Significance of tourmaline-rich rocks in the Grenville Complex of St. Lawrence County, New York: U.S. Geological Survey Bulletin 1626–C, Contributions to the Geology of Mineral Deposits, p. C1–C33. [Also available at https://doi.org/10.3133/b1626C.]

Buddington, A.F., 1939, Adirondack igneous rocks and their metamorphism: Geological Society of America Memoir, v. 7, 354 p. [Also available at https://doi.org/10.1130/MEM7-p1.]

Buddington, A.F., and Leonard, B.F., 1962, Regional geology of the St. Lawrence County magnetite district, northwest Adirondacks, New York: U.S. Geological Survey Professional Paper 376, 145 p., 4 pls. in pocket, scales 1:62,500 and 1:500,000 [plates 1 and 3]. [Also available at https://doi.org/10.3133/pp376.]

Burton, W.C., and Southworth, S., 2010, A model for Iapetan rifting of Laurentia based on Neoproterozoic dikes and related rocks, *in* Tollo, R.P., Bartholomew, M.J., Hibbard, J.P., and Karabinos, P.M., eds., From Rodinia to Pangea—The lithotectonic record of the Appalachian region: Geological Society of America Memoir 206, p. 455–476, accessed April 12, 2021, at https://doi.org/10.1130/2010.1206(20).

Cerny, P., and Ercit, T.S., 2005, The classification of granitic pegmatites revisited: The Canadian Mineralogist, v. 43, no. 6, p. 2005–2026. [Also available at https://doi.org/10.2113/gscanmin.43.6.2005.]

Chiarenzelli, J., Kratzmann, D., Selleck, B., and deLorraine, W., 2015, Age and provenance of Grenville supergroup rocks, Trans-Adirondack basin, constrained by detrital zircons: Geology, v. 43, no. 2, p. 183–186, accessed April 13, 2021, at https://doi.org/10.1130/G36372.1.

Chiarenzelli, J., and Regan, S., 2015, Recent developments in the understanding of the geology of the Adirondack Lowlands: St. Lawrence University Geology Alumni Conference IX, Canton, N.Y., Sept. 25–27, 2015, Canton, N.Y., St. Lawrence University, 22 p., accessed April 8, 2019, at http://it.stlawu.edu/~geoclub/alumni/SLUGACIX-FieldGuide.pdf.

Chiarenzelli, J.R., Selleck, B., Lupulescu, M., Regan, S., Bickford, M.E., Valley, P., and McLelland, J., 2017, Lyon Mountain ferroan leucogranite suite—Magmatic response to extensional thinning of overthickened crust in the core of the Grenville orogeny: Geological Society of America Bulletin, v. 129, nos. 11–12, p. 1472–1488. [Also available at https://doi.org/10.1130/B31697.1.]

Coble, M.A., Vazquez, J.A., Barth, A.P., Wooden, J., Burns, D., Kylander□Clark, A., Jackson, S., and Vennari, C.E., 2018, Trace element characterisation of MAD□559 zircon reference material for ion microprobe analysis: Geostandards and Geoanalytical Research, v. 42, no. 4, p. 481–497. [Also available at https://doi.org/10.1111/ggr.12238.]

Coish, R.A., and Sinton, C.W., 1992, Geochemistry of mafic dikes in the Adirondack Mountains—Implications for late Proterozoic continental rifting: Contributions to Mineralogy and Petrology, v. 110, p. 500–514. [Also available at https://doi.org/10.1007/BF00344084.]

Crosby, P., 1969, Petrogenetic and statistical implications of modal studies of Adirondack anorthosite, *in* Isachsen, Y.W., ed., Origin of anorthosite and related rocks: New York State Museum Memoir 18, p. 289–303.

Cushing, H.P., 1898, Syenite porphyry dikes in the northern Adirondacks: Geological Society of America Bulletin, v. 9, no. 1, p. 239–256. [Also available at https://doi.org/10.1130/GSAB-9-239.]

Cushing, H.P., 1917, Structure of the anorthosite body in the Adirondacks: Journal of Geology, v. 25, no. 6, p. 501–509. [Also available at https://www.jstor.org/stable/30062032.]

Davidson, A., 1998, Geological map of the Grenville province, Canada and adjacent parts of the United States of America: Geological Survey of Canada Map 1947A, 2 sheets, scale 1:2,000,000. [Also available at https://doi.org/10.4095/210351.]

Davis, W.J., Pestaj, T., Rayner, N., and McNicoll, V.M., 2019, Long-term reproducibility of $^{207}Pb/^{206}Pb$ age at the GSC SHRIMP lab based on the GSC Archean reference zircon z1242: Geological Survey of Canada, Scientific Presentation 111, 1 poster, accessed January 25, 2025, at https://doi.org/10.4095/321203.

DeLucia, M.S., Guenthner, W.R., Marshak, S., Thomson, S.N., and Ault, A.K., 2017, Thermochronology links denudation of the Great Unconformity surface to the supercontinental cycle and snowball Earth: Geology, v. 46, no. 2, p. 167–170. [Also available at https://doi.org/10.1130/G39525.1.]

de Waard, D., 1965, The occurrence of garnet in the granulite-facies terrane of the Adirondack highlands: Journal of Petrology, v. 6, no. 1, p. 165–191. [Also available at https://doi.org/10.1093/petrology/6.1.165.]

de Waard, D., and Walton, M., 1967, Precambrian geology of the Adirondack highlands, a reinterpretation: Geological Review, v. 56, p. 596–629. [Also available at https://doi.org/10.1007/BF01848745.]

Dicken, C.L., Nicholson, S.W., Horton, J.D., Kinney, S.A., Gunther, G., Foose, M.P., and Mueller, J.A.L., 2005, Preliminary integrated geologic map databases for the United States—Delaware, Maryland, New York, Pennsylvania, and Virginia (ver. 1.0): U.S. Geological Survey Open-File Report 2005–1325, scale 1:250,000. [Also available at https://pubs.er.usgs.gov/publication/ofr20051325.]

Eby, G.N., 1992, Chemical subdivision of the A-type granitoids—Petrogenetic and tectonic implications: Geology, v. 20, no. 7, p. 641–644. [Also available at https://doi.org/10.1130/0091-7613(1992)020<0641:CSOTAT>2.3.CO;2.]

Emslie, R.F., 1978, Anorthosite massifs, rapakivi granites, and late Proterozoic rifting of North America: Precambrian Research, v. 7, no. 1, p. 61–98. [Also available at https://doi.org/10.1016/0301-9268(78)90005-0.]

Farrell, P.F., 1996, Through the light hole—A saga of Adirondack mines and men: Utica, N.Y., North Country Books, 291 p.

Foose, M.P., and McLelland, J.M., 1995, Proterozoic low-Ti iron-oxide deposits in New York and New Jersey—Relation to Fe-oxide (Cu-U-Au-rare element) deposits and tectonic implications: Geology, v. 23, no. 7, p. 665–668. [Also available at https://doi.org/10.1130/0091-7613(1996)024<0475:PLTIOD>2.3.CO;2.]

Force, E.R., Grosz, A.E., Loferski, P.J., and Maybin, A.H., 1982, Aeroradioactivity maps in heavy-mineral exploration—Charleston, South Carolina, area: U.S. Geological Survey Professional Paper 1218, 19 p., 2 pls., scale 1:500,000. [Also available at https://doi.org/10.3133/pp1218.]

Frost, B.R., Barnes, C.G., Collins, W.J., Arculus, R.J., Ellis, D.J., and Frost, C.D., 2001, A geochemical classification for granitic rocks: Journal of Petrology, v. 42, no. 11, p. 2033–2048. [Also available at https://doi.org/10.1093/petrology/42.11.2033.]

Frost, B.R., and Frost, C.D., 2008a, On charnockites: Gondwana Research, v. 13, p. 30–44. [Also available at https://www.uwyo.edu/geolgeophys/people/faculty/cfrost/_files/docs/2008-frost2-gondwana.pdf.]

Frost, B.R., and Frost, C.D., 2008b, A geochemical classification for feldspathic igneous rocks: Journal of Petrology, v. 49, no. 11, p. 1955–1969, accessed December 13, 2022, at https://doi.org/10.1093/petrology/egn054.

Geer, P.S., 2020, Magnetite mineralization of the Hammondville pluton—Poly-phase Kiruna type IOCG magnetite-apatite deposits in the Lyon Mountain Granite: Amherst, Mass., University of Massachusetts Amherst, M.S. thesis, 101 p., accessed December 16, 2022, at https://doi.org/10.7275/19182236.

Hamilton, M.A., McLelland, J., and Selleck, B., 2004, SHRIMP U-Pb zircon geochronology of the anorthosite-mangerite-charnockite-granite suite, Adirondack Mountains, New York—Ages of emplacement and metamorphism, *in* Tollo, R.P., Corriveau, L., McLelland, J., and Bartholomew, M.J., eds., Proterozoic tectonic evolution of the Grenville orogen in North America: Geological Society of America Memoir 197, p. 337–355. [Also available at https://doi.org/10.1130/0-8137-1197-5.337.]

Heumann, M.J., Bickford, M.E., Hill, B.M., Selleck, B.W., and Jercinovic, M.J., 2006, Timing of anatexis in metapelites from the Adirondack Lowlands and Southern Highlands—Manifestation of the Shawinigan orogeny and subsequent anorthosite-mangerite-charnockite-granite (AMCG) magmatism: Geological Society of America Bulletin, v. 118, p. 1283–1298. [Also available at https://doi.org/10.1130/B25927.1.]

Hibbard, J.P., van Staal, C.R., Rankin, D.W., and Williams, H., 2006, Lithotectonic map of the Appalachian Orogen, Canada-United States of America: Geological Survey of Canada Map 2096A, 2 sheets, scale 1:1,500,000. [Also available at https://ngmdb.usgs.gov/Prodesc/proddesc_81463.htm.]

Hoskin, P.W.O., and Schaltegger, U., 2003, The composition of zircon and igneous and metamorphic petrogenesis, *in* Hanchar, J.M., and Hoskin, P.W.O., eds., Zircon: Washington, D.C., Mineralogical Society of America, Reviews in Mineralogy and Geochemistry, v. 53, p. 27–62. [Also available at https://doi.org/10.1515/9781501509322-005.]

Hyndman, D.W., 1972, Petrology of igneous and metamorphic rocks: McGraw-Hill, New York, 533 p.

Isachsen, Y.W., 1981, Contemporary doming of the Adirondack Mountains—Further evidence from releveling: Developments in Geotectonics, v. 16, p. 95–96, accessed April 13, 2021, at https://doi.org/10.1016/B978-0-444-41953-8.50016-5.]

Isachsen, Y.W., and Fisher, D.W., 1970, Geologic map of New York—Adirondack sheet: New York State Museum, Map and Chart Series 15, 1 sheet, scale 1:250,000. [Also available at http://www.nysm.nysed.gov/staff-publications/geologic-map-new-york-adirondack-sheet-1250000.]

Isachsen, Y.W., Kelly, W.M., Sinton, C., Coish, R.A., and Heisler, M.T., 1988, Dikes of the northeast Adirondack region—Introduction to their distribution, orientation, mineralogy, chronology, magmatism, chemistry, and mystery, *in* Isachsen, Y.W., ed., New York State Geological Association 60th Annual Meeting field trip guidebook: Albany, N.Y., New York State Geological Association, p. 215–243.

Kamo, S.L., Krogh, T.E., and Kumarapeli, P.S., 1995, Age of the Grenville dyke swarm, Ontario-Quebec—Implications for the timing of Iapetan rifting: Canadian Journal of Earth Sciences, v. 32, p. 273–280. [Also available at https://cdnsciencepub.com/doi/pdf/10.1139/e95-022.]

Kemp, J.F., 1898, Geology of the magnetites near Port Henry, N.Y. and especially those of Mineville: Transactions of the American Institute of Mining and Engineers, v. 27, p. 146–203.

Kemp, J.F., and Alling, H.L., 1925, Geology of the Ausable quadrangle, New York: New York State Museum Bulletin 261, 126 p., map scale 1:62,500.

Kemp, J.F., and Marsters, V.F., 1893, The trap dikes of the Lake Champlain region: U.S. Geological Survey Bulletin 107, 62 p. [Also available at https://doi.org/10.3133/b107.]

Krestianinov, E., Amelin, Y., Neymark, L.A., and Aleinikoff, J.N., 2021, U-Pb systematics of uranium-rich apatite from Adirondacks—Inferences about regional geological and geochemical evolution, and evaluation of apatite reference materials for in situ dating: Chemical Geology, v. 581, no. 120417, accessed August 25, 2022, at https://doi.org/10.1016/j.chemgeo.2021.120417.

Landing, E., 2012, The great American carbonate bank in eastern Laurentia—Its births, deaths, and linkage to paleooceanic oxygenation (Early Cambrian-Late Ordovician), *in* Derby, J., Fritz, R., Longacre, S., Morgan, W., and Sternbach, C., eds., The great American carbonate bank—The geology and economic resources of the Cambrian–Ordovician Sauk megasequence of Laurentia: American Association of Petroleum Geologists Memoir 98, p. 451–492.

Le Bas, M.J., Le Maitre, R.W., Streckeisen, A., and Zanettin, B., 1986, A chemical classification of volcanic rocks based on the total alkali-silica diagram: Journal of Petrology, v. 27, no. 3, p. 745–750. [Also available at https://doi.org/10.1093/petrology/27.3.745.]

Le Bas, M.J., and Streckeisen, A.L., 1991, The IUGS systematics of igneous rocks: Journal of the Geological Society, v. 148, no. 5, p. 825–833. [Also available at https://doi.org/10.1144/gsjgs.148.5.0825.]

Ludwig, K.R., 2009, SQUID 2, A user's manual (rev. 2.50): Berkeley Geochronology Center Special Publication 5, 110 p.

Lupulescu, M.V., 2018, An historical–economic description of several iron deposits from the Adirondack Region of New York, chap. 2 *in* Pickands, M., ed., Iron In New York: Albany, N.Y., The University of the State of New York, v. 8, p. 44–58, accessed February 15, 2023, at https://www.nysm.nysed.gov/staff-publications/iron-new-york.

Lupulescu, M.V., Chiarenzelli, J.R., and Bailey, D.G., 2012, Mineralogy, classification, and tectonic setting of the granitic pegmatites of New York State, USA: The Canadian Mineralogist, v. 50, no. 6, p. 1713–1728, accessed April 14, 2021, at https://doi.org/10.3749/canmin.50.6.1713.

Lupulescu, M.V., Chiarenzelli, J.R., Pullen, A.T., and Price, J.D., 2011, Using pegmatite geochronology to constrain temporal events in the Adirondack Mountains: Geosphere, v. 7, no. 1, p. 23–39, accessed April 14, 2021, at https://doi.org/10.1130/GES00596.1.

Maniar, P.D., and Piccoli, P.M., 1989, Tectonic discrimination of granitoids: Geological Society of America Bulletin, v. 101, no. 5, p. 635–643. [Also available at https://doi.org/10.1130/0016-7606(1989)101<0635:TDOG>2.3.CO;2.]

Martin, R.F., 2012, The petrogenesis of anorogenic felsic magmas and AMCG suites—Insights on element mobility and mutual cryptic contamination from polythermal experiment: Lithos, v. 151, p. 35–45, accessed January 25, 2025, at https://doi.org/10.1016/j.lithos.2011.12.016.

McAleer, R.J., Jubb, A.M., Hackley, P.C., Walsh, G.J., Merschat, A.J., Regan, S.P., Burton, W.C., and Vazquez, J.A., 2020, Photoluminescence imaging of whole zircon grains on a petrographic microscope—An underused aide for geochronologic studies: Minerals, v. 10, no. 10, accessed December 13, 2022, at https://doi.org/10.3390/min10100876.

McCafferty, A.E., Stoeser, D.B., and Van Gosen, B.S., 2014, Geophysical interpretation of U, Th, and rare earth element mineralization of the Bokan Mountain peralkaline granite complex, Prince of Wales Island, southeast Alaska: Interpretation, v. 2, no. 4, p. SJ47–SJ63. [Also available at https://doi.org/10.1190/INT-2014-0010.1.]

McLelland, J., Ashwal, L., and Moore, L., 1994, Composition and petrogenesis of oxide-, apatite-rich gabbronorites associated with Proterozoic anorthosite massifs—Examples from the Adirondack Mountains, New York: Contributions to Mineralogy and Petrology, v. 116, p. 225–238, accessed December 13, 2022, at https://doi.org/10.1007/BF00310702.

McLelland, J., Chiarenzelli, J., and McLelland, J., 2016, The intrusion breccia in the valley of Roaring Brook, Giant Mountain, Adirondack Highlands, New York—A modern interpretation: Geosphere, v. 12, no. 2, p. 572–584, accessed June 6, 2023, at https://doi.org/10.1130/GES01260.1.

McLelland, J., Chiarenzelli, J., Whitney, P., and Isachsen, Y., 1988a, U-Pb zircon geochronology of the Adirondack Mountains and implications for their geologic evolution: Geology, v. 16, no. 10, p. 920–924, accessed April 14, 2021, at https://doi.org/10.1130/0091-7613(1988)016<0920:UPZGOT>2.3.CO;2.

McLelland, J., Lochhead, A., and Vyhnal, C., 1988b, Evidence for multiple metamorphic events in the Adirondack Mountains, N.Y.: Journal of Geology, v. 96, no. 3, p. 279–298. [Also available at https://www.jstor.org/stable/30068728.]

McLelland, J., Morrison, J., Selleck, B., Cunningham, B., Olson, C., and Schmidt, K., 2002, Hydrothermal alteration of late- to post-tectonic Lyon Mountain Granitic Gneiss, Adirondack Mountains, New York—Origin of quartz-sillimanite segregations, quartz-albite lithologies, and associated Kiruna-type low-Ti Fe-oxide deposits: Journal of Metamorphic Geology, v. 20, no. 1, p. 175–190. [Also available at https://doi.org/10.1046/j.0263-4929.2001.00345.x.]

McLelland, J., Wong, M., Grover, T., Willliams, M., and Jercinovic, M., 2011, Geology and geochronology of the eastern Adirondacks, Trip B–2, *in* West, D.P., Jr., ed., Guidebook for field trips in Vermont and adjacent New York: New England Intercollegiate Geological Conference, 103rd Annual Meeting, Middlebury, Vt., Sept. 29 to Oct. 1, 2011, Middlebury, Vt., Middlebury College, p. B2–1 to B2–19.

McLelland, J.M., Bickford, M.E., Hill, B.M., Clechenko, C.C., Valley, J.W., and Hamilton, M.A., 2004, Direct dating of Adirondack massif anorthosite by U-Pb SHRIMP analysis of igneous zircon—Implications for AMCG complexes: Geological Society America Bulletin, v. 116, nos. 11–12, p. 1299–1317, accessed April 14, 2021, at https://doi.org/10.1130/B25482.1.

McLelland, J.M., Hamilton, M., Selleck, B.W., McLelland, J., Walker, D., and Orrell, S., 2001, Zircon U-Pb geochronology of the Ottawan orogeny, Adirondack Highlands, New York—Regional and tectonic implications: Precambrian Research, v. 109, nos. 1–2, p. 39–72, accessed April 14, 2021, at https://doi.org/10.1016/S0301-9268(01)00141-3.

McLelland, J.M., Selleck, B.W., and Bickford, M.E., 2013, Tectonic evolution of the Adirondack Mountains and Grenville orogen inliers within the USA: Geoscience Canada, Harold Williams series, v. 40, no. 4, p. 318–352, accessed April 14, 2021, at https://doi.org/10.12789/geocanj.2013.40.022.

Meleik, M.L., Fouad, K.M., Wassef, S.N., Ammar, A.A., and Dabbour, G.A., 1978, Aerial and ground radiometry in relation to the sedimentation of radioactive minerals in the Damietta beach sands, Egypt: Economic Geology, v. 73, no. 8, p. 1738–1748, accessed April 14, 2021, at https://doi.org/10.2113/gsecongeo.73.8.1738.

Miller, W.J., 1918, Adirondack anorthosite: Geological Society of America Bulletin, v. 29, no. 1, p. 399–462. [Also available at https://doi.org/10.1130/GSAB-29-399.]

Miller, W.J., 1919a, Geology of the Lake Placid quadrangle: New York State Museum Bulletin 211–212, 106 p. [Also available at http://purl.org/net/nysl/nysdocs/2583156.]

Miller, W.J., 1919b, Magnetic iron ores of the Clinton County, New York: Economic Geology, v. 14, no. 7, p. 509–535. [Also available at https://doi.org/10.2113/gsecongeo.14.7.509.]

Miller, W.J., 1926, Geology of the Lyon Mountain quadrangle: New York State Museum Bulletin 271, 101 p.

Mineral Resources Data System, 2005, Mineral Resources Data System [MRDS], edition 20160315: U.S. Geological Survey database, accessed July 10, 2019, at https://mrdata.usgs.gov/mrds/.

Morse, S.A., 1968, Layered intrusions and anorthosite genesis, *in* Isachsen, Y.W., ed., Origin of anorthosite and related rocks: New York State Museum and Science Service Memoir 18, p. 175–188.

Murphy, J.B., Shellnutt, J.G., and Collins, J.C., 2018, Late Neoproterozoic to Carboniferous genesis of A-type magmas in Avalonia of northern Nova Scotia—Repeated partial melting of anhydrous lower crust in contrasting tectonic environments: International Journal of Earth Sciences, v. 107, p. 587–599. [Also available at https://doi.org/10.1007/s00531-017-1512-7.]

Newland, D.H., 1921, The mineral resources of the State of New York: New York State Museum Bulletin 223–224, p. 69–76.

Newland, D.H., and Kemp, J.F., 1908, Geology of the Adirondack magnetic iron ores, with a report on the Mineville-Port Henry mine group: New York State Museum Bulletin 119, 182 p.

North American Commission on Stratigraphic Nomenclature, 2021, North American stratigraphic code: Stratigraphy, v. 18, no. 3, p. 153–204, accessed April 14, 2021, at https://www.micropress.org/microaccess/stratigraphy/issue-372/article-2251.

Northey, W.C., 1940, Letter to E. Eugene Barker, 30 September 1940, reprinted under the title “Former Engineer Describes Hammondville Ore Mines”: Ticonderoga, New York, Ticonderoga Sentinel, July 5, 1962, p. 7, accessed January 23, 2023, at https://nyshistoricnewspapers.org.

O’Connor, J.T., 1965, A classification for quartz-rich igneous rocks based on feldspar ratios: U.S. Geological Survey Professional Paper 0525–B, p. B79–B84. [Also available at https://doi.org/10.3133/pp525B.]

Ogilvie, I.H., 1905, Geology of the Paradox Lake quadrangle, New York: New York State Museum Bulletin 96, p. 461–516, 1 sheet in pocket, scale 1:62,500.

Parsons, I., Thompson, P., Lee, M.R., and Cayzer, N., 2005, Alkali feldspar microtextures as provenance indicators in siliciclastic rocks and their role in feldspar dissolution during transport and diagenesis: Journal of Sedimentary Research, v. 75, no. 5, p. 921–942, accessed April 14, 2021, at https://doi.org/10.2110/jsr.2005.071.

Passchier, C.W., Myers, J.S., and Kröner, A., 1990, Field geology of high-grade gneiss terranes: Heidelberg, Germany, Springer-Verlag, 150 p.

Pearce, J.A., Harris, N.B.W., and Tingle, A.G., 1984, Trace element discrimination diagrams for the tectonic interpretation of granitic rocks: Journal of Petrology, v. 25, no. 4, p. 956–983. [Also available at https://doi.org/10.1093/petrology/25.4.956.]

Peck, W.H., Bickford, M.E., McLelland, J.M., Nagle, A.N., and Swarr, G.J., 2010, Mechanism of metamorphic zircon growth in a granulite-facies quartzite, Adirondack Highlands, Grenville Province, New York: American Mineralogist, v. 95, nos. 11–12, p. 1796–1806. [Also available at https://doi.org/10.2138/am.2010.3547.]

Peck, W.H., Quinan, M.P., and Selleck, B.W., 2019, Detrital zircon constraints on Grenville sedimentation at the margin of Laurentia: Precambrian Research, v. 331, article 105342. [Also available at https://doi.org/10.1016/j.precamres.2019.105342.]

Peck, W.H., Selleck, B.W., Regan, S.P., Howard, G.E., and Kozel, O.O., 2018, In-situ dating of metamorphism in Adirondack anorthosite: American Mineralogist, v. 103, no. 10, p. 1523–1529. [Also available at https://doi.org/10.2138/am-2018-6481.]

Peters, S.E., and Gaines, R.R., 2012, Formation of the "Great Unconformity" as a trigger for the Cambrian explosion: Nature, v. 484, p. 363–366. [Also available at https://doi.org/10.1038/nature10969.]

Pickands, M., 2018, Preface to iron in New York, *in* Pickands, M., ed., Iron in New York: New York State Museum Record No. 8, p. xiii–xv, accessed February 15, 2023, at http://www.nysm.nysed.gov/staff-publications/iron-new-york.

Pope, C., 1971, Hammondville—Essex County ghost town: York State Tradition, v. 25, no. 1, p. 33–44.

Postel, A.W., 1951, Geology of the Dannemora quadrangle, New York: U.S. Geological Survey Geologic Quadrangle Map GQ–14, 1 sheet, scale 1:62,500. [Also available at https://pubs.er.usgs.gov/publication/gq14.]

Postel, A.W., 1952, Geology of Clinton County magnetite district, New York: U.S. Geological Survey Professional Paper 237, 88 p., 3 pls. in pocket, map scale 1:62,500. [Also available at https://doi.org/10.3133/pp237.]

Ramsay, J.G., 1962, Interference patterns produced by the superposition of folds of "similar" type: Journal of Geology, v. 60, no. 4, p. 466–481. [Also available at https://doi.org/10.1086/626837.]

Ramsay, J.G., 1967, Folding and fracturing of rocks: New York, N.Y., McGraw-Hill, 568 p.

Ratcliffe, N.M., Aleinikoff, J.N., Burton, W.C., and Karabinos, P.A., 1991, Trondhjemitic 1.35–1.31 Ga gneisses of the Mount Holly Complex of Vermont—Evidence for an Elzevirian event in the Grenville basement of the United States Appalachians: Canadian Journal of Earth Sciences, v. 28, no. 1, p. 77–93. [Also available at https://doi.org/10.1139/e91-007.]

Ratcliffe, N.M., Stanley, R.S., Gale, M.H., Thompson, P.J., and Walsh, G.J., 2011, Bedrock geologic map of Vermont: U.S. Geological Survey Scientific Investigations Map 3184, 1 sheet, scale 1:100,000. [Also available at https://doi.org/10.3133/sim3184.]

Regan, S., Lupulescu, M., Jercinovic, M., Chiarenzelli, J., Williams, M., Singer, J., and Bailey, D., 2019b, Age and origin of monazite symplectite in an iron oxide-apatite deposit in the Adirondack Mountains, New York, USA—Implications for tracking fluid conditions: Minerals, v. 9, no. 1, 17 p., accessed April 15, 2021, at https://doi.org/10.3390/min9010065.

Regan, S.P., Chiarenzelli, J.R., McLelland, J.M., and Cousens, B.L., 2011, Evidence for an enriched asthenospheric source for coronitic metagabbros in the Adirondack Highlands: Geosphere, v. 7, no. 3, p. 694–709. [Also available at https://doi.org/10.1130/GES00629.1.]

Regan, S.P., Geer, P.S., Walsh, G.J., Aleinikoff, J.N., Baird, G.B., Valley, P.M., Williams, M.L., Jercinovic, M.J., and Grover, T.W., 2015, Precambrian geology of the Eagle Lake quadrangle, Essex County, New York, *in* Franzi, D., ed., Geology of the Northeastern Adirondack Mountains and Champlain-St. Lawrence Lowlands of New York, Vermont and Quebec: New York State Geological Association, 87th Annual Meeting, Plattsburgh, N.Y., Sept. 12–13, 2015, Field Trip Guidebook, Plattsburgh, N.Y., State University of New York at Plattsburgh, p. 30–59.

Regan, S.P., Walsh, G.J., Williams, M.L., Chiarenzelli, J.R., Toft, M., and McAleer, R., 2019a, Syn-collisional exhumation of hot middle crust in the Adirondack Mountains (New York, USA)—Implications for extensional orogenesis in the southern Grenville province: Geosphere, v. 15, no. 4, p. 1240–1261, accessed April 15, 2021, at https://doi.org/10.1130/GES02029.1.

Rickard, L.V., Isachsen, Y.W., and Fisher, D.W., 1970, Geologic map of New York: New York State Museum, Map and Chart Series 15, 6 sheets, scale 1:250,000. [Also available at https://ngmdb.usgs.gov/Prodesc/proddesc_98670.htm.]

Rivers, T., 2012, Upper-crustal orogenic lid and mid-crustal core complexes—Signature of a collapsed orogenic plateau in the hinterland of the Grenville province: Canadian Journal of Earth Science, v. 49, no. 1, p. 1–42, accessed April 15, 2021, at https://doi.org/10.1139/E11-014.

Rivers, T., 2015, Tectonic setting and evolution of the Grenville Orogen—An assessment of progress over the last 40 Years: Geoscience Canada, v. 42, no. 1, p. 77–124, accessed April 15, 2021, at https://doi.org/10.12789/geocanj.2014.41.057.

Robbins, L.S., and Amidon, W.H., 2018, Evaluating geochemical signatures and tectonic implications of calcite veins within the Champlain Valley, VT [abs.]: Geological Society of America Abstracts with Programs, v. 50, no 2. [Also available at https://doi.org/10.1130/abs/2018NE-311357.]

Roden-Tice, M.K., and Tice, S.J., 2005, Regional-scale mid-Jurassic to Late Cretaceous unroofing from the Adirondack Mountains through central New England based on apatite fission-track and (U-Th)/He thermochronology: Journal of Geology, v. 113, no. 5, p. 535–552. [Also available at https://doi.org/10.1086/431908.]

Roden-Tice, M.K., Tice, S.J., and Schofield, I.S., 2000, Evidence for differential unroofing in the Adirondack Mountains, New York State, determined by apatite fission-track thermochronology: Journal of Geology, v. 108, no. 2, p. 155–169. [Also available at https://doi.org/10.1086/314395.]

Rowley, E.B., 1962a, Rare-earth pegmatite discovered in Adirondack Mountain area, Essex County, New York: Rocks & Minerals, v. 37, nos. 7–8, p. 341–347, accessed October 14, 2022, at https://doi.org/10.1080/00357529.1962.11766273.

Rowley, E.B., 1962b, Rare-earth pegmatite discovered in Adirondack Mountain area, Essex County, New York Part II: Rocks & Minerals, v. 37, nos. 9–10, p. 453–460, accessed October 14, 2022, at https://doi.org/10.1080/00357529.1962.11766306.

Salvini, F., 2016, DAISY 3—The structural data integrated system analyser (version 5.08-9): Rome, Italy, Roma Tre University, Department of Geological Sciences.

Salvini, F., Billi, A., and Wise, D.U., 1999, Strike-slip fault-propagation cleavage in carbonate rocks—The Mattinata fault zone, Southern Apennines, Italy: Journal of Structural Geology, v. 21, no. 12, p. 1731–1749. [Also available at https://doi.org/10.1016/S0191-8141(99)00120-0.]

Selleck, B.W., McLelland, J.M., and Bickford, M.E., 2005, Granite emplacement during tectonic exhumation—The Adirondack example: Geology, v. 33, no. 10, p. 781–784, accessed April 15, 2021, at https://doi.org/10.1130/G21631.1.

Seman, S., Stock, D.F., and McLean, N.M., 2017, U-Pb geochronology of grossular-andradite garnet: Chemical Geology, v. 460, p. 106–116, accessed July 12, 2018, at https://doi.org/10.1016/j.chemgeo.2017.04.020.

Shah, A.K., 2016, Airborne geophysical surveys over the eastern Adirondacks, New York State: U.S. Geological Survey data release, accessed April 16, 2021, at https://doi.org/10.5066/F72R3PT0.

Shah, A.K., Bern, C.R., Van Gosen, B.S., Daniels, D.L., Benzel, W.M., Budahn, J.R., Ellefsen, K.J., Karst, A., and Davis, R., 2017, Rare earth mineral potential in the southeastern U.S. Coastal Plain from integrated geophysical, geochemical, and geological approaches: Geological Society of America Bulletin, v. 129, nos. 11–12, p. 1140–1157, accessed April 16, 2021, at https://doi.org/10.1130/B31481.1.

Shah, A.K., Taylor, R., Walsh, G., and Phillips, J., 2021, Integrated geophysical imaging of rare earth element-bearing iron oxide-apatite deposits in the eastern Adirondack Highlands, New York: Geophysics, v. 86, no. 1, p. B37–B54, accessed April 16, 2021, at https://doi.org/10.1190/geo2019-0783.1.

Shah, A.K., Walsh, G.J., Klein, A.J., and Suarez, K.A., 2019, Petrophysical data collected on outcrops and rock samples from the eastern Adirondack Highlands, New York: U.S. Geological Survey data release, accessed April 16, 2021, at https://doi.org/10.5066/P9E6P7S2.

Shand, S.J., 1951, Eruptive rocks—Their genesis, composition, classification, and their relation to ore-deposits, with a chapter on meteorites (4th ed.): New York, John Wiley & Sons, Inc., 488 p.

Singer, J.W., and Lupulescu, M.V., 2016, REE-rich fluorapatite textures from eastern Adirondack iron ore deposits [abs.]: Geological Society of America Abstracts with Programs, v. 48, no. 2, accessed March 30, 2016, at https://doi.org/10.1130/abs/2016NE-272533.

Spear, F.S., and Markussen, J.C., 1997, Mineral zoning, P-T-X-M phase relations, and metamorphic evolution of some Adirondack granulites: Journal of Petrology, v. 38, no. 6, p. 757–783, accessed March 9, 2022, at https://doi.org/10.1093/petroj/38.6.757.

Sportman, S.P., 2011, Halcyon days—The historical archaeology of community and identity, 1870–1900: Storrs, Conn., University of Connecticut, Ph.D. dissertation, 444 p. [Also available at https://digitalcommons.lib.uconn.edu/dissertations/AAI3476610.]

Storm, L.C., and Spear, F.S., 2005, Pressure, temperature and cooling rates of granulite facies migmatitic pelites from the southern Adirondack Highlands, New York: Journal of Metamorphic Geology, v. 23, no. 2, p. 107–130, accessed April 16, 2021, at https://doi.org/10.1111/j.1525-1314.2005.00565.x.

Streckeisen, A., 1976, To each plutonic rock its proper name: Earth-Science Reviews, v. 12, no. 1, p. 1–33, accessed July 7, 2023, at https://doi.org/10.1016/0012-8252(76)90052-0.

Suarez, K.A, Walsh, G.J., and Tjapkes, D.J., 2025b, Whole rock and portable XRF geochemistry data from Mesoproterozoic granitic rocks in the eastern Adirondack Mountains, New York: U.S. Geological Survey data release, https://doi.org/10.5066/P1XP5HHS.

Suarez, K.A., Walsh, G.J., Williams, M.L., Jercinovic, M.J., Tjapkes, D.J., and Hillenbrand, I.W., 2023, Alteration mapping using geophysical and geochemical instrumentation—Implications for IOA and REE exploration [abs.]: Geological Society of America Abstracts with Programs, v. 55, no. 2, accessed April 24, 2023, at https://doi.org/10.1130/abs/2023SE-385700.

Suarez, K.A., Williams, M.L., Walsh, G.J., Harlov, D.E., Jercinovic, M.J., Tjapkes, D.J., and Hillenbrand, I.W., 2025a, Alteration mapping in granitic gneiss using handheld geophysical and geochemical instruments—Implications for IOA and REE exploration: Ore and Energy Resource Geology, v. 19, no. 100116, p. 1–16, accessed September 14, 2025, at https://doi.org/10.1016/j.oreoa.2025.100116.

Tan, L., 1966, Major pegmatite deposits of New York State: New York State Museum and Science Bulletin 408, 138 p.

Taylor, R.D., and Adams, D.T., 2019, Electron microprobe geochemistry of apatite crystals in the iron oxide-apatite ores of the Adirondack Mountains, New York, 2016–2017: U.S. Geological Survey data release, accessed January 25, 2025, at https://doi.org/10.5066/P9GVYTXB.

Taylor, R.D., Shah, A.K., Walsh, G.J., and Taylor, C.D., 2019, Geochemistry and geophysics of iron oxide-apatite deposits and associated waste piles with implications for potential rare earth element resources from ore and historic mine waste in the eastern Adirondack Highlands, New York, USA: Economic Geology, v. 114, no. 8, p. 1569–1598, accessed April 16, 2021, at https://doi.org/10.5382/econgeo.4689.

Valley, J.W., and O'Neil, J.R., 1981, $^{13}C/^{12}C$ exchange between calcite and graphite—A possible thermometer in Grenville marbles: Geochimica et Cosmochimica Acta, v. 45, no. 3, p. 411–419. [Also available at https://doi.org/10.1016/0016-7037(81)90249-0.]

Valley, P.M., Fisher, C.M., Hanchar, J.M., Lam, R., and Tubrett, M., 2010, Hafnium isotopes in zircon—A tracer of fluid-rock interaction during magnetite-apatite ("Kiruna-type") mineralization: Chemical Geology, v. 275, nos. 3–4, p. 208–220, accessed April 16, 2021, at https://doi.org/10.1016/j.chemgeo.2010.05.011.

Valley, P.M., Hanchar, J.M., and Whitehouse, M.J., 2009, Direct dating of Fe oxide-(Cu-Au) mineralization by U/Pb zircon geochronology: Geology, v. 37, no. 3, p. 223–226, accessed April 16, 2021, at https://doi.org/10.1130/G25439A.1.

Valley, P.M., Hanchar, J.M., and Whitehouse, M.J., 2011, New insights on the evolution of the Lyon Mountain Granite and associated Kiruna-type magnetite-apatite deposits, Adirondack Mountains, New York State: Geosphere, v. 7, no. 2, p. 357–389, accessed April 16, 2021, at https://doi.org/10.1130/GES00624.1.

Valley, P.M., Walsh, G.J., McAleer, R.J., Holm-Denoma, C., and Odom, W., 2023, Neoproterozoic dikes of the northeastern Adirondack Mountains [abs.]: Geological Society of America Abstracts with Programs, v. 55, no. 2, accessed November 21, 2023, at https://doi.org/10.1130/abs/2023SE-385695.

Vermeesch, P., 2018, IsoplotR—A free and open toolbox for geochronology: Geoscience Frontiers, v. 9, no. 5, p. 1479–1493, accessed January 24, 2025, at https://doi.org/10.1016/j.gsf.2018.04.001.

Walsh, G.J., Aleinikoff, J.N., and Ratcliffe, N.M., 2016, New U-Pb zircon ages and field studies support Shawinigan deformation in the eastern Adirondacks [abs.]: Geological Society of America Abstracts with Programs, v. 48, no. 2, accessed April 16, 2021, at https://doi.org/10.1130/abs/2016NE-272135.

Walsh, G.J., McAleer, R.J., Geer, P.S., and Regan, S.P., 2023, Whole rock geochemistry and uranium-lead isotopic data from Mesoproterozoic rocks in the Eagle Lake quadrangle, Essex County, New York: U.S. Geological Survey data release, accessed January 24, 2025, at https://doi.org/10.5066/P9BRVJSI.

Walsh, G.J., Orndorff, R.C., and McAleer, R.J., 2022, Bedrock geologic map of the Crown Point quadrangle, Essex County, New York, and Addison County, Vermont: U.S. Geological Survey Scientific Investigations Map 3491, 1 sheet, scale 1:24,000, 44-p. pamphlet [Also available at https://doi.org/10.3133/sim3491.]

Walsh, G.J., Regan, S.P., Geer, P.S., Merschat, A.J., Suarez, K.A., McAleer, R.J., Walton, M.S., Jr., and Crider, E.A., Jr., 2026, Database for the bedrock geologic map of the Eagle Lake quadrangle, Essex County, New York: U.S. Geological Survey data release, https://doi.org/10.5066/P9D6XYEL.

Walsh, G.J., and Walsh, M.C., 2023, Percent-slope map showing historical anthracite coal mining infrastructure at the north end of the Lackawanna syncline, Wayne, Susquehanna, and Lackawanna Counties, Pennsylvania: U.S. Geological Survey Scientific Investigations Map 3507, 1 sheet, scale 1:40,000, accessed January 24, 2025, at https://doi.org/10.3133/sim3507.

Walton, M.S., 1954, Draft geologic maps of the Paradox Lake northeast 1/4, Eagle Lake 7 1/2' quadrangle: New York State Geological Survey Open-File Reports 1g1377.1 and 1g1377.2, unpublished archived manuscript maps, scale 1:24,000.

Walton, M.S., 1960, Geologic map of the Eagle Lake quadrangle, NY: New York State Geological Survey Open-File Report 1g584, unpublished archived manuscript map, scale 1:24,000.

Walton, M.S., 1966, Explanation for bedrock maps of the Paradox Lake, Elizabethtown, Port Henry and Ticonderoga 15′ quadrangles, and contained 7-1/2′ quadrangles: New York State Geological Survey Open-File Report 1m4628, unpublished archived manuscript text, 47 p.

Walton, M.S., and de Waard, D., 1963, Orogenic evolution of the Precambrian in the Adirondack Highlands, a new synthesis: Koninklijke Nederlandse Akademie van Wetenschappen [Royal Dutch Academy of Sciences] Proceedings, ser. B, v. 66, no. 3, p. 98–106.

Wang, C., Slack, J.F., Shah, A.K., Yates, M.G., Lentz, D.R., Whittaker, A.T.H., and Marvinney, R.G., 2023, A recently discovered trachyte-hosted rare earth element-niobium-zirconium occurrence in northern Maine, USA: Economic Geology, v. 118, no. 1, p. 1–13, accessed January 24, 2025, at https://doi.org/10.5382/econgeo.4993.

Wasteneys, H., McLelland, J., and Lumbers, S., 1999, Precise zircon geochronology in the Adirondack Lowlands and implications for revising plate-tectonic models of the Central Metasedimentary Belt and Adirondack Mountains, Grenville Province, Ontario and New York: Canadian Journal of Earth Science, v. 36, no. 6, p. 967–984. [Also available at https://doi.org/10.1139/e99-020.]

Whalen, J.B., and Hildebrand, R.S., 2019, Trace element discrimination of arc, slab failure, and A-type granitic rocks: Lithos, v. 348–349, article 105179, accessed January 24, 2025, at https://doi.org/10.1016/j.lithos.2019.105179.

Whitney, P.R., and McLelland, J.M., 1973, Origin of coronas in metagabbros of the Adirondacks Mts., N.Y.: Contributions to Mineralogy and Petrology, v. 39, p. 81–98. [Also available at https://link.springer.com/article/10.1007/BF00374247.

Whitney, P.R., and McLelland, J.M., 1983, Origin of biotite-hornblende-garnet coronas between oxides and plagioclase in olivine metagabbros, Adirondack region, New York: Contributions to Mineralogy and Petrology, v. 82, p. 34–41. [Also available at https://link.springer.com/article/10.1007/BF00371173.]

Whitney, P.R., and Olmsted, J.F., 1988, Geochemistry and origin of albite gneisses, northeastern Adirondack Mountains, New York: Contributions to Mineralogy and Petrology, v. 99, p. 476–484, accessed April 16, 2021, at https://doi.org/10.1007/BF00371938.

Whitney, P.R., and Olmsted, J.F., 1993, Bedrock geology of the Au Sable Forks quadrangle, northeastern Adirondack Mountains, New York: New York State Museum, Map and Chart Series 43, 48 p., scale 1:62,500. [Also available at https://nysl.ptfs.com/data/Library1/81266.PDF.]

Williams, M.L., Grover, T.W., Jercinovic, M.J., Regan, S.P., Pless, C.R., and Suarez, K.A., 2019, Constraining the timing and character of crustal melting in the Adirondack Mountains using multi-scale compositional mapping and in-situ monazite geochronology: American Mineralogist, v. 104, no. 11, p. 1585–1602, accessed April 16, 2021, at https://doi.org/10.2138/am-2019-6906.

Williams, M.L., Grover, T.W., Pless, C.R., Suarez, K.A., Regan, S.P., and Baird, G.B., 2018, Migmatites of the eastern Adirondack Mountains—New constraints on the timing, petrology, and tectonic setting of partial melting, Trip A–1, *in* Grover, T.W., and Mango, H., eds., Guidebook for field trips in New York and Vermont: New England Intercollegiate Geological Conference, 110th Annual Meeting, and New York State Geological Association, 90th Annual Meeting, Castleton, Vt., Oct. 12–14, 2018, Field Trip Guidebook, Castleton, Vt., Castleton University, p. A1–1 to A1–34. [Also available at https://castleton.s3.amazonaws.com/files/pages/a1-final.pdf.]

Witherbee, F.S., 1906, History of the iron industry of Essex County, New York: Essex County Republican, Keeseville, N.Y., Princeton University, 39 p.

Wong, M.S., Williams, M.L., McLelland, J.M., Jercinovik, M.J., and Kowalkoski, J., 2012, Late Ottawan extension in the eastern Adirondack Highlands—Evidence from structural studies and zircon and monazite geochronology: Geological Society of America Bulletin, v. 124, nos. 5–6, p. 857–869. [Also available at https://doi.org/10.1130/B30481.1.]

Wynne-Edwards, H.R., 1972, The Grenville province, *in* Price, R.A., and Douglas, R.J.W., ed., Variations in tectonic styles in Canada: The Geological Association of Canada, Special Paper 11, p. 263–334.

Yochelson, E.L., 2006, The Lipalian interval—A forgotten, novel, concept in the geologic column: Earth Science History, v. 25, no. 2, p. 251–269. [Also available at https://doi.org/10.17704/eshi.25.2.772747j430w13n61.]

Appendix 1. Representative Photographs of Map Units From the Eagle Lake Quadrangle

The appendix contains representative photographs (figs. 1.1–1.12) of bedrock geologic map units from the Eagle Lake quadrangle, Essex County, New York. Photographs were taken during fieldwork. Units Ylg (Lyon Mountain Granite Gneiss), Ygb (metagabbro), and Ybg (migmatitic biotite gneiss member of the Grenville Complex) are shown in photographs in figures within the report and are not duplicated here. All locations are north latitude, west longitude in decimal degrees (World Geodetic System of 1984).

Figure 1.1. Photograph of a waste rock pile (unit wt) at the Penfield mine in Hammondville. Geologist is shown in the background (center right) wearing an orange vest for scale. Photograph by Gregory J. Walsh, U.S. Geological Survey. Location of photograph: 43.913096°, –73.616098° (World Geodetic System of 1984).

Figure 1.2. Light tan to buff weathering quartz arenite in the Potsdam Sandstone (unit Cpt) with near horizontal bedding near McMurty Road. Hammer for scale. Photograph by Gregory J. Walsh, U.S. Geological Survey. Location of photograph: 43.990396°, –73.518049° (World Geodetic System of 1984).

Figure 1.3. Photograph of dark-colored, olive-brown weathered mafic dike (unit Zd) (center) that intruded very coarse-grained, light-yellowish-tan to gray pegmatite (unit Yp) at the Spar Bed Hill deposit. Hammer for scale. Photograph by Gregory J. Walsh, U.S. Geological Survey. Location of photograph: 43.982505°, –73.539459° (World Geodetic System of 1984).

Figure 1.4. Photograph of hornblende granitoid gneiss (unit Ych) in the upper plate of the Moose Mountain detachment, on the south slopes of Moose Mountain. Hammer for scale. Photograph by Gregory J. Walsh, U.S. Geological Survey. Location of photograph: 43.944485°, –73.620112° (World Geodetic System of 1984).

Figure 1.5. Photograph of hornblende granitoid gneiss (unit Ych) on the north slopes of Dudley Mountain. Gray pen for scale. Photograph by Sean P. Regan, U.S. Geological Survey and University of Alaska. Location of photograph: 43.949814°, –73.600245° (World Geodetic System of 1984).

Figure 1.6. Photograph of white-weathered anorthosite (unit Yan) block within anorthosite, leucogabbro, and gabbroic gneiss (unit Yanw) on the north slopes of Moose Mountain. Anorthosite block is bordered by a black metamorphic reaction rim of magnetite, ilmenite, clinopyroxene, and hornblende. Host rock contains smaller blocks of anorthosite and andesine megacrysts. Hammer for scale. Photograph by Sean P. Regan, U.S. Geological Survey and University of Alaska. Location of photograph: 43.964558°, –73.615855° (World Geodetic System of 1984).

Figure 1.7. Photograph of anorthosite, leucogabbro, and gabbroic gneiss (unit Yanw) showing complex, tectonically interlayered (a) dark-gray metagabbro to ferrodiorite gneiss with andesine megacrysts; (b) light-colored leucogabbro gneiss; and (c) tan weathered, heterogenous and banded syenitic and leuocogabbroic gneiss on the north slope of Moose Mountain. A small brittle fault cuts through the left center of the exposure. Compass for scale. Photograph by Gregory J. Walsh, U.S. Geological Survey. Location of photograph: 43.968815°, –73.61884833° (World Geodetic System of 1984).

Figure 1.8. Photograph of megacrystic leucogabbroic gneiss within the anorthosite, leucogabbro, and gabbroic gneiss (unit Yanw), on the west side of Moose Mountain. Rock contains blue-gray megacrystic augen (porphyroclasts) of andesine that are likely deformed phenocrysts. Hammer for scale. Photograph by Gregory J. Walsh, U.S. Geological Survey. Location of photograph: 43.951874°, –73.63132° (World Geodetic System of 1984).

Figure 1.9. Photograph of granitic augen gneiss (unit Yggn) with white microcline augen on an unnamed ridge east of Penfield Pond. Pen for scale. Photograph by Gregory J. Walsh, U.S. Geological Survey. Location of photograph: 43.90580333°, –73.53135167° (World Geodetic System of 1984).

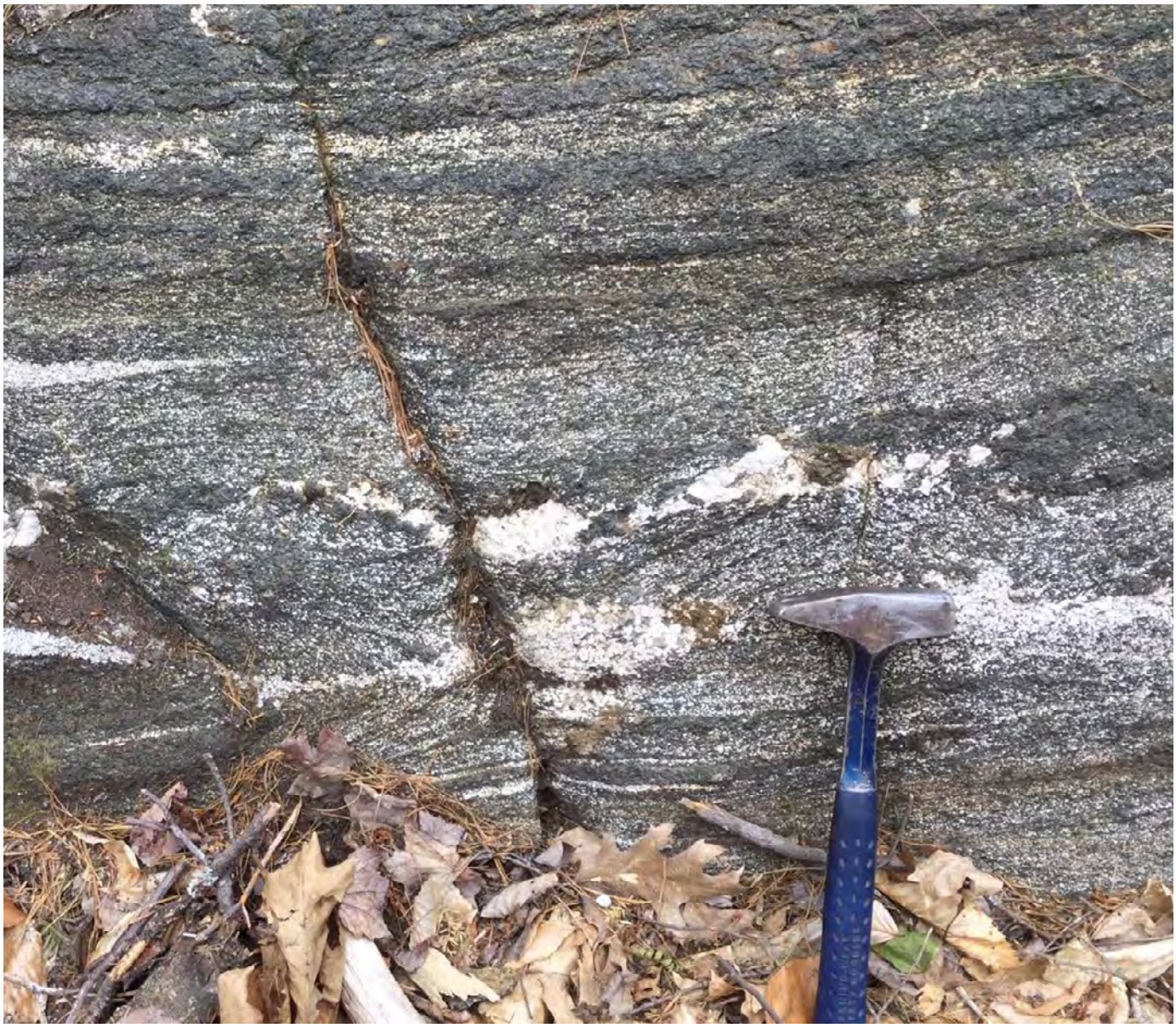

Figure 1.10. Photograph of amphibolite gneiss member of the Grenville Complex (unit Ya) with late pegmatite occurring as sills and infilled dilatant zones in boudin necks on the southwest ridge of Mount Lewis. Hammer for scale. Photograph by Gregory J. Walsh, U.S. Geological Survey. Location of photograph: 43.963584°, –73.566777° (World Geodetic System of 1984).

Figure 1.11. Photographs of the marble member of the Grenville Complex (unit Ym). *A*, Photograph of typical deeply weathered exposure north of Sherman Lake; and *B*, photograph of typical rusty weathered, white calcite marble with dark-green diopside. Geologist's legs (tan pants) for scale in *A*. Photographs by Gregory J. Walsh, U.S. Geological Survey. Location of photographs: 43.99224667°, –73.54443° (World Geodetic System of 1984).

Figure 1.12. Photographs of rusty garnet-sillimanite gneiss member of the Grenville Complex (unit Ysi) on the east-west trending ridge east of Chilson. *A*, Photograph shows abundant light-pink garnet; and *B*, photograph shows a white to very light gray vitreous quartzite layer. Hammer for scale. Photograph by Gregory J. Walsh, U.S. Geological Survey. Locations of photographs: 43.880143°, –73.515376° (top); 43.880692°, –73.517467° (bottom); World Geodetic System of 1984.

For more information regarding this publication, contact:
Director, USGS Florence Bascom Geoscience Center
12201 Sunrise Valley Drive, MS 926A
Reston, VA 20192

For additional information visit
USGS Florence Bascom Geoscience Center at
https://www.usgs.gov/centers/florence-bascom-geoscience-center.

Prepared by the USGS Science Publishing Network
Reston Publishing Service Center
Edited by David A. Shields
Illustration support by David Bruce and D. Paul Mathieux
Layout support by David Bruce and Cathy Y. Knutson

ISSN 2329-132X (online)
https://doi.org/10.3133/sim3542